

**DAHLGREN DIVISION  
NAVAL SURFACE WARFARE CENTER**

Panama City, Florida 32407-7001



**CSS/TR-96/29**

**OPTICAL CORRELATIONS FOR MINELIKE TARGET  
DETECTION: THEORY, MODELING, AND EVALUATION**

*DTIC QUALITY INSPECTED 4*

**MUSTAFA A.G. ABUSHAGUR**

**UNIVERSITY OF ALABAMA HUNTSVILLE**

**GIRARDEAU L. HENDERSON**

**COASTAL RESEARCH AND TECHNOLOGY DEPARTMENT**

**APRIL 1996**

Approved for public release; distribution is unlimited.

19960826 143

# REPORT DOCUMENTATION PAGE

Form Approved  
OMB No. 0704-0188

Public reporting burden for this collection of information is estimated to average 1 hour per response, including the time for reviewing instructions, searching existing data sources, gathering and maintaining the data needed, and completion and reviewing the collection of information. Send comments regarding this burden estimate or any other aspect of this collection of information, including suggestions for reducing this burden, to Washington Headquarters Services, Directorate for Information Operations and Reports, 1215 Jefferson Davis Highway, Suite 1204, Arlington, VA 22202-4302, and to the Office and Management and Budget, Paperwork Reduction Project (0704-0188), Washington, DC 20503.

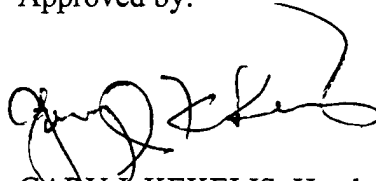
1. AGENCY USE ONLY (Leave blank)		2. REPORT DATE April 1996	3. REPORT TYPE AND DATES COVERED	
4. TITLE AND SUBTITLE Optical Correlators for Minelike Target Detection: Theory, Modeling, and Evaluation			5. FUNDING NUMBERS  RN15C52/11029	
6. AUTHOR(S) Mustafa A.G. Abushagur Girardeau L. Henderson				
7. PERFORMING ORGANIZATION NAME(S) AND ADDRESS(ES) Attn: Code 110A Commanding Officer CSSDD NSWC 6703 W. Highway 98 Panama City, FL 32407-7001			8. PERFORMING ORGANIZATION REPORT NUMBER  CSS/TR-96/29	
9. SPONSORING/MONITORING AGENCY NAME(S) AND ADDRESS(ES) Chief of Naval Research Ballston Tower 1 800 North Quincy Street Arlington, VA 22217-5660			10. SPONSORING/MONITORING AGENCY REPORT NUMBER	
11. SUPPLEMENTARY NOTES				
12a. DISTRIBUTION/AVAILABILITY STATEMENT  Approved for public release; distribution is unlimited.			12b. DISTRIBUTION CODE	
13. ABSTRACT (Maximum 200 words) Optical correlators were analyzed and simulated with emphasis on the evaluation of their performance in minelike target detection. Diffraction theory was used in analyzing correlator performance. A model of a correlator system using discrete optoelectronic devices, spatial light modulators, and detector arrays was formulated. Discretization and quantization effects on correlator performance were analyzed. It was shown that at least eight gray levels are needed for a satisfactory detection performance. Filter displacement in the Fourier plan of a few pixels was shown to cause a drastic reduction in the correlation peak and the detectability of the targets. Additive noise to the input image was considered in the simulation studies. A minimum signal-to-noise ratio of -2 dB (low CSNR) is needed for target detection in the specific examples used. Limited resolution images were evaluated and results show small (<20 percent) degradation in the performance of the correlator. It has been shown that a target with 50 pixels or more can be detected if its CSNR is 1.5 or higher. This suggests the advantage of reducing computation time significantly by reducing the pixel resolution of the images. Thresholding was studied for the detection of minelike targets. The peak-to-average intensity of the correlation was found to be the best parameter for thresholding.				
14. SUBJECT TERMS  optical correlators, target detection, pattern recognition, Fourier optics			15. NUMBER OF PAGES	
			16. PRICE CODE	
17. SECURITY CLASSIFICATION OF REPORT UNCLASSIFIED	18. SECURITY CLASSIFICATION OF THIS PAGE UNCLASSIFIED	19. SECURITY CLASSIFICATION OF ABSTRACT UNCLASSIFIED	20. LIMITATION OF ABSTRACT  UL	

## FOREWORD

This study was sponsored by the Chief of Naval Research; Ocean, Atmospheric, and Space Science and Technology Department (ONR 322). The work was performed under Coastal Systems Station (CSS) project/task RN15C52/11029, in the Mine Countermeasures Technology Program, SD3C.

This work was performed during FY94 and FY95 in the Electro-Optics/Magnetics Division (Code 110), Coastal Research and Technology Department (Code 10), CSS, Dahlgren Division, Naval Surface Warfare Center, Panama City, Florida.

Approved by:

A handwritten signature in black ink, appearing to read 'Gary J. Kekelis', is written over a horizontal line.

GARY J. KEKELIS, Head  
Coastal Research and Technology Department

## CONTENTS

<u>Chapter</u>	<u>Page</u>
1.0 INTRODUCTION .....	1-1
2.0 OPTICAL PATTERN RECOGNITION SYSTEMS .....	2-1
2.1 OPTICAL CORRELATORS .....	2-1
2.2 CORRELATOR ARCHITECTURES .....	2-2
2.3 INPUT IMAGE AND FILTER PARAMETERS .....	2-6
3.0 THEORY .....	3-1
3.1 DEFINITIONS .....	3-1
3.2 POWER BUDGET ANALYSIS .....	3-1
3.3 TIME ANALYSIS .....	3-3
3.4 BEAM PROPAGATION .....	3-3
3.5 LENS TRANSMITTANCE FUNCTION .....	3-4
3.6 SPATIAL LIGHT MODULATORS .....	3-5
3.7 DETECTOR ARRAY .....	3-6
3.8 OTHER OPTICAL COMPONENTS .....	3-7
4.0 OPTICAL SYSTEM MODELING .....	4-1
4.1 FOURIER OPTICS-BASED MODELING .....	4-2
4.2 SAMPLING AND DISCRETIZATION .....	4-3
4.3 SCALING .....	4-3
5.0 CATEGORIZATION OF CORRELATOR COMPONENT PARAMETERS.....	5-1
6.0 FILTER IN-PLANE TRANSLATION .....	6-1
7.0 QUANTIZATION EFFECTS ON CORRELATOR PERFORMANCE .....	7-1
7.1 MATHEMATICAL MODELING .....	7-1
7.2 QUANTIZING DATA FOR SLMs .....	7-4
7.3 CORRELATION PERFORMANCE CRITERIA .....	7-4
7.4 NUMERICAL EXPERIMENTS .....	7-5
8.0 IMAGES WITH LIMITED PIXEL RESOLUTION .....	8-1
8.1 LIMITED PIXEL RESOLUTION SIMULATION .....	8-1
8.2 LIMITED PIXEL RESOLUTION AND CORRELATOR .....	8-5

**CONTENTS (Continued)**

<u>Chapter</u>	<u>Page</u>
9.0 THRESHOLDING.....	9-1
9.1 MINELIKE TARGET CHARACTERIZATION .....	9-1
9.2 THRESHOLDING PARAMETER.....	9-5
10.0 SUMMARY AND CONCLUSIONS .....	10-1
11.0 REFERENCES .....	11-1
APPENDIXES	
A-SYSTEM COMPONENTS AND PARAMETERS .....	A-1
B-MINELIKE TARGETS DATA .....	B-1
C-COMPUTER MODEL FOR OPTICAL CORRELATOR .....	C-1
DISTRIBUTION.....	(1)

**ILLUSTRATIONS**

<u>Figure</u>	<u>Page</u>
2.1 LENS FT SYSTEM.....	2-2
2.2 TRANSMISSIVE SLM-BASED CORRELATOR .....	2-3
2.3 REFLECTIVE SLM-BASED CORRELATOR .....	2-4
2.4 JTC .....	2-5
3.1 ELECTRIC FIELD PROPAGATION THROUGH A DISTANCE.....	3-4
3.2 PIXELIZED SPATIAL LIGHT MODULATOR .....	3-5
3.3 TWO-DIMENSIONAL PHOTODIODE ARRAY.....	3-7
4.1 REPRESENTATION OF A LINEAR SYSTEM .....	4-1
4.2 REPRESENTATION OF OPTICAL CORRELATOR .....	4-2
6.1 RECTANGULAR TEST FUNCTION .....	6-1
6.2 CORRELATION PEAK AS A FUNCTION OF HORIZONTAL DISPLACEMENT OF FILTER .....	6-2
6.3 CORRELATION PEAK AS A FUNCTION OF DIAGONAL DISPLACEMENT OF FILTER .....	6-2

## ILLUSTRATIONS (Continued)

<u>Figure</u>		<u>Page</u>
6.4	CORRELATION PEAK AS A FUNCTION OF DIAGONAL DISPLACEMENT OF FILTER .....	6-3
6.5	CORRELATION PEAK AS A FUNCTION OF HORIZONTAL DISPLACEMENT OF FILTER .....	6-3
6.6	TEST PATTERN OF LETTER "E" .....	6-4
6.7	CORRELATION PEAK AS A FUNCTION OF HORIZONTAL DISPLACEMENT OF FILTER .....	6-4
6.8	CORRELATION PEAK AS A FUNCTION OF VERTICAL DISPLACEMENT OF FILTER .....	6-5
6.9	CORRELATION PEAK AS A FUNCTION OF DIAGONAL DISPLACEMENT OF FILTER .....	6-5
7.1	SIGNAL QUANTIZATION WITH SEVEN QUANTIZATION LEVELS .....	7-1
7.2	SIGNAL AND ITS QUANTIZED SIGNALS FOR Q=2 AND 8.....	7-2
7.3	INPUT IMAGE, TARGET, AND THEIR POWER SPECTRUMS .....	7-6
7.4	CORRELATION PATTERN FOR DIFFERENT QUANTIZATION LEVELS, Q, OF FILTER .....	7-7
7.5	CORRELATOR PERFORMANCE MEASURES FOR QUANTIZED FILTER EXPERIMENT.....	7-8
7.6	QUANTIZED INPUT IMAGES .....	7-9
7.7	CORRELATION PATTERN FOR QUANTIZED INPUT IMAGE FOR DIFFERENT $Q_i$ 's .....	7-11
7.8	CORRELATION PATTERN FOR QUANTIZED INPUT IMAGE AND FILTER .....	7-11
7.9	PERFORMANCE MEASURES FOR QUANTIZED INPUT IMAGE .....	7-12
7.10	CORRELATION PATTERNS FOR QUANTIZED INPUT AND FILTER .....	7-13
7.11	PERFORMANCE PARAMETERS.....	7-13
7.12	NOISE CORRUPTED INPUT SCENE.....	7-15
7.13	CORRELATION PATTERN OF NOISY INPUTS WITH TARGET .....	7-17
7.14	PERFORMANCE PARAMETERS AS A FUNCTION OF $SNR_i$ .....	7-19
7.15	CORRELATION PATTERNS FOR NOISY INPUT SCENE USING A BPOF... ..	7-21
7.16	PERFORMANCE PARAMETERS FOR NOISY INPUT AND BPOF .....	7-23
7.17	BINARIZED NOISY INPUT SCENE .....	7-25
7.18	CORRELATION PATTERNS FOR BINARIZED NOISY INPUT SCENE USING A CMF .....	7-26
7.19	PERFORMANCE PARAMETERS FOR BINARIZED NOISY INPUT AND CMF .....	7-29
7.20	EXPERIMENTALLY COLLECTED IMAGES .....	7-30

## ILLUSTRATIONS (Continued)

<u>Figure</u>		<u>Page</u>
7.21	REFERENCE TARGET IMAGE .....	7-32
7.22	AUTOCORRELATION PATTERN OF TARGET .....	7-33
7.23	CROSS-CORRELATION OF INPUT SCENES WITH TARGET .....	7-33
7.24	AUTOCORRELATION OF TARGET USING POF .....	7-35
7.25	CROSS-CORRELATION INTENSITY PATTERNS FOR INPUT SCENES WITH TARGET .....	7-36
7.26	AUTOCORRELATION PATTERN OF TARGET USING BPOF .....	7-38
7.27	CROSS-CORRELATION INTENSITY PATTERNS FOR INPUT SCENES USING BPOF .....	7-38
7.28	BINARIZED INPUT IMAGES .....	7-41
7.29	CROSS-CORRELATION OF BINARIZED INPUT SCENES WITH TARGET .....	7-42
7.30	CROSS-CORRELATION OF BINARIZED INPUT SCENES WITH TARGET USING BPOF .....	7-44
7.31	QUANTIZED INPUT SCENE b1 WITH Q=16 AND 32 .....	7-46
7.32	QUANTIZED INPUT SCENE w1 WITH Q=c, 2, 4, 8, 16, AND 32 .....	7-47
7.33	CROSS-CORRELATION INTENSITY PATTERN FOR QUANTIZED b1 USING CMF .....	7-48
7.34	CROSS-CORRELATION INTENSITY PATTERN FOR QUANTIZED w1 USING CMF .....	7-49
8.1	IMAGE BEACH1 .....	8-2
8.2	IMAGE BEACH7 .....	8-2
8.3	IMAGE DUNE1 .....	8-3
8.4	IMAGE DUNE2 .....	8-3
8.5	IMAGE WATER1 .....	8-4
8.6	IMAGE WATER2 .....	8-4
8.7	PERFORMANCE MEASURE PAR AS A FUNCTION OF IMAGE PIXEL RESOLUTION .....	8-6
8.8	PERFORMANCE MEASURE PMSR AS A FUNCTION OF IMAGE PIXEL RESOLUTION .....	8-7
9.1	PERFORMANCE PARAMETERS AS A FUNCTION OF CSNR FOR CMF CASE .....	9-4
9.2	PERFORMANCE PARAMETERS AS A FUNCTION OF CSNR FOR POF CASE .....	9-4
9.3	PERFORMANCE PARAMETERS AS A FUNCTION OF CSNR FOR BPOF CASE .....	9-5
9.4	IMAGES AND TARGET LOCATION AS DETECTED BY CORRELATOR (SPATIAL FILTER USED IS CMF AND PAR <sub>th</sub> =3) .....	9-6

## ILLUSTRATIONS (Continued)

<u>Figure</u>		<u>Page</u>
9.5	IMAGES AND TARGET LOCATION AS DETECTED BY CORRELATOR (SPATIAL FILTER USED IS POF AND PAR <sub>th</sub> =3).....	9-7
9.6	IMAGES AND TARGET LOCATION AS DETECTED BY CORRELATOR (SPATIAL FILTER USED IS BPOF AND PAR <sub>th</sub> =3).....	9-7
9.7	IMAGES AND TARGET LOCATION AS DETECTED BY CORRELATOR (SPATIAL FILTER USED IS BPOF AND PAR <sub>th</sub> =5).....	9-8

## TABLES

<u>Table</u>		<u>Page</u>
5.1	PARAMETER CATEGORIZATION .....	5-1
5.2	PARAMETER SIMULATION .....	5-2
7.1	AVERAGE SIGNAL-TO-QUANTIZER NOISE POWER RATIO .....	7-4
7.2	SNR <sub>i</sub> FOR CORRUPTED IMAGES.....	7-15
7.3	CORRELATION PERFORMANCE FOR MATCHED FILTER.....	7-35
7.4	CORRELATION PERFORMANCE FOR POF.....	7-37
7.5	CORRELATION PERFORMANCE FOR BPOF .....	7-40
7.6	CORRELATION PERFORMANCE FOR BINARY INPUT AND BPOF .....	7-45
7.7	CORRELATION PERFORMANCE FOR QUANTIZED b <sub>1</sub> SCENE .....	7-51
7.8	CORRELATION PERFORMANCE FOR QUANTIZED w <sub>1</sub> SCENE.....	7-51
8.1	REDUCED RESOLUTION PIXEL COUNT.....	8-1
8.2	REDUCED RESOLUTION PERFORMANCE RESULTS.....	8-5
9.1	CORRELATOR PERFORMANCE RESULTS .....	9-3



## 1.0 INTRODUCTION

Optical correlators play a major role in a wide range of signal processing systems,<sup>1</sup> such as optical pattern recognition.<sup>2,3,4,5</sup> Correlator systems operate in parallel and provide the high speed throughput required for such an application. In this study, theoretical analysis, computer modeling, and simulation of an optical correlator system for detecting minelike targets are considered. The practical characteristics and limitations of the different components are implemented to make the model of practical use. The computer model was designed in such a way to allow the user to specify the parameters for each component and the layout of the system. This study is limited to the VanderLugt 4f correlator system.<sup>6</sup>

Optical pattern recognition fundamentals and optical correlator architectures are presented in Section 2.0. In Section 3.0, the theoretical foundation for the correlator system is presented using diffraction theory. Optical correlator modeling based on Fourier optics is given in Section 4.0. Simulation parameters prioritization is given in Section 5.0. The rest of the report contains simulation results to study a number of critical issues in the performance of optical correlators in minelike target detection. The affects on the correlator performance of in-plane translation of the spatial filter are given in Section 6.0. Section 7.0 studies the affects of quantization on the performance of the optical correlator. Limitation on image pixel resolution is investigated and reported in Section 8.0. In Section 9.0 thresholding of the output data is examined and a thresholding parameter is introduced for minelike target detection. Limited resolution affects on the performance of the system are given in Section 8.0. Thresholding and choosing the thresholding parameter are presented in Section 9.0. Summary and conclusions are presented in Section 10.0. Optical and optoelectronic components for a typical optical correlator system are listed in Appendix A. The statistical parameters of the experimental minelike targets are given in Appendix B. The optical correlator model description and operation procedure are presented in Appendix C.

## 2.0 OPTICAL PATTERN RECOGNITION SYSTEMS

Optics with its parallelism attracted much attention in the development of pattern recognition systems. Patterns to be recognized usually are in an optical format; i.e., an image. This format lends itself to the optical domain and is natural to be processed optically. In the last three decades since the invention of the laser, a great deal of research has been directed towards developing optical pattern recognition systems. Coherent optical Fourier processors capable of performing vital mathematical operations such as Fourier transformation, correlation, and convolution of two-dimensional signals became the center of attention for such applications. The introduction of the VanderLugt filter<sup>6</sup> was the breakthrough needed at that time to initiate such efforts. Since then, many system architectures and filter designs have been introduced. A major problem hindering the development of such systems is the interface device limitations, spatial light modulators in particular. Recently, technological advances in such devices has made pattern recognition systems more feasible.

Pattern recognition here is meant in the general sense; i.e., character, image, speech, or signal recognition. The fundamental objective of pattern recognition is the classification of the input pattern. Pattern recognition in general uses two broad techniques-*template matching* and *feature extraction*.<sup>2,3,4</sup> Template matching is based on comparing an input pattern to a template of all possible patterns. This comparison can be done by performing correlation using either space or frequency domain techniques. In feature extraction, the system is considered as a two-stage device. The first stage is feature extraction, and the second stage is classification. Features are defined as measurements taken on the pattern. A set of measured features are supplied to the classifier. The classifier's task is to map these input features onto a classification state. In this report, the concentration is on the correlator with its application in detecting minelike targets.

### 2.1 OPTICAL CORRELATORS

Correlation is an operation to compare two patterns. Consider two functions  $f(x)$  and  $g(x)$ , the correlation is defined using the following mathematical operation.

$$c(x) = \int_{-\infty}^{\infty} f(\beta) g'(\beta - x) d\beta, \quad (2.1)$$

where  $c(x)$  is the correlation, and ' denotes the complex conjugate. Correlation of two functions is the area of overlap as one function is scanned over the other. Let the Fourier transforms (FTs) of  $f(x)$ ,  $g(x)$ , and  $c(x)$  be  $F(u)$ ,  $G(u)$ , and  $C(u)$ , respectively. By taking the FT of both sides of Equation (2.1)

$$C = FG^* \quad (2.2)$$

From Equations (2.1) and (2.2) another way to perform correlation is by inverse Fourier transforming the product of the FT of one of the functions with the complex conjugate of the FT of the other.

Consider an object that is placed in the front focal plane of a lens and illuminated by a coherent plane wave as shown in Figure 2.1. The output of this optical system is determined by using the Fresnel propagation integrals taking into account the quadratic phase term of the lens transfer function.<sup>7</sup> The output is the FT of the input function except for simple phase terms. This output is a two-dimensional transform of the input function. This FT operation is performed in parallel and the time required is the time it takes for the light beam to travel from the input to the output plane. Consider a system with a lens of 5-cm focal length, the time required for the FT operation is 0.3 nsec.

This capability of optics to perform FTs is employed in performing the correlation operation.

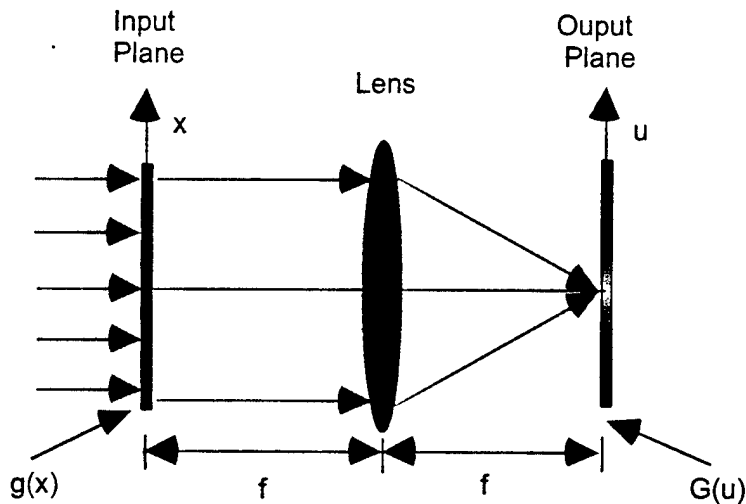


FIGURE 2.1 LENS FT SYSTEM  
(f IS FOCAL LENGTH OF LENS)

## 2.2 CORRELATOR ARCHITECTURES

Correlation as discussed earlier is performed by taking the inverse FT of the product of the FT of both functions. There are two major correlator systems, the 4f in-line or VanderLugt and the joint transform correlators.<sup>8</sup>

### 2.2.1 4f In-Line Correlator

This system can be designed using either transmissive or reflective type spatial light modulators (SLMs). The study is limited to the transmissive type. As shown in Figures 2.2 and 2.3, a beam emitted by a coherent light source is filtered, expanded, and collimated then used to illuminate the input SLM. The electric field emanating from this SLM is modulated by the input image. Lens 1 operates on this electric field to produce its FT, within the Fourier optics concept, and project it on the filter SLM. The filter SLM, in a simple correlator system, represents the conjugate of the FT of the target. The light emanating from this SLM is the product of the FT of the input image and the conjugate FT of the target. Lens 2 produces the inverse FT of the field emanating from the filter SLM. This results in the correlation of the input scene and the target. This correlation pattern is detected by the charge coupled device (CCD) array and processed by the computer system.

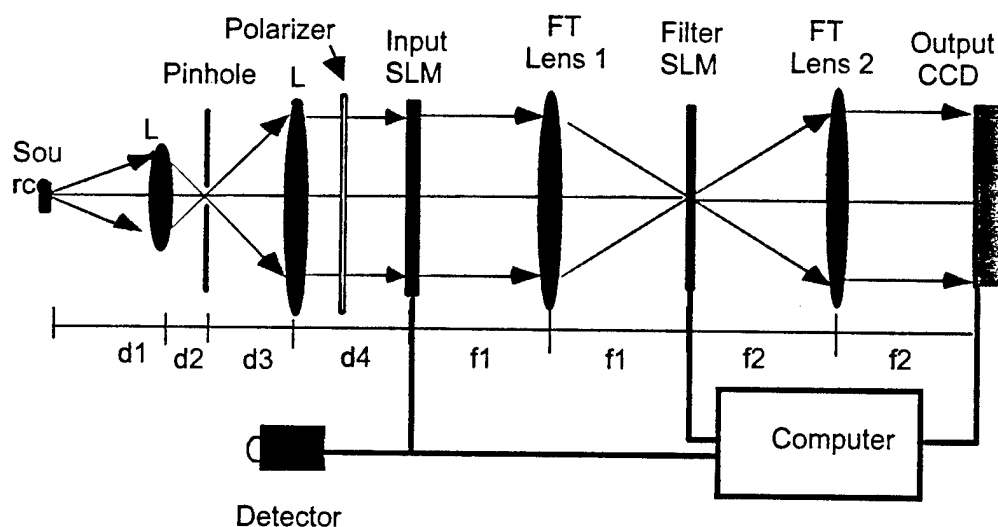


FIGURE 2.2. TRANSMISSIVE SLM-BASED CORRELATOR

The correlation is performed in parallel in two-dimensions. As in the case of Fourier transformation, the speed of the correlation operation is limited only by the time required for the light to travel from the input to the output plane. This system is referred to as the *4-f in-line correlator*. It is the basic building block of most coherent optical signal processing systems.

The complex conjugate of the FT of the reference target is placed in the frequency domain and it is referred to as the *filter function*. A large body of literature exists regarding these filters and their design.

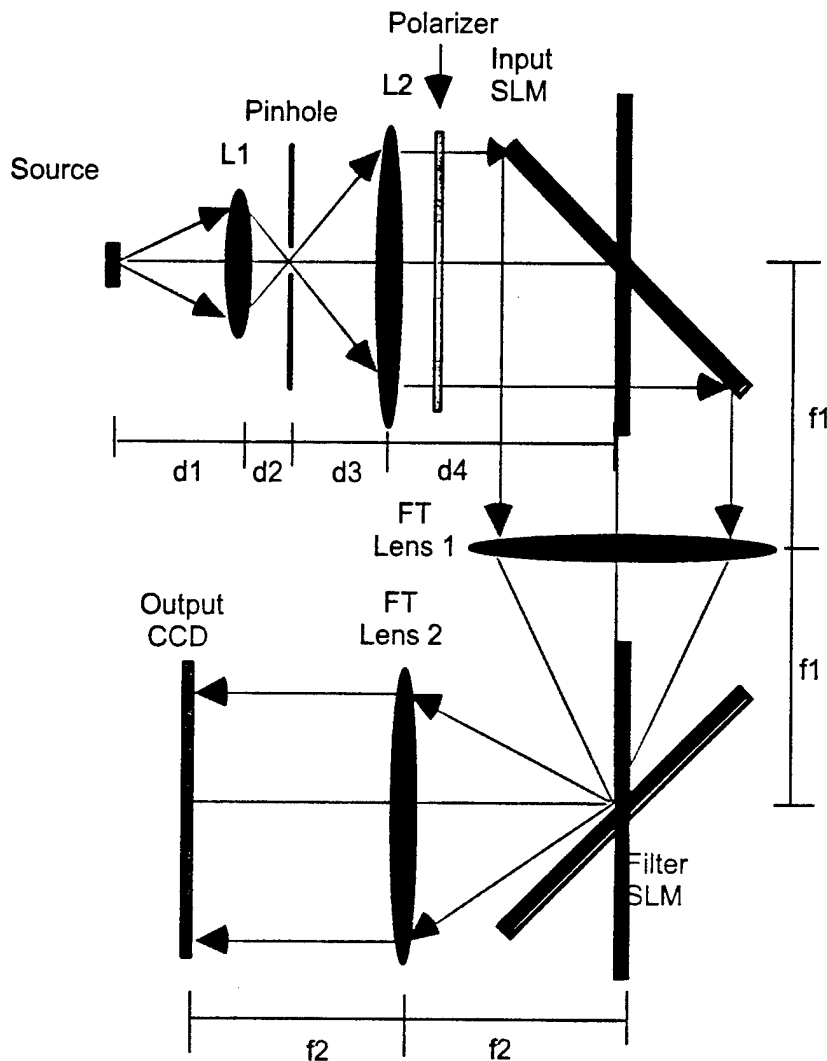


FIGURE 2.3. REFLECTIVE SLM-BASED CORRELATOR

This system is translation invariant. Translating the object in the input plane does not affect the position of its FT. Its transform remains centered with some phase change. The correlation spot tracks the object indicating its exact position in the scene. The classical matched filter introduced by VanderLugt<sup>1</sup> is holographically recorded. Placing the filter in the Fourier plane is critical, it allows only a few microns of tolerance perpendicular to the optic axis and tens of microns along the optic axis.<sup>9,10</sup> This is a severe requirement on such systems and places a great emphasis on filter positioning. Changing the scale or the orientation of the input object will reflect directly on the scale and rotation of its FT. If this takes place in the correlator system, the correlation peak becomes small and the system fails to recognize the object. This sensitivity to scale and rotation changes is considered one of the major problems facing such correlator

systems. A number of techniques have been proposed to design filters that can accommodate the in-plane scale and rotation changes.<sup>11,12,13,14,15,16</sup> Some of these techniques will be discussed in a later section in this report.

### 2.2.2 Joint Transform Correlator (JTC)

The positioning of the filter in the frequency plane (focal plane of the lens) presents a severe restriction especially for high data inputs. The JTC was proposed as an improvement to the 4-f in-line correlator for objects of great similarity and also relaxes the filter positioning problem mentioned earlier.<sup>8,17,18,19</sup>

In this correlator architecture, both target and scene patterns are presented at the input plane simultaneously. Patterns are placed in the front focal plane of a Fourier transforming lens and illuminated by a coherent plane wave. Electric field distribution of FTs of both patterns are added up to produce an interference pattern at the back focal plane of the lens, as shown in Figure 2.4. This interference pattern is recorded on a photographic plate as a hologram. The processed hologram is illuminated by a plane wave and the correlation of the target with the scene is produced at the back focal plane of the lens.

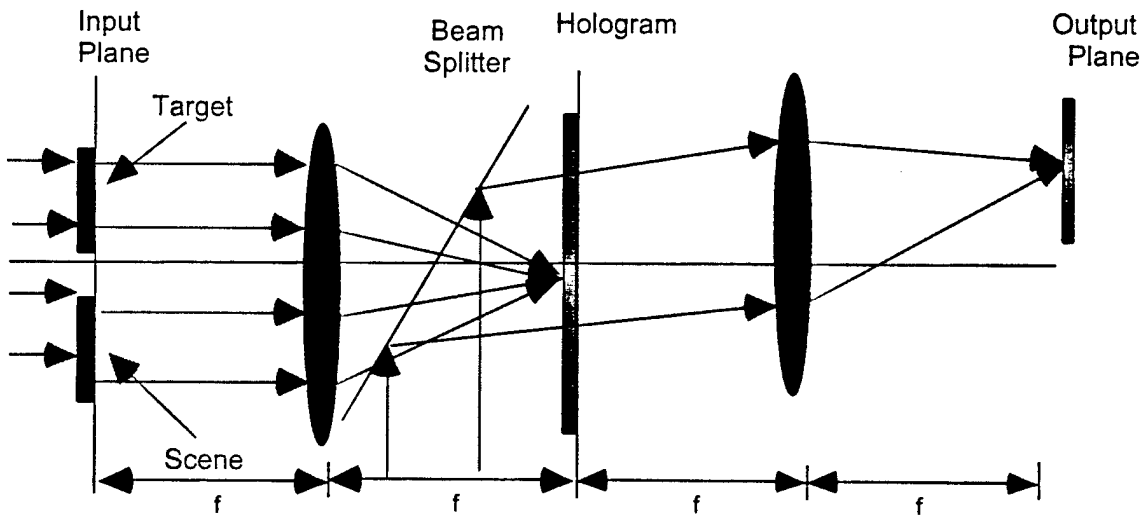


FIGURE 2.4. JTC (BOTH RECORDING AND READING ARE SUPERIMPOSED)

As in the case of 4-f in-line correlators using a holographic filter, the output plane contains convolution, correlation, and distorted images of the two function. These are located in different positions in the output plane.

The JTC system is advantageous in two respects. First, provided that the hologram is to be replaced by a real-time optoelectronic device such as an SLM or a detector and SLM combination,<sup>20</sup> its parallelism is achieved. The input and filter patterns can be displayed on the same SLM or two different SLMs. This makes the system operate in near real-time and the reference filter need not be recorded in advance. Second, the problem in positioning the filter in the Fourier plane is also alleviated since the FT of the input and filter patterns are formed by the same lens.

### 2.3 INPUT IMAGE AND FILTER PARAMETERS

A correlator system is used to search a scene for a particular target. The scene is typically captured using a detector. The scene is referred to in this study as the input image. The image is displayed using the input SLM. The target or set of targets to be searched for are recorded off-line as a set of spatial filters. The spatial filters use one or more of the typical filter formats such as the conventional matched filter (CMF), phase-only filter (POF), binary phase-only filters (BPOF), etc. These filters, for practical system applications are designed with the capability to detect the target regardless of its orientation, projection, or scale. Such filters use composite filter formats. The following is a list of some of the important parameters of the input image and filters that are needed for designing the computer model of the correlator.

#### Input Image

- Image Size
- Gray Levels
- Updating Speed
- Jitter
- Signal-to-Noise Ratio (SNR)

#### Filter

- Filter Size
- Filter Type (Complex, POF, BPOF, etc.)
- Number of Reference Filters
- Filter Search and Retrieval Time
- Gray Levels

### 3.0 THEORY

This section presents the theoretical foundations for the design and operation of optical correlator systems. This includes power and time budget analysis and propagation of optical beams through the different optical components and in the space between them.

#### 3.1 DEFINITIONS

$W_s$	=	Width of the emitting area of the light source
$R_l$	=	Lens reflectance per surface (assuming all lenses have similar reflectance's)
$T_{slm}$	=	SLM transmittance (transmissive type SLM)
$R_{slm}$	=	SLM reflectance (reflective type SLM)
$T_{pl}$	=	Polarizer transmittance
$D_1, D_2, D_{fl}$	=	Diameters of lenses $L_1$ , $L_2$ , and FT lenses
$P_s$	=	Source emitted power in Watts
$P_d$	=	Power falling on the detector array
$m$	=	Light source radiation coefficient
$w_p$	=	Pinhole diameter
$t_s$	=	Source rise time
$t_i$	=	Image refresh time
$t_f$	=	Filter search and retrieval time
$t_d$	=	Detector array reading time

#### 3.2 POWER BUDGET ANALYSIS

The power of the emitted light beam is

$$P_s = P_o \cos^m \theta , \quad (3.1)$$

where  $\theta$  is the angle between the emitted rays and the optical axis, and  $P_o$  is the power emitted normal to the light source surface. The power of the light beam after lens  $L_1$  in Figure 2.2 is given by

$$P_1 = (1 - R_l)^2 P_o \int_{-\theta_1}^{\theta_1} \cos^m \theta \, d\theta , \quad (3.2)$$

where



$$\theta_1 = \tan^{-1} \left( \frac{D_1}{2d_1} \right). \quad (3.3)$$

The power as it emerges from lens L<sub>2</sub> is

$$P_2 = 0.83 (1-R_l)^2 P_1, \quad (3.4)$$

or

$$P_2 = 0.83(1-R_l)^4 P_o \int_{-\theta_1}^{\theta_1} \cos^m \theta \, d\theta, \quad (3.5)$$

In some cases, the laser diode assembly will include a collimator that is made of the source, lenses L<sub>1</sub> and L<sub>2</sub>, and the pinhole. The power output from such an assembly is equivalent to P<sub>2</sub> and the beam usually has a Gaussian profile. In such cases, the beam needs to be collimated and expanded. That involves similar assembly and Equation (3.5) can still be used to determine the power of the collimated beam.

The power at the detector, considering all the optical elements between lens L<sub>2</sub> and the CCD array, for a transmissive SLM system is given by

$$P_d = (1-R_l)^4 \cdot T_{pl} \cdot T_{slm}^2 \cdot P_2, \quad (3.6)$$

and for a reflective SLM system is given by

$$P_d = (1-R_l)^4 \cdot T_{pl} \cdot R_{slm}^2 \cdot P_2. \quad (3.7)$$

In this analysis, the size of the source is assumed to be small compared with the size of the pinhole, and the diameters of L<sub>2</sub> and the FT lenses are larger than the beam.

Laser diodes emit an elliptical optical beam. To convert this through the pinhole-lens assembly to a circular Gaussian beam considerable power loss will result. Let the emitted beam have two diverging angles j<sub>1</sub> and j<sub>2</sub>. The resulting power conversion can be approximated by

$$\eta = \frac{\int_{-\pi\phi_1/\phi_2}^{\pi\phi_1/\phi_2} \frac{\sin\left(\frac{\pi\theta}{\phi_2}\right)}{\left(\frac{\theta}{\phi_2}\right)} d\theta}{\int_{-\pi}^{\pi} \frac{\sin\left(\frac{\pi\theta}{\phi_2}\right)}{\left(\frac{\theta}{\phi_2}\right)} d\theta} \quad (3.8)$$

So the total power at the detector array is

$$P_d = \eta \cdot (1 - R_l)^4 \cdot T_{pl} \cdot T_{slm}^2 \cdot P_2 \quad (3.9)$$

### 3.3 TIME ANALYSIS

The system speed depends on the response time of the different optoelectronic components and the light beam propagation time. The propagation time is extremely small so it will not be considered. The system response time can be approximately expressed as

$$t_{sys} = 1.1 \sqrt{t_s^2 + t_i^2 + t_{fl}^2 + t_d^2} \quad (3.10)$$

### 3.4 BEAM PROPAGATION

Beam propagation analysis, from one plane to another in the optical system, uses diffraction theory. The Fresnel diffraction integral is to be used for such an analysis.<sup>2</sup> Linear system techniques can be used effectively in this case. Propagation of electric fields can be reduced to convolution between the input electric field and the impulse response of the system, which is in this case the Fresnel kernel. Propagation through optical elements can be achieved by multiplying the electric field by the transmission function of the optical element.

Let an input electric field be represented by  $g(x,y)$ . After propagating a distance  $z$ , as shown in Figure 3.1, the output electric field,  $u(p,q)$ , can be given by (using Fresnel diffraction integral)

$$u(p,q) = Q \int_{-\infty}^{\infty} g(x,y) e^{j \frac{k}{2z} [(x-p)^2 + (y-q)^2]} dx dy \quad (3.11)$$

where  $Q$  is a constant phase factor given by

$$Q = \frac{e^{jkz}}{j\lambda z} \quad (3.12)$$

Using linear system theory Equation (3.11) can be rewritten as

$$u(p, q) = g(p, q) * e^{j\frac{k}{2z}(p^2 + q^2)} \quad (3.13)$$

where \* denotes the convolution operation.

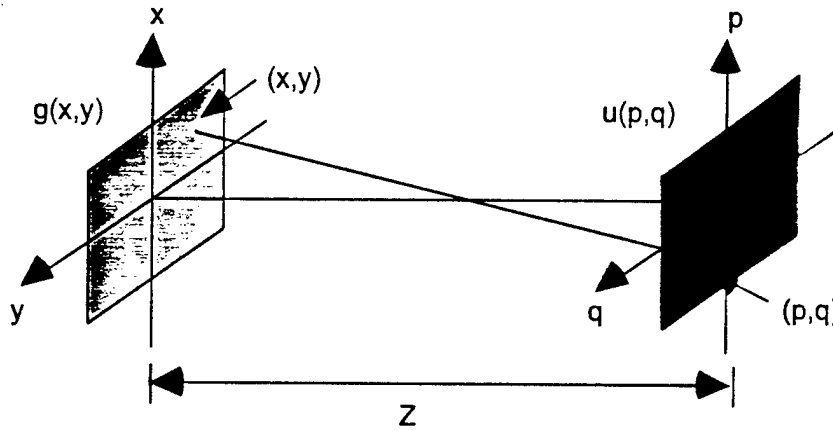


FIGURE 3.1. ELECTRIC FIELD PROPAGATION THROUGH A DISTANCE

### 3.5 LENS TRANSMITTANCE FUNCTION

The lens as an optical element reshapes the electric field wavefront. It can be considered as a phase transformer. For a spherical thin lens with a focal length  $F$ , the transmittance function is given by

$$t_l(x, y) = e^{-j\frac{\pi}{\lambda F}(x^2 + y^2)} \quad (3.14)$$

This formula is based on a first-order approximation, assuming the spherical lens can be represented by parabolic surfaces. Aberration effects can be included by taking into account the thickness and aperture size of the lens, index of refraction wavelength dependence, and the deviation from the parabolic representation of the lens.

### 3.6 SPATIAL LIGHT MODULATORS

A SLM plays a major role in all optical systems. It modulates the light beams either reflected off it or transmitted through it with a modulating function impressed on it either electronically or optically. The amplitude transmittance of the SLM can be represented by

$$t_s(x, y) = t_{os}(x, y) \cdot e^{j\phi(x, y)}, \quad (3.15)$$

where  $t_{os}(x, y)$  and  $\phi(x, y)$  are the amplitude and phase modulation of the SLM, respectively. The effect of the SLM as well as the lens is a multiplication with the input electric field. The SLM representation given in Equation (3.15) is for a continuous analog device. The discrete nature of the SLM can be considered by modifying Equation (3.15). Let the SLM have  $N \times N$  pixels; each pixel be a square with a side dimension  $d_s$ ; and the pixel center spacing  $s_c$ ; and the SLM overall size  $D_s$  as shown in Figure 3.2.

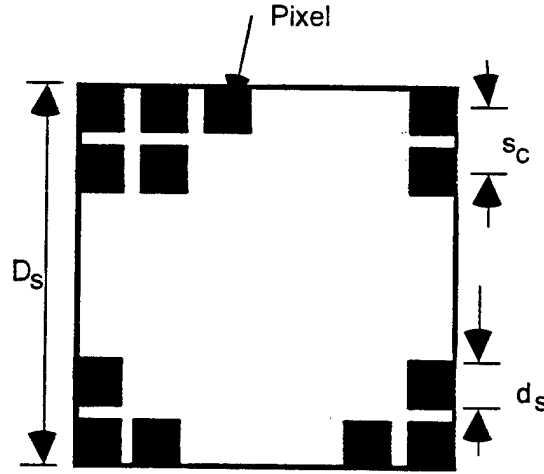


FIGURE 3.2. PIXELIZED SPATIAL LIGHT MODULATOR

The amplitude transmittance function of such an SLM can be given by

$$t_s(x, y) = \sum_{n=-N/2}^{N/2} \left[ \text{rect} \left( \frac{x}{d_s}, \frac{y}{d_s} \right) * \delta(x - ns_c, y - ns_c) \right] \cdot t_{os}(x, y) \cdot e^{j\phi(x, y)} \quad (3.16)$$

where  $\text{rect}(\cdot)$  is the rectangular function, which is defined as

$$\text{rect} \left( \frac{x}{d} \right) = \begin{cases} 1 & , -d/2 \leq x \leq d/2 \\ 0 & , -d/2 > x > d/2 \end{cases} \quad (3.17)$$

and  $\delta(x)$  is the Dirac delta function. The fill factor,  $f_f$ , of the SLM is the ratio of the active area of the pixels to the total area

$$f_f = \frac{(N \cdot d_s)^2}{D_2} . \quad (3.18)$$

The dynamic range of the SLM can be represented through the amplitude modulation  $t_s(x,y)$ .

### 3.7 DETECTOR ARRAY

Photodetector arrays are used to convert the output optical signal to an electronic one.<sup>21</sup> The electronic representation of the output of the system depends on the speed, resolution, and dynamic range of the detector array. The output of the detector array is a discrete representation of the image, even if the image is continuous. The relation between the input optic power  $P_i$  and the output current  $I$ , for a discrete photodetector element, is given by

$$I = R_O P_i \quad (3.19)$$

where  $R_O$  is the responsivity of the detector, which depends on a number of factors including the quantum efficiency and the wavelength. There are three important factors in choosing a detector array: the number of elements,  $M \times M$ , in the array; the spacing,  $s_d$ , between the individual detector elements; and the dynamic range and speed.

Sampling theory requires a sampling rate at least equal to the Nyquist frequency. For a detector array in the spatial frequency plane (as in the case of the optical correlator) at least two detector elements per frequency are needed. For a signal with a spatial length of  $L$  this requires

$$2s_d \leq \frac{\lambda F}{L} . \quad (3.20)$$

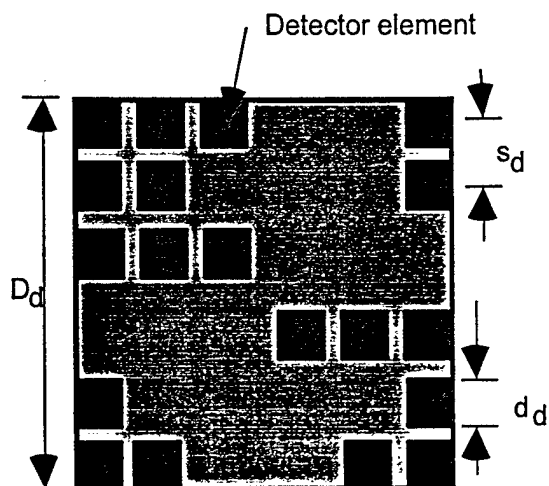


FIGURE 3.3. TWO-DIMENSIONAL PHOTODIODE ARRAY

The number of detector elements,  $M$ , should be larger than twice the space bandwidth product (SBP) of the system. In optical systems, the detector array and the SLM restrict the SBP.

### 3.8 OTHER OPTICAL COMPONENTS

Other optical components such as plane mirrors, polarizers, and beam splitters can be represented by their reflection and transmission coefficients.

#### 4.0 OPTICAL SYSTEM MODELING

This study uses the linear system notation for the analysis and simulation of the optical correlator. In linear system notation, each system component is represented by its impulse response,  $h(x,y)$ . Figure 4.1 shows a basic representation of a linear system and the relationship between the input and output.

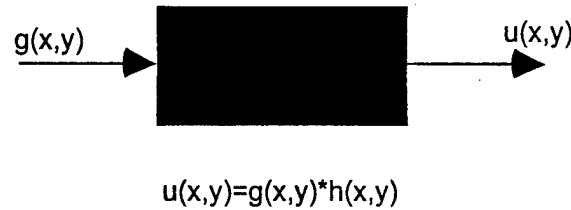


FIGURE 4.1. REPRESENTATION OF A LINEAR SYSTEM

The correlator system shown in Figure 2.2 can be represented by the block diagram shown in Figure 4.2. This block diagram represents the system starting at the plane wave illuminating the input SLM. Let the input image, the filter, and the output be  $u_i(x,y)$ ,  $u_f(x,y)$ , and  $u_o(x,y)$ , respectively. Using the notation described for the different optical elements the output image is

$$u_o(x,y) = \left\{ \left[ \left( u_i(x,y) * e^{j\frac{k}{2F}(x^2+y^2)} \right) \cdot t_l(x,y) \right] * e^{j\frac{k}{2F}(x^2+y^2)} \right\} \cdot u_f(x,y) * e^{j\frac{k}{2F}(x^2+y^2)} \cdot t_l(x,y) * e^{j\frac{k}{2F}(x^2+y^2)} \quad (4.1)$$

Where \* and • denote convolution and multiplication, respectively.

In this simulation, the fast FT operation will be used to perform convolution. From the FT properties, taking the inverse FT of the product of the FT of the two functions results in a convolution operation.

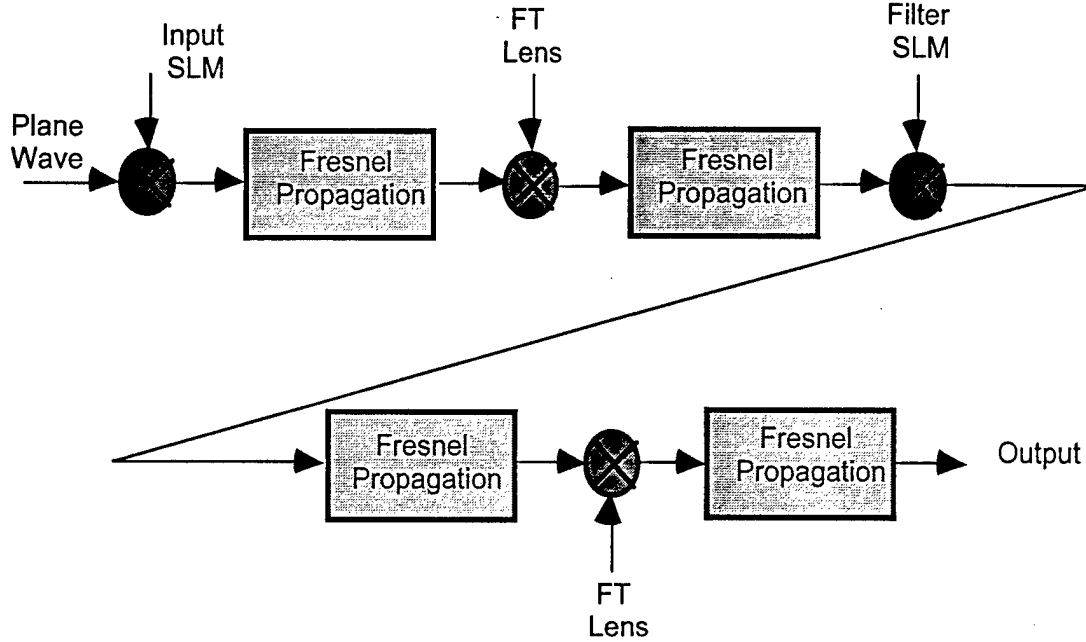


FIGURE 4.2. REPRESENTATION OF OPTICAL CORRELATOR

#### 4.1 FOURIER OPTICS-BASED MODELING

In this model, the FT property of the lens is used, which is a good approximation for many applications. Also considered is the general case in which the object can be placed any distance in front of the lens instead of restricting it to the front focal plane. The finite size of lens 1 aperture, which leads to the *vignetting* effect will be considered. Let an object with an amplitude transmittance  $u_i(x,y)$  be placed a distance,  $d$ , in front of a lens with pupil function  $P(x,y)$ . The output field at the back focal plane of the lens is given by

$$u_o(x_f, y_f) = \frac{e^{\left[ j \frac{k}{2F} \left( 1 - \frac{d}{F} \right) (x_f^2 + y_f^2) \right]}}{j\lambda F} \cdot \int_{-\infty}^{\infty} \int_{-\infty}^{\infty} u_i(x, y) P\left(x + \frac{d}{F} x_f, y + \frac{d}{F} y_f\right) e^{\left[ -j \frac{2\pi}{\lambda F} (x_o x_f + y_o y_f) \right]} dx dy \quad (4.2)$$



where  $(x_f, y_f)$  is the spatial coordinates of the FT plane. Equation (4.2) can be represented by the following operator notation

$$u_o(x_f, y_f) = Q_o F \left\{ u_i(x, y) \cdot \left[ P(x, y) * \delta \left( x + \frac{d}{F} x_f, y + \frac{d}{F} y_f \right) \right] \right\}, \quad (4.3)$$

where  $F\{\dots\}$  is the FT operator and  $Q_o$  is the phase factor preceding the integral in Equation (4.2).

## 4.2 SAMPLING AND DISCRETIZATION

The input image, the spatial filter, and output signal are all represented in a discrete form due to the nature of the optoelectronic devices involved. Modeling the system components on the computer also involves discretization. In this model, it is assumed that all sampling satisfies the Nyquist criterion. The discrete nature of the data will affect the SBP and the frequency content of the system.

## 4.3 SCALING

In the correlator system, as light propagates from one plane to another, it carries along information about the object, plane separation distances, and sizes of pixels and devices. In the simulation model, the input is represented by a matrix with size equal to the number of pixels in the input SLM. The spatial input dimensions depend on the SLM pixel size. For example, the output of the FT is also represented by a matrix. The dimensions of the spatial features depend on the wavelength, the focal length and size of the lens, and the input SLM dimensions. These dimensions are important when the field at this plane is being modulated by another function; e.g., the filter SLM. Scaling of these planes becomes an important factor in representing the physical system in the simulation.

For example, the pixels in the input SLM are squares with size  $d_s$ . For this analysis, consider a one-dimensional case. The input to the optical FT system is  $\text{rect}(x/d_s)$ . The output is

$$F \left\{ \text{rect} \left( \frac{x}{d_s} \right) \right\} = d_s \text{sinc} \left( \frac{d_s x_f}{\lambda F} \right). \quad (4.4)$$

The width of the main lobe will define the size of the FT plane. If the number of pixels in the output plane is  $N$  (which is the same as of the input), then for the zeros of the sinc function

$$N d_o = \frac{2\lambda F}{d_s}, \quad (4.5)$$

where  $d_o$  is the output pixel size; i.e., spatial size of the output matrix element, and is given by

$$d_o = \frac{2\lambda F}{Nd_s} . \quad (4.6)$$

If the size of the pixel of the following SLM or detector does not match  $d_o$ , then an averaging will take place. For input and output SLMs with identical pixel sizes, the system requires  $d_o=d_s$ , which can be achieved by choosing a proper focal length

$$F = \frac{Nd_o^2}{2\lambda} . \quad (4.7)$$

Consider the case where  $N=128$ ,  $d_s=d_o=30$  mm, which is what should be expected for a typical Ferro-electric SLM, and  $\lambda=690$  nm, then the focal length should be  $F=83.478$  mm.

## 5.0 CATEGORIZATION OF CORRELATOR COMPONENT PARAMETERS

In Table 5.1, the different component parameters are tabulated and categorized according to their affect on the overall performance of the correlator system. Also the parameters are categorized in terms of the analysis (power budget, speed analysis, or correlator performance) they influence the most. In Table 5.2, the different versions of the computer model designed are listed as part of this study and the different parameters included in each version. The study in its current state includes only the first version of the model.

TABLE 5.1. PARAMETER CATEGORIZATION

Parameter	0 <sup>th</sup> Order	1 <sup>st</sup> Order	2 <sup>nd</sup> Order
Light Source			
Power Emitted	X (PA)		
Beam Profile		X	
Wavelength	X (CP)		
Spectral Width			X (SA)
Coherence Length			X
Source Size	X (PA)		
Rise Time	X (SA)		
Lenses			
Focal Length	X (CP)		
Aperture Size	X (PA)	X (CP)	
Surface Curvature			X (CP)
Surface Tolerance			X (CP)
Glass Type			X (CP)
Transmissivity or Reflectivity	X (PA)		
Physical Size	X (PA)		
Resolution	X (CP)		
Pixel Size	X (CP)		
Pixel Spacing	X (CP)		
Fill Factor	X (PA)		
Surface Flatness			X (CP)
Addressing Speed	X (SA)		
Gray Levels	X (CP)		
Detector Array			
Physical Size	X (PA)		
Array Size	X (CP)		
Active Area Size	X (CP)		
Detector Spacing	X (CP)		

TABLE 5.1. PARAMETER CATEGORIZATION (CONTINUED)

Parameter	0 <sup>th</sup> Order	1 <sup>st</sup> Order	2 <sup>nd</sup> Order
Fill Factor	X (PA)		
Responsivity	X (PA)		
Reading Speed	X (SA)		
Dynamic Range	X (CP)		
Input Image			
Image Size		X (CP)	
Gray Levels	X (CP)		
Updating Speed	X (SA)		
Jitter		X (CP)	
SNR		X (CP)	
Filter			
Filter Size	X (CP)		
Filter Type	X (CP)		
Number of Reference Filters	X (CP)		
Search and Retrieval Time	X (CP)		
Gray Levels	X (CP)		

PA = power analysis

CP = correlator performance

SA = speed analysis

TABLE 5.2. PARAMETER SIMULATION

Parameter	1 <sup>st</sup> Version	2 <sup>nd</sup> Version	3 <sup>rd</sup> Version
Power Analysis		X	
Beam Profile		X	
Coherence			X
Time Analysis		X	
Fourier Optics	X		
Fresnel Propagation		X	
Reflection Architecture		X	
Transmissive Architecture	X		
JTC		X	
Lens Aperture Size	X		
Lens Aberration		X	X
SLM Fill Factor		X	
SLM Size	X		
SLM Nonlinearities		X	
Noise and Jitter		X	X
Gray Level (Input)	X	X	
Gray Level (Filter)		X	
Filter Design	X	X	X

TABLE 5.2. PARAMETER SIMULATION (CONTINUED)

Parameter	1st Version	2nd Version	3rd Version
Preprocessing		X	
Postprocessing		X	
Detector Array Size	X		
Detector Array Fill Factor		X	
Detector Array Resolution	X		
Polarization		X	
Optical Alignment	X		
Filter Placing Accuracy		X	

## 6.0 FILTER IN-PLANE TRANSLATION

In optical systems, the alignment of the different components plays a major role in its performance. In the correlator system, the projection of the FT of the input image upon the spatial filter is probably the most crucial alignment requirement. In this plane, a point-by-point product is performed between the two FTs. When the pixels of the two transforms are misaligned, a degradation of the performance is expected. The other important misalignment degradation results from the positioning of the filter SLM in a plane that is not exactly at the focal plane of the FT lens. This situation requires a more complex modeling using Fresnel diffraction integrals and will not be considered at this stage of study.

This section addresses the problem of in-plane misalignment of the filter and its affect on the correlator performance. Two patterns will be used for the numerical experiments: a rectangular function and a letter 'E' pattern.

The first experiment is done using an input background with 32x32 pixels while the rectangular function is 5x5 pixels as shown in Figure 6.1.

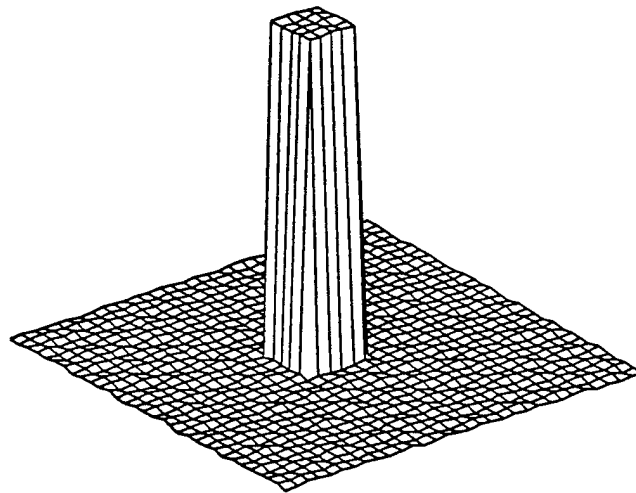


FIGURE 6.1. RECTANGULAR TEST FUNCTION

The autocorrelation peak is computed as a function of the filter displacement and is plotted in Figure 6.2. The location of the correlation peak did not change but its value decreases rapidly by the increase of the translation. In the considered example, a displacement of four pixels resulted in a 3-dB drop of its peak.

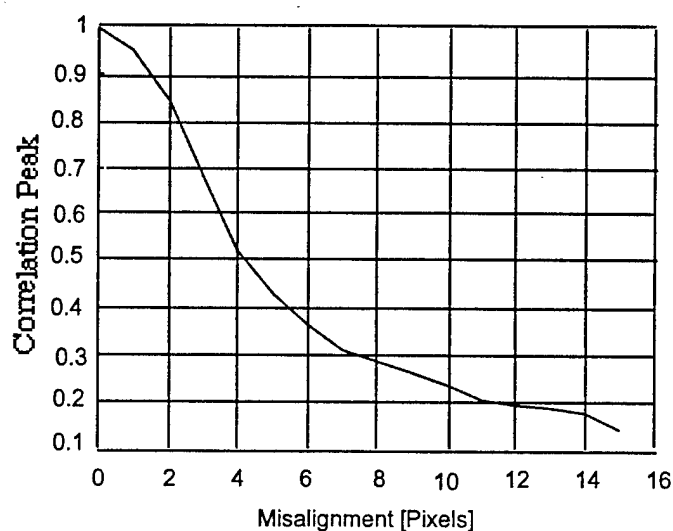


FIGURE 6.2. CORRELATION PEAK AS A FUNCTION OF HORIZONTAL DISPLACEMENT OF FILTER

In Figure 6.3, the displacement is done along both axes at the same time; i.e., one pixel misalignment corresponds to one pixel horizontal and one pixel vertical displacement. The correlation peaks drops by 3 dB for a translation of three pixels (about four diagonal pixels).

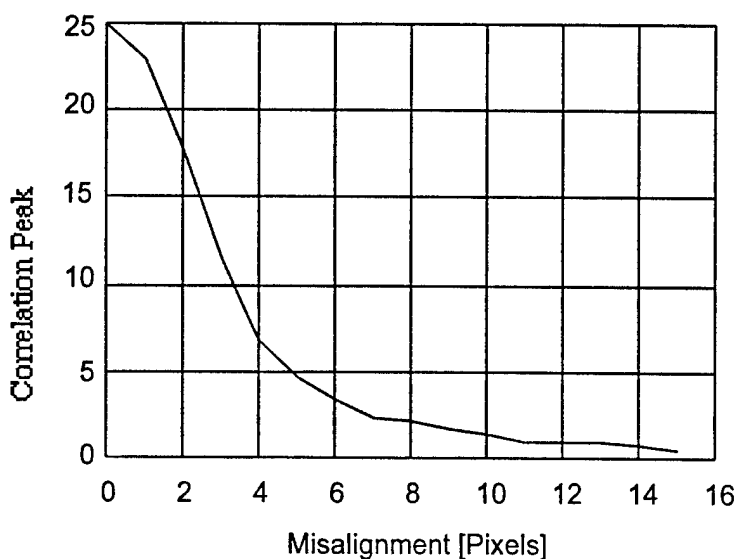


FIGURE 6.3. CORRELATION PEAK AS A FUNCTION OF DIAGONAL DISPLACEMENT OF FILTER

Considered next is the same rectangular function with a 64x64 pixel background. This effectively reduces the rectangular function to half its original size. The correlation peak is plotted in Figure 6.4. The correlation drops by 3 dB with a misalignment approximately of six pixels.

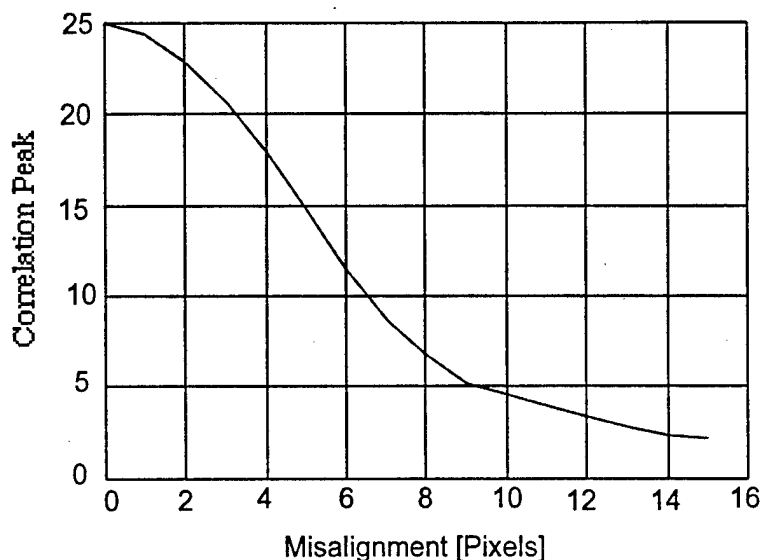


FIGURE 6.4. CORRELATION PEAK AS A FUNCTION OF DIAGONAL DISPLACEMENT OF FILTER

Figure 6.5 shows the correlation peak for an input of a 32x32 randomly generated image. The correlation peak is more sensitive to the displacement because of the uncorrelated nature of the signal. The correlation peaks drops by 3 dB for one pixel misalignment.

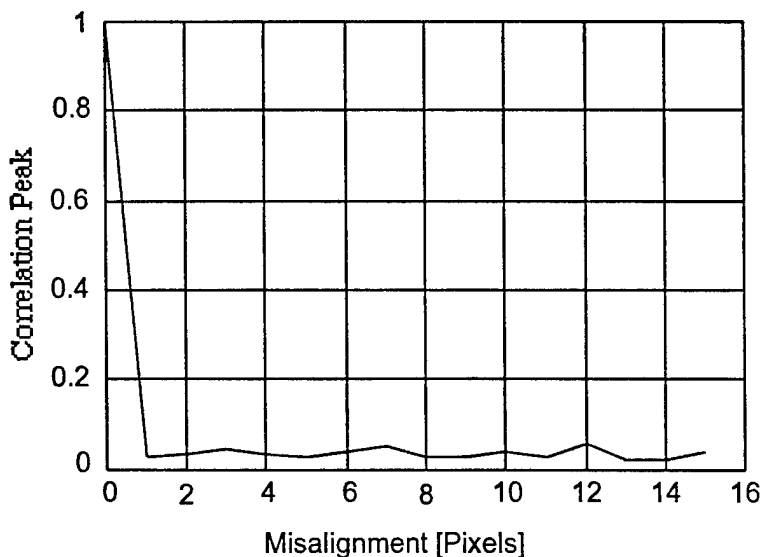


FIGURE 6.5. CORRELATION PEAK AS A FUNCTION OF HORIZONTAL DISPLACEMENT OF FILTER



The third test pattern considered is a letter 'E' as shown in Figure 6.6. This image does not have the symmetry that the rectangular function has and its correlation length is different along the two axes.

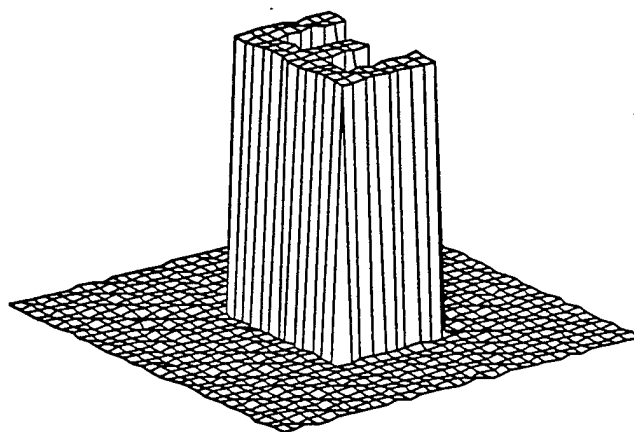


FIGURE 6.6. TEST PATTERN OF LETTER 'E'

The correlation peak as a function of the displacement along the horizontal, vertical, and diagonal direction of the filter is given in Figures 6.7 to 6.9, respectively.

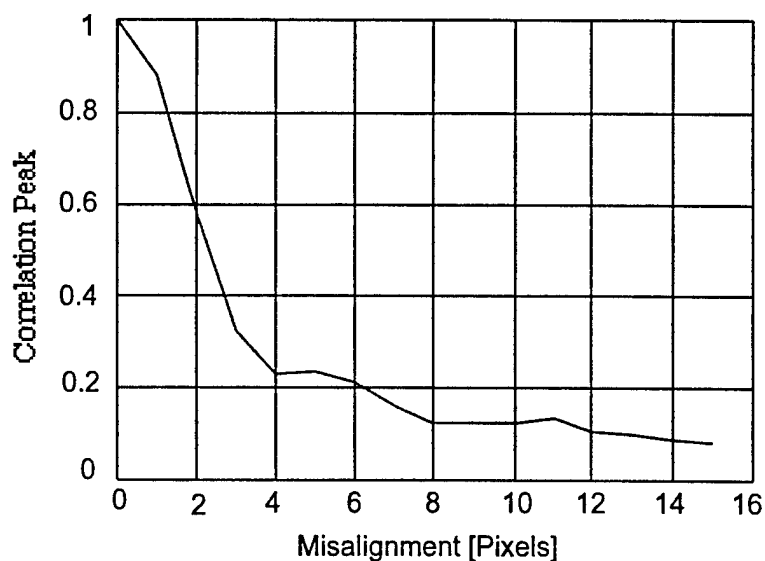


FIGURE 6.7. CORRELATION PEAK AS A FUNCTION OF HORIZONTAL DISPLACEMENT OF FILTER

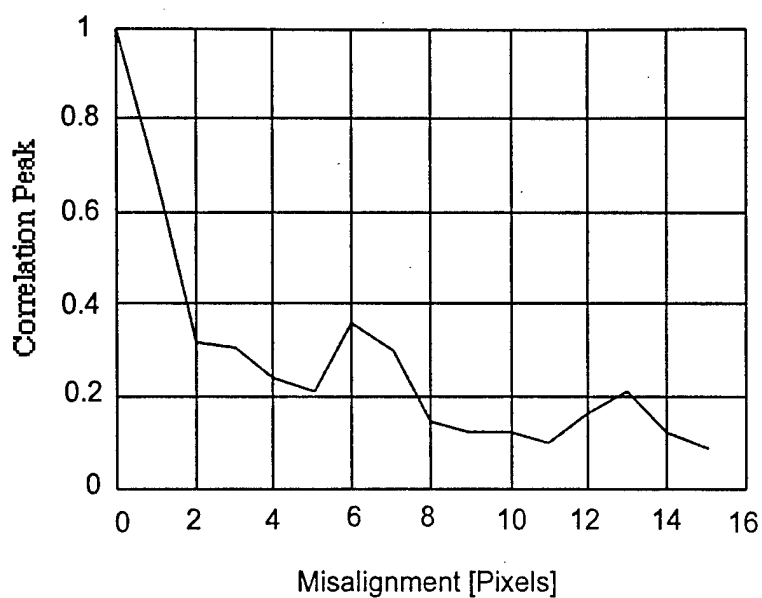


FIGURE 6.8. CORRELATION PEAK AS A FUNCTION OF VERTICAL DISPLACEMENT OF FILTER



FIGURE 6.9. CORRELATION PEAK AS A FUNCTION OF DIAGONAL DISPLACEMENT OF FILTER

Results of displacement given in Figures 6.7 to 6.9 show that a filter displacement of two or three pixels results in a 3-dB drop in the correlation peak.

From the test examples that have been considered, a displacement of a few pixels, three to four for the rectangular and 'E' patterns and only one for the randomly generated pattern, results in a 3-dB drop of the correlation peak. This leads to an increase in the false detection of a target. So aligning the filter properly is crucial to the correlator performance. The misalignment sensitivity increases when the correlation length of the function decreases.

## 7.0 QUANTIZATION EFFECTS ON CORRELATOR PERFORMANCE

Optical correlator performance depends on a number of factors. Among these are the optoelectronic devices used for feeding information in and out of the system. SLM and CCD arrays available for use in correlator systems have a limited dynamic range. A large number of available fast SLMs are binary. Using these devices for both displaying the input image and reference filters require the conversion of such signals from the analog, or continuous mode into the appropriate quantized form with finite quantization levels. Quantization of the analog signal plays a major role in determining the quality and performance of the correlator system. In the optics literature, few studies have addressed this issue.<sup>22</sup> This section addresses the issue of quantization and its affects on the performance of a typical correlator system.

### 7.1 MATHEMATICAL MODELING

Consider the signal  $X(t)$  as shown in Figure 7.1. Assume that the signal varies in the range  $a \leq (t) \leq b$ .

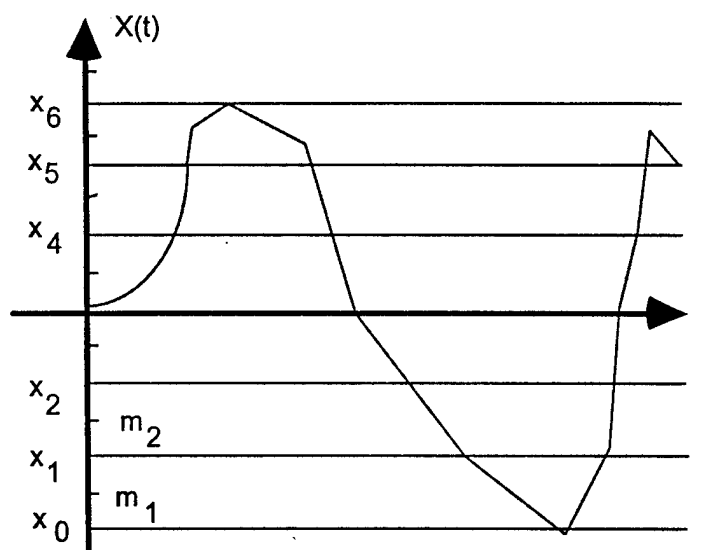


FIGURE 7.1. SIGNAL QUANTIZATION WITH SEVEN QUANTIZATION LEVELS

Let the function  $X(t)$  be quantized into  $Q$  levels. The quantization will be at intervals of  $t$  that satisfy the Nyquist theorem. The quantization levels for uniform quantizing, as shown in Figure 7.1, will be separated by

$$\Delta = \frac{b - a}{Q} \quad (7.1)$$

The quantized function  $X_q$  will be given by

$$X_q = m_i, \text{ if } x_{i-1} < X \leq x_i, \quad (7.2)$$

where

$$\begin{aligned} x_i &= a + i \cdot \Delta, \\ m_i &= \frac{x_{i-1} + x_i}{2} \end{aligned} \quad (7.3)$$

and  $i=0, 1, 2, \dots, (Q-1)$ .

An arbitrary function and its quantized forms at quantization levels  $Q=2$  and  $8$  are shown in Figure 7.2.

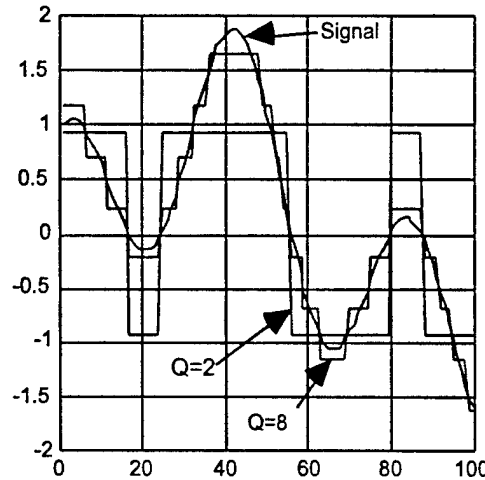


FIGURE 7.2. SIGNAL AND ITS QUANTIZED SIGNALS FOR  $Q=2$  AND  $8$

The measure of performance of a quantizing scheme is defined as the ratio of the output quantized signal to the quantizing noise power<sup>23</sup>

$$\frac{S_q}{N_q} = \frac{E\{[X_q]^2\}}{E\{[X - X_q]^2\}} \quad (7.4)$$

where  $E\{ \cdot \}$  is the expected value. Let  $X(t)$  be a zero mean stationary random process with probability density function (pdf)  $p_X(x)$ , then

$$\begin{aligned} N_q &= E\{[X - X_q]^2\} \\ &= \int_a^b (x - x_q)^2 p_X(x) dx \\ &= \sum_{i=1}^Q \int_{x_{i-1}}^{x_i} (x - m_i)^2 p_X(x) dx \end{aligned} \quad (7.5)$$

and

$$\begin{aligned} S_q &= E\{[X_q]^2\} \\ &= (m_i)^2 \sum_{i=1}^Q \int_{x_{i-1}}^{x_i} p_X(x) dx \end{aligned} \quad (7.6)$$

If the input to a  $Q$ -step uniform quantizer has a uniform pdf over  $[-a, a]$ , the average signal-to-quantizer noise power ratio at the output is

$$\begin{aligned} \frac{S_q}{N_q} &= Q^2 - 1 \\ &\approx Q^2, \quad \text{for } Q \gg 1. \end{aligned} \quad (7.7)$$

A random function of 100 points is generated using uniform distribution statistics. The average signal-to-quantizer noise power is computed for  $Q=2, 4, 8, 16, 32, 64, 128$ , and 256. The results are shown in Table 7.1, and they agree with the predicted results, using Equation (7.7). A larger data set will give more accurate results.

TABLE 7.1. AVERAGE SIGNAL-TO-QUANTIZER NOISE POWER RATIO  
(COMPUTED AS A FUNCTION OF QUANTIZATION LEVEL, Q, FOR A  
RANDOMLY GENERATED FUNCTION WITH A UNIFORM DISTRIBUTION)

Q	2	4	8	16	32	64	128	256
$S_q/N_q$	3.3	12.5	51.2	213.7	971.1	3636.9	13,405	59,953

## 7.2 QUANTIZING DATA FOR SLMs

In optical systems, SLMs are used as the input/output devices for displaying the information to be impressed on a beam. The transmittance function of these devices vary between the values "0" and "1", "0" indicates complete block of the optical beam and "1" for full transmission of the beam. This is for amplitude modulation. Phase modulation can be also performed by SLMs and the phase can assume values between "0" and " $\pi$ ". Low cost liquid crystal television (LCTV) SLMs are analog with a limited dynamic range. These can be used for either amplitude or phase modulation. Cascading two LCTVs can perform complex data modulation.

## 7.3 CORRELATION PERFORMANCE CRITERIA

Several performance criteria are proposed in the literature for quantitative measures of the correlator and comparison between the different correlation schemes.<sup>24,25</sup> In this study, the following performance measures will be used.

*Correlation Peak:* Correlation peak intensity value.

*Peak-to-Average Intensity Ratio (PAR):* Correlation-peak intensity to the average intensity of the entire correlation plane.

*Peak-to-Maximum-Sidelobe Ratio (PMSR):* The intensity of the primary peak in the correlation plane to the intensity of the successive highest value around the primary peak. To find this second peak value, a square-shaped portion of the correlation plane centered upon the primary peak was deleted. This square is made of about 11x11 pixels, which constitutes about 2.95 and .75 percent of the correlation plane area for a 64x64 and 128x128 pixel image, respectively.

These performance measures indicate the sharpness of the correlation peak. Correlation peak depends on a number of factors including the energy content of the signal. For the quantization experiments, it might not be a good measure because of the bias added by the quantization process.

## 7.4 NUMERICAL EXPERIMENTS

In this section, a set of numerical experiments are reported to analyze the affect of quantization on optical correlator performance. In such correlators, the input image (test image) is captured using a CCD camera and displayed into the correlator through an SLM, then its FT is computed optically. This transform of the input image is projected on an SLM that displays the filter. The filter in its simplest form is the complex conjugate of the FT of the reference image. The product of these two signals is inverse Fourier transformed optically to produce the correlation between the input image and the reference. The correlation pattern is detected on a CCD array.

Quantization of signals can take place in a number of ways in this correlator system, namely at the CCD camera, input SLM, filter SLM, and output CCD array. In the following numerical experiments three cases will be considered.

- (1) Input is continuous and the filter is quantized.
- (2) Input and the filter are both quantized.
- (3) Input is quantized and the filter is continuous.

In each of these cases, it is first assumed that SLMs can display any quantized value, then the limitations of the optical SLMs mentioned in the previous section are considered. The quantization of the filter signal, which is complex in the CMF case, is performed separately on the magnitude and phase. For the case of POF, only the phase will be quantized since the magnitude is unity.

The numerical experiments are performed using two sets of test patterns. The first set is a computer-generated pattern using image processing software. This pattern consists of two objects, a vehicle and another object with circular cross-section and a Gaussian-type amplitude. This pattern is used in two sets of experiments; i.e., as it is and by adding different levels of noise and studying the effect. The third set of experiments uses experimentally collected data for a spherical-shaped target in different environments. In each of these experiments, the spatial filter of the target to be recognized is computer generated. Correlator performance criteria is plotted or tabulated for each of these cases and compared.

### 7.4.1 Vehicle Pattern

The input image to the correlator system consists of a vehicle, which is the target, and a circular object. The pattern is made out of 64x64 pixels with continuous variation of the amplitude. In this report, continuous amplitude is limited by computer accuracy. The circular object included has about 67 percent of the vehicle energy. Its function is to present a false target and to test the correlator system for false target rejection. The input image and the target are both shown along with their power spectrum in Figure 7.3.



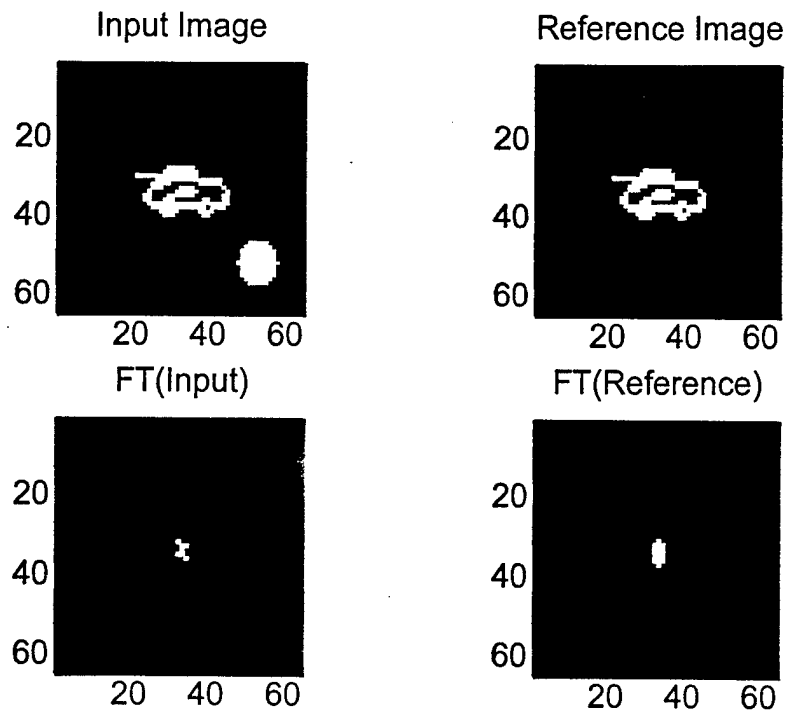


FIGURE 7.3. INPUT IMAGE, TARGET, AND THEIR POWER SPECTRUMS

**7.4.1.1 Continuous Input Image and Quantized Filter.** In the correlator testing, the input image is used as a continuous pattern along with its FT. The reference image is used to compute its corresponding spatial filter. This filter is quantized with a range of levels  $Q=2, 4, 8, 16, 32, 64, 128$ , and  $256$ , which correspond to  $1, 2, 3, 4, 5, 6, 7$ , and  $8$  bits, respectively. In each of these cases, a plot of the maximum correlation intensity of each column of the correlation pattern is given. Figure 7.4 shows the results of the correlation for the continuous,  $Q=c$ , and CMF. The pattern labeled  $Q=c$  is the fundamental limit since it assumes both the input and filter can be displayed with continuous amplitudes and phases. For  $Q=2$ , the correlation pattern is quite different from that for  $Q=c$ . As  $Q$  approaches eight or higher, the correlation pattern becomes close to that of  $Q=c$ .

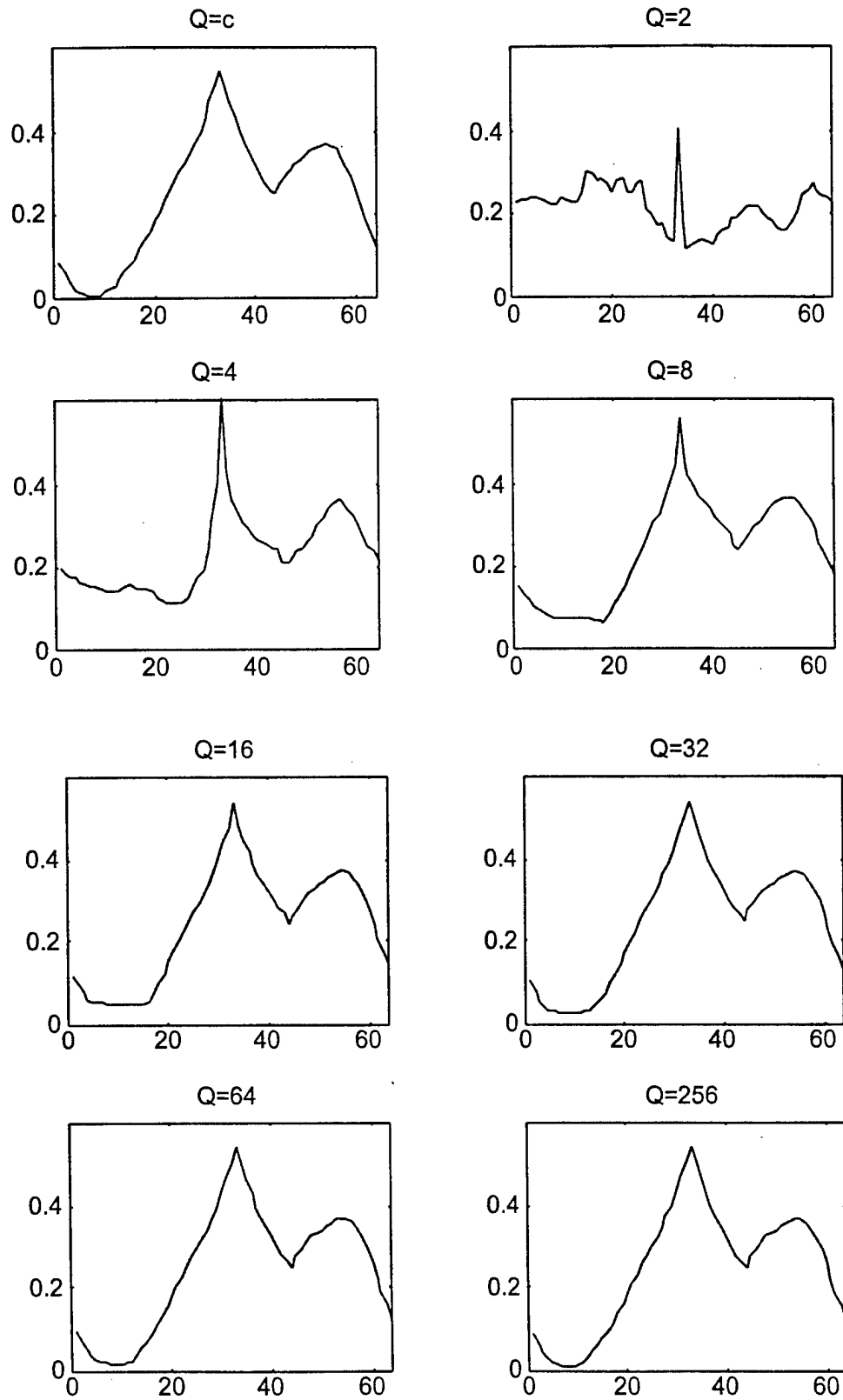


FIGURE 7.4 CORRELATION PATTERN FOR DIFFERENT QUANTIZATION LEVELS,  $Q$ , OF FILTER

The resulting correlation patterns are used to compute performance measures, namely the correlation peak, PAR, and the PMSR defined previously. These performance measures are shown in Figure 7.5.

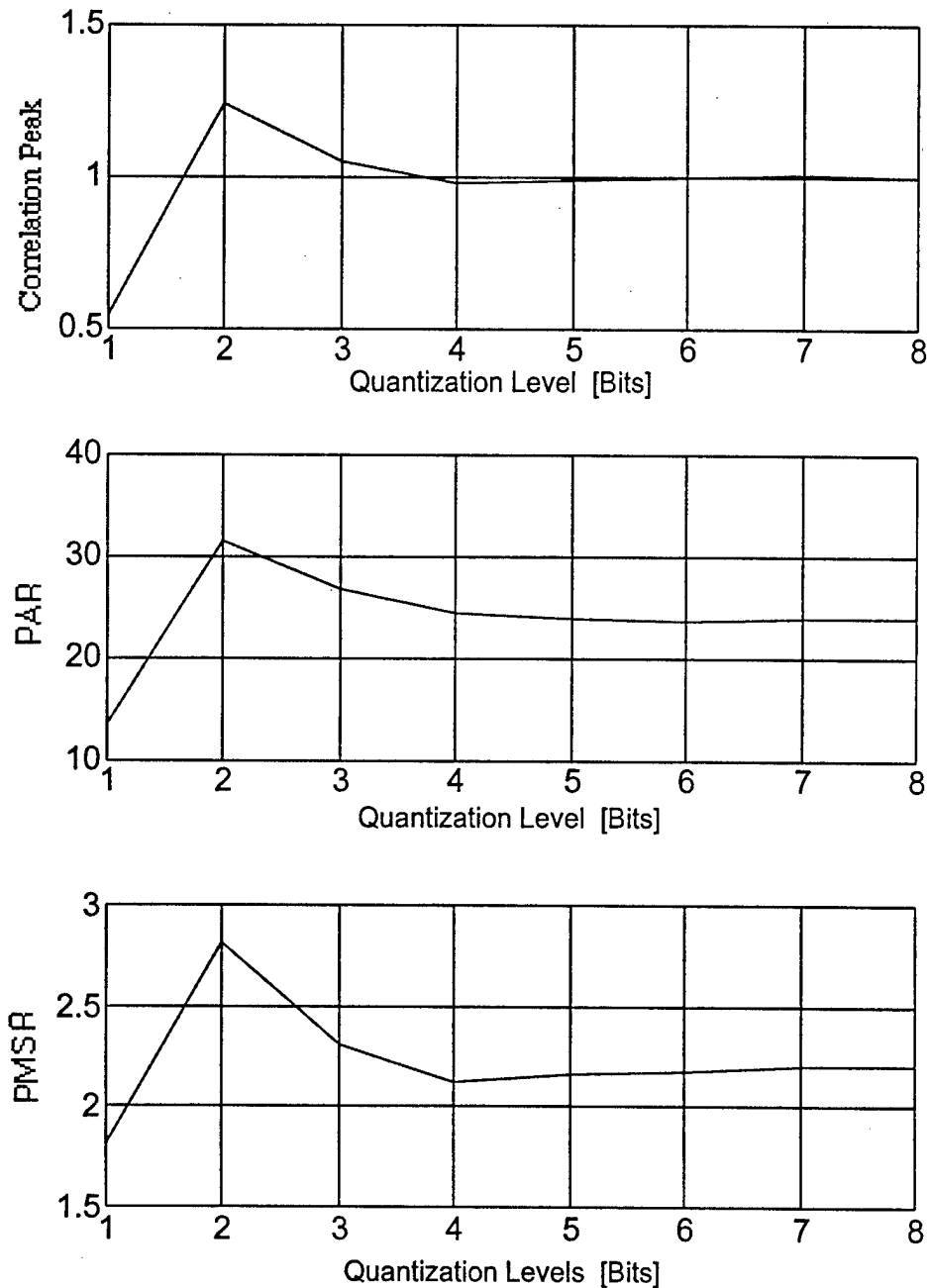


FIGURE 7.5. CORRELATOR PERFORMANCE MEASURES  
FOR QUANTIZED FILTER EXPERIMENT

The correlator performance measures resemble the correlation peak curve. The correlation peak in these experiments is not an accurate measure of the performance. It depends on the energy content of the input and filter patterns. Quantizing the filter biases the pattern, especially the binary case  $Q=2$ . The previous curves, Figure 7.4, show that as  $Q$  approaches eight PAR and PMSR converge to the continuous limit.

**7.4.1.2 Quantized Input Image.** In this series of experiments, the input image is quantized while the filter is either continuous or quantized. The input image is shown for the different quantization levels in Figure 7.6.

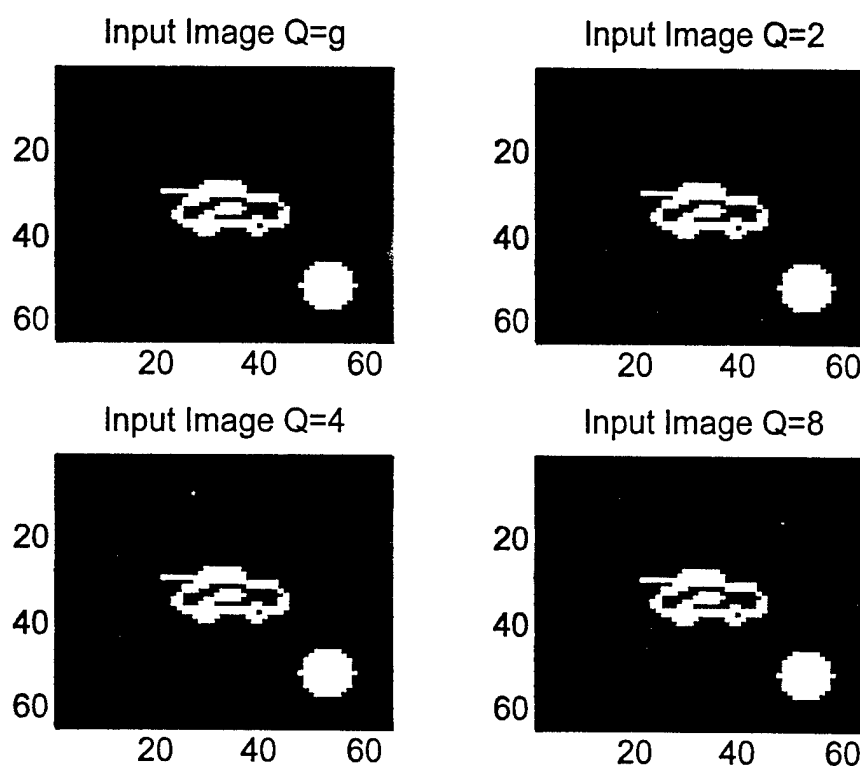


FIGURE 7.6. QUANTIZED INPUT IMAGES

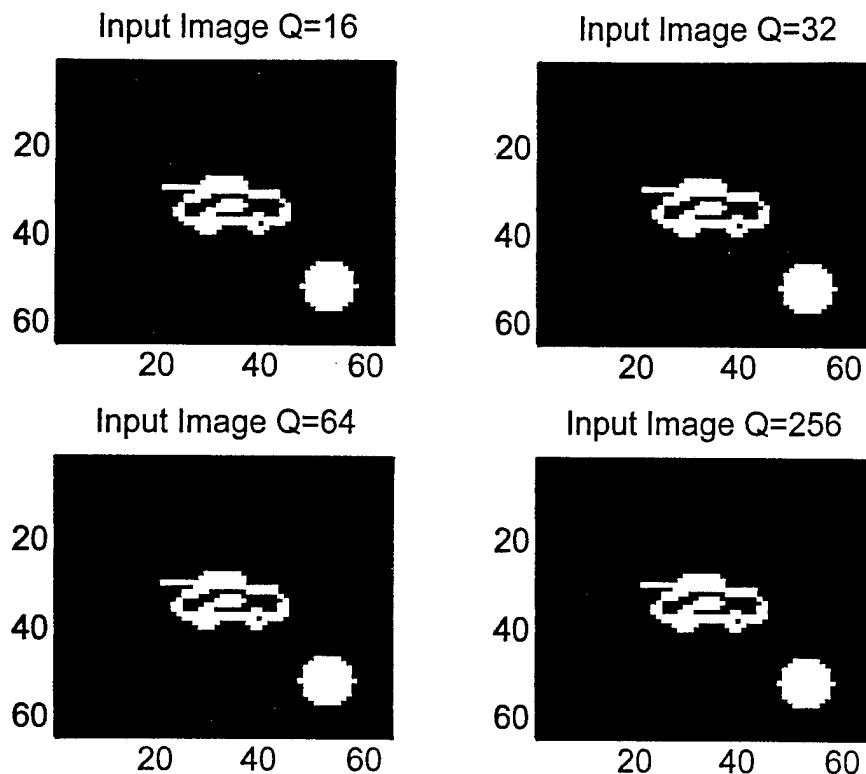


FIGURE 7.6. QUANTIZED INPUT IMAGES (CONTINUED)

The correlation pattern for the quantized input image using a continuous spatial filter is shown in Figure 7.7. The effect of the quantization is not as dramatic as for the case of quantizing the spatial filter, especially for the binary case. In Figure 7.7,  $Q_i$  and  $Q_c$  represent the quantization levels for the input image and the filter, respectively. Quantization of both the input image and the filter correlation patterns are shown in Figure 7.8 for a filter with  $Q=2$ . Clearly binarization of the filter results in unacceptable performance. The performance parameters, peak, PAR, and PMSR are shown in Figure 7.9. The correlation peak again increases for low values of  $Q$  due to the energy bias caused by the quantization. The PAR and PMSR both increase with the increase of the quantization level of the input image. PAR doubles as  $Q$  increases from two to eight, then it keeps increasing with a much slower rate. PMSR also increases with a higher rate for  $Q=2$  to 8. PAR and PMSR are a measure of the correlation peak sharpness and false target rejection, respectively.

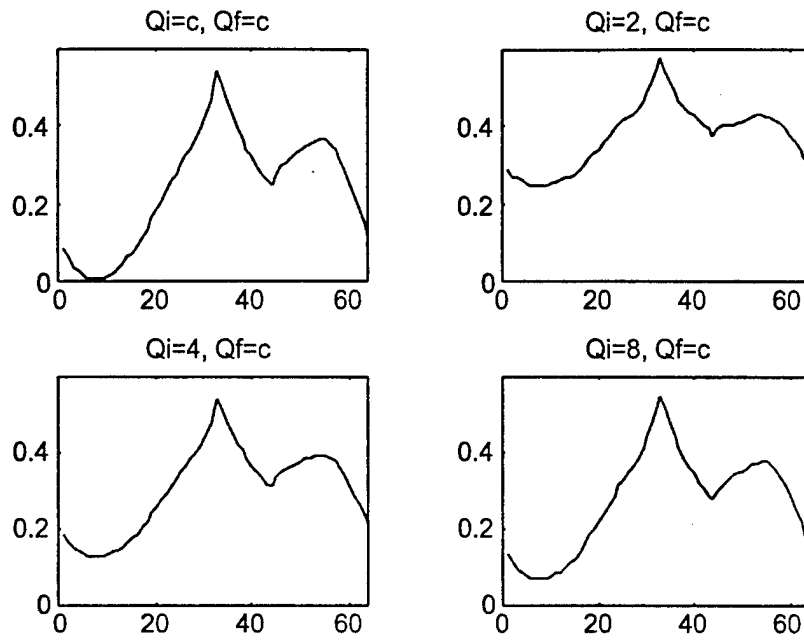


FIGURE 7.7. CORRELATION PATTERN FOR QUANTIZED INPUT IMAGE FOR DIFFERENT  $Q_i$ 's

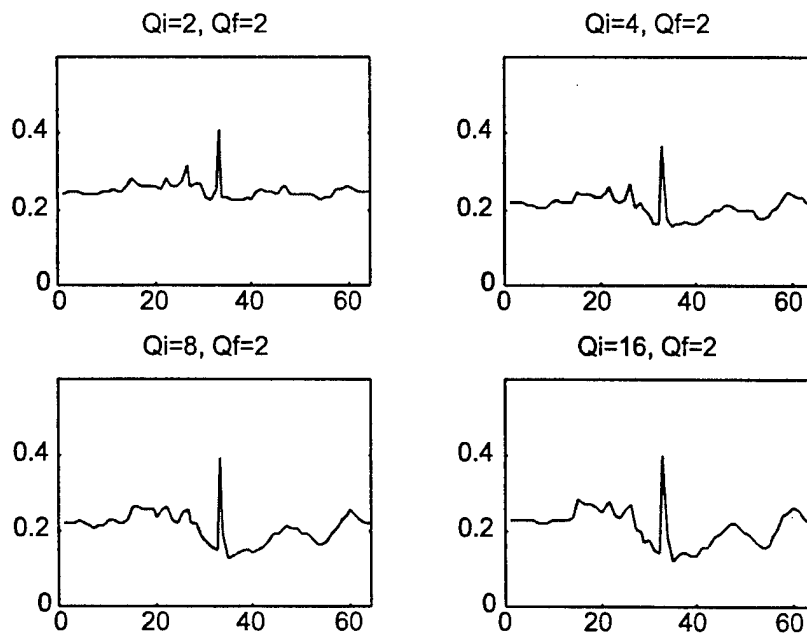


FIGURE 7.8. CORRELATION PATTERN FOR QUANTIZED INPUT IMAGE AND FILTER

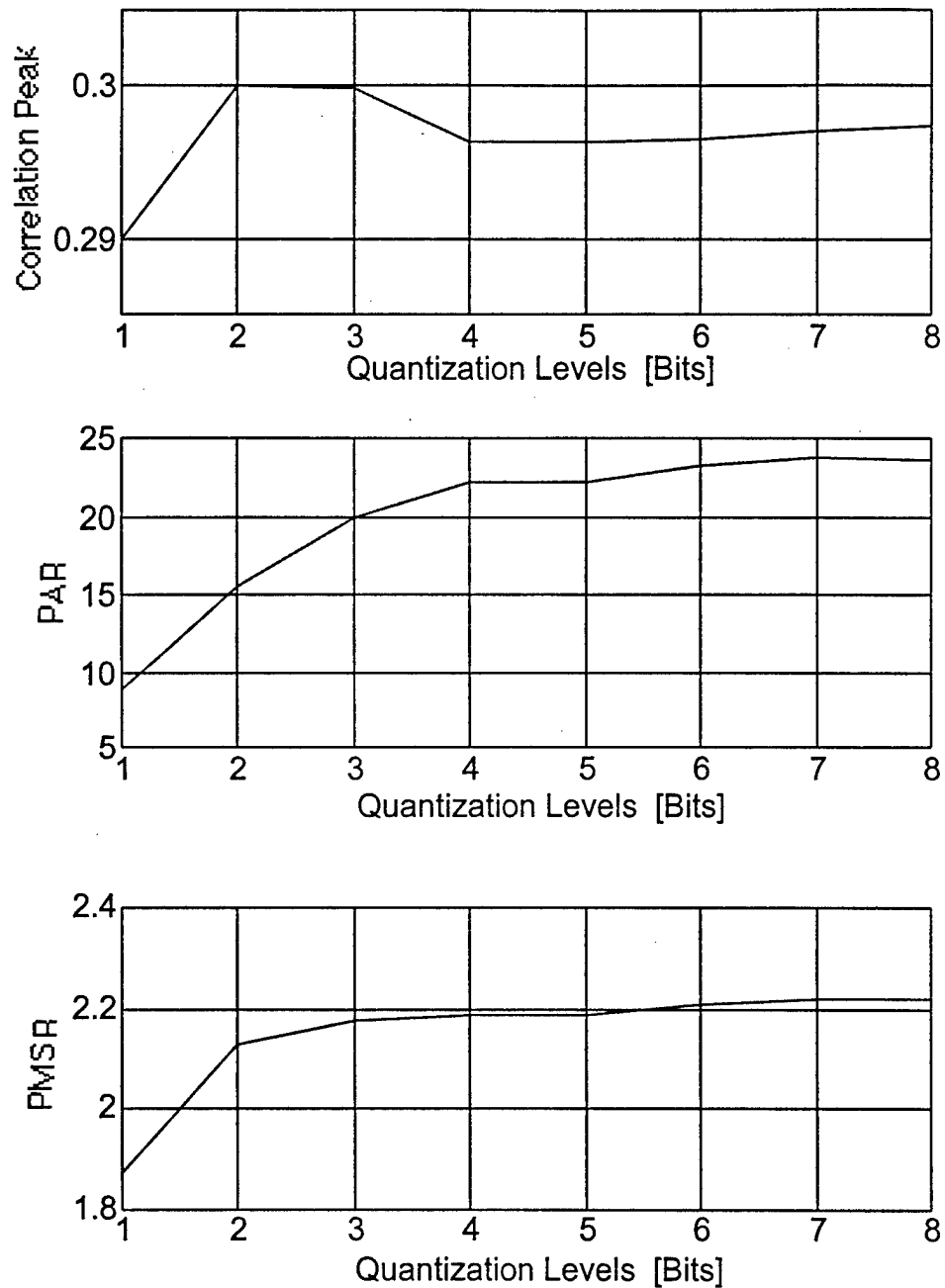


FIGURE 7.9. PERFORMANCE MEASURES FOR QUANTIZED INPUT IMAGE

Correlation patterns for a quantized input image and four-level quantized filter are shown in Figure 7.10. PAR and PMSR are shown in Figure 7.11, which shows the same results as before where about eight levels of quantization gives good results.

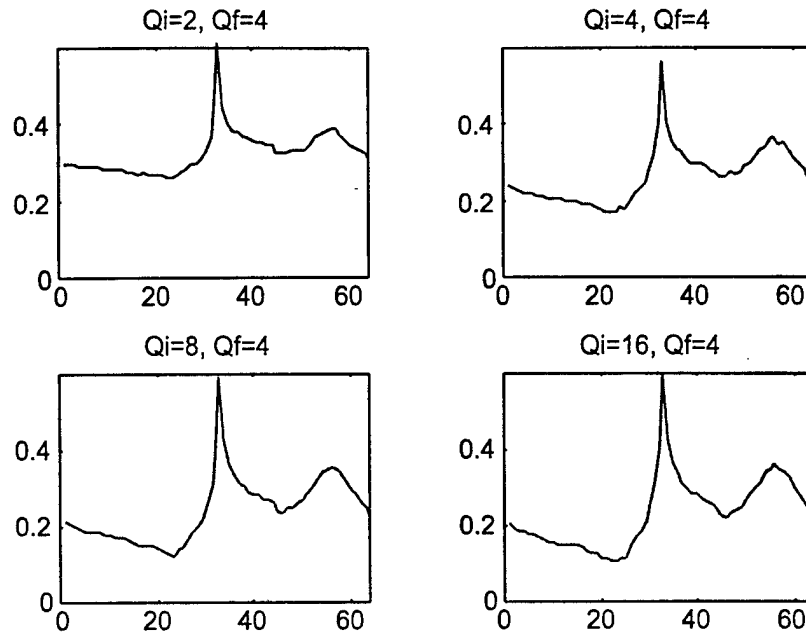


FIGURE 7.10. CORRELATION PATTERNS FOR QUANTIZED INPUT AND FILTER

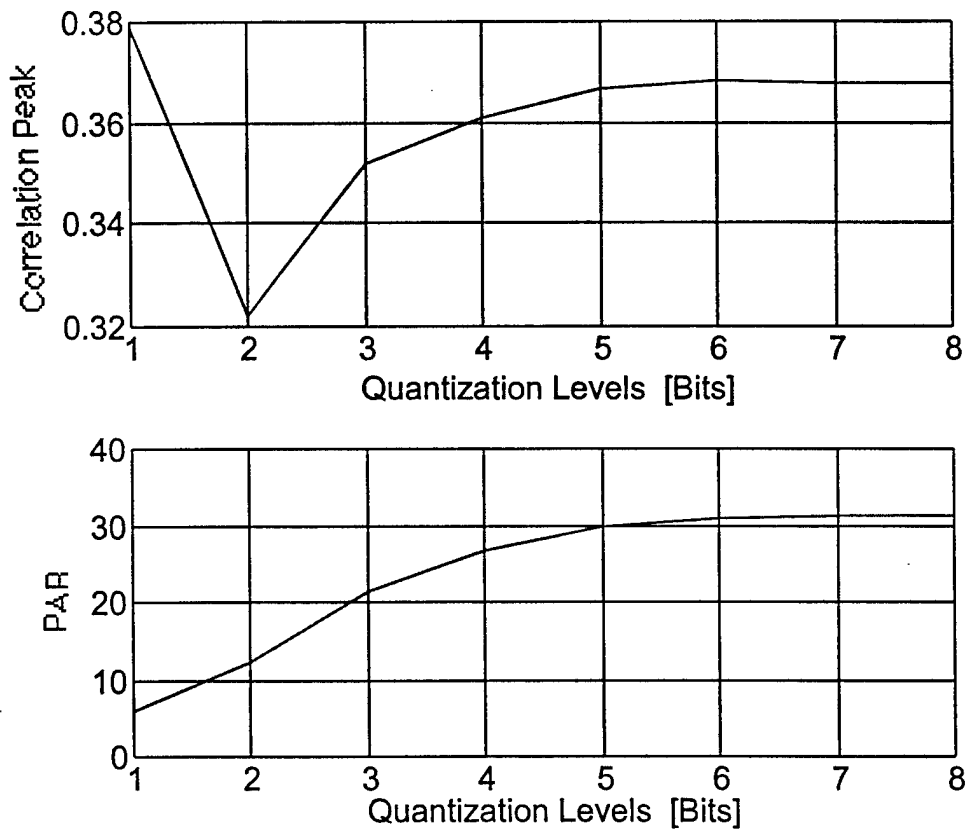


FIGURE 7.11. PERFORMANCE PARAMETERS



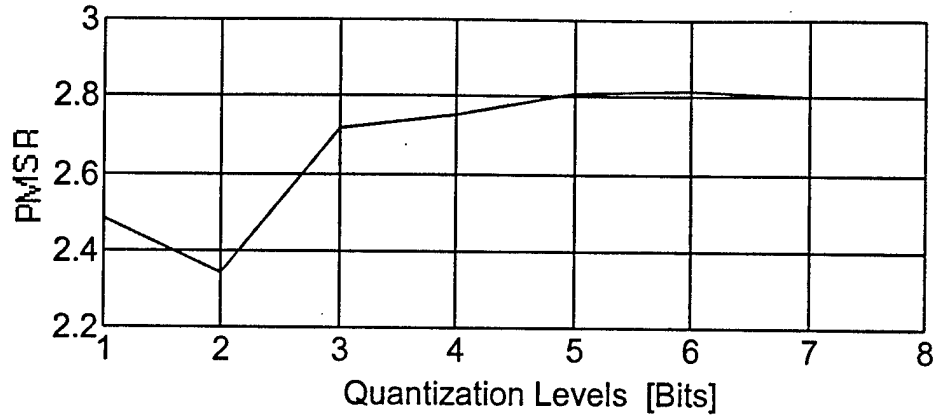


FIGURE 7.11. PERFORMANCE PARAMETERS (CONTINUED)

**7.4.1.3 Input Image Corrupted With Noise.** In the previous section for the numerical experiments, an image on a dark background and no noise were considered. In this section, the move will be away from the ideal situation to more of a practical one. By corrupting the input image with additive noise, a more realistic image can be created. The input image consists of positive numbers. The way the noisy input image is generated is as follows:

Let the input image be given by  $f(x,y)$ , the noisy input image by  $g(x,y)$ , and the additive noise signal by  $n(x,y)$ .  $n(x,y)$  is generated using a random number generator with Gaussian statistics with a zero mean and a variable standard deviation (STD). This noise signal contains both positive and negative numbers. The noisy image is given by

$$g(x,y) = |f(x,y) + n(x,y)| \quad (7.8)$$

Ten noise corrupted images were generated using 10 values for the STD of  $n(x,y)$ . These images will be referred to as  $g_1, g_2, g_3, \dots, g_{10}$ . The input SNR is defined as

$$SNR_i = \frac{\sqrt{E \{f^2(x,y)\}}}{\sqrt{E \{[g(x,y) - f(x,y)]^2\}}} \quad (7.9)$$

where  $E\{ \cdot \}$  denotes the expected value. The subtraction in the denominator is a pixel-by-pixel operation. The  $SNR_i$  associated with each of the noisy input signal is tabulated in Table 7.2.

TABLE 7.2.  $SNR_i$  FOR CORRUPTED IMAGES

Noise Signal	STD	Noisy input	$SNR_i$	$SNR_i$ [dB]
n1	1	g1	55.5	17.4
n2	10	g2	4.84	6.8
n3	20	g3	2.45	3.9
n4	30	g4	1.6	2
n5	40	g5	1.2	0.8
n6	50	g6	0.9387	-0.27
n7	100	g7	0.48	-3.2
n8	200	g8	0.24	-6.2
n9	500	g9	0.098	-10
n10	1000	g10	0.048	-13.2

The noise corrupted images  $g_i(x,y)$  are given in Figure 7.12, and are referred to as tmgn1 to tmgn10. The target can still be visually recognized until tmgn7, where the SNR is -3.2 dB.

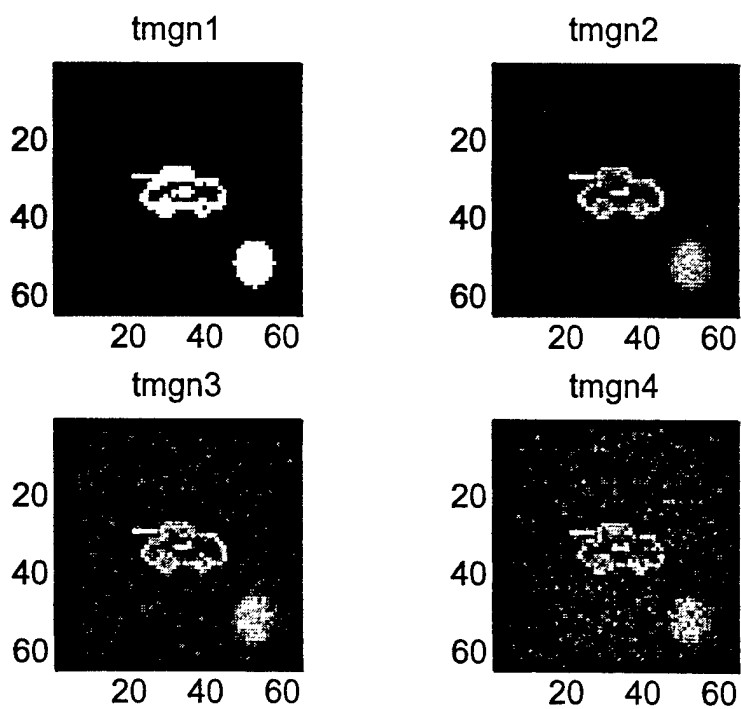


FIGURE 7.12. NOISE CORRUPTED INPUT SCENE

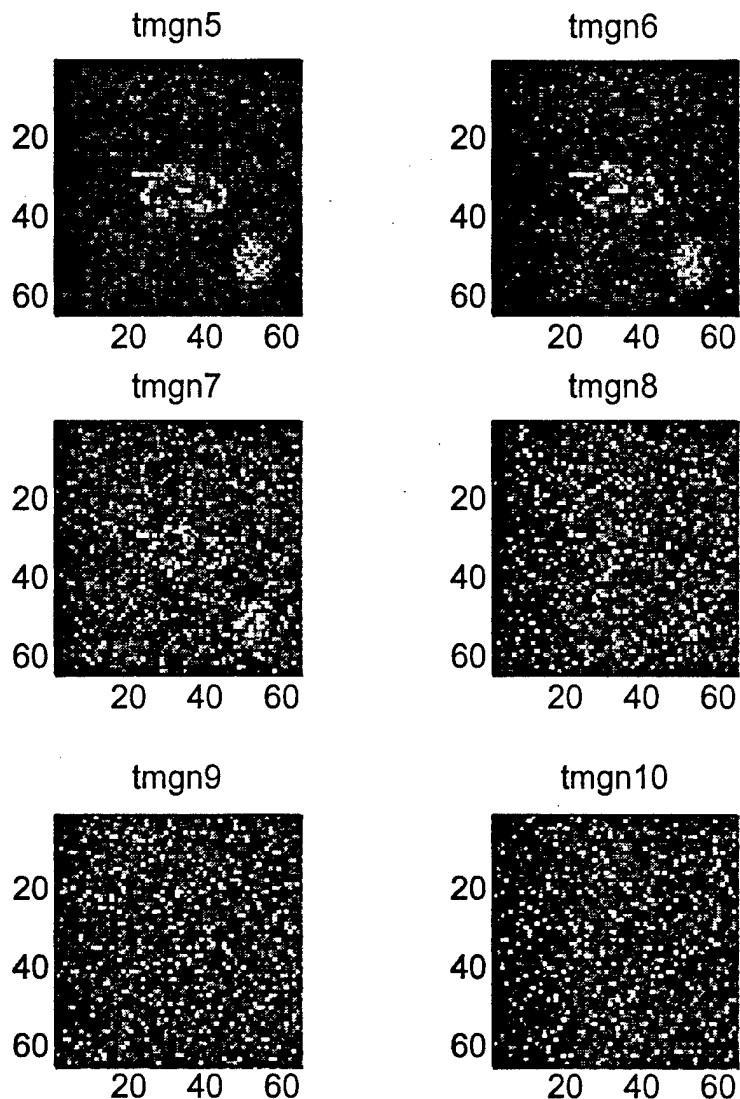


FIGURE 7.12. NOISE CORRUPTED INPUT SCENE (CONTINUED)

A complex matched filter was generated for the target  $t(x,y)$  and used in the optical correlator. The correlation was performed between each noisy input and the target,  $t(x,y)$ . The correlation pattern is shown in Figure 7.13. For each correlation, a plot of the maximum intensity along each column (y-axis) of the pattern is plotted below it. The pattern of the correlation between  $g_1(x,y)$  and  $t(x,y)$  (indicated as  $tmgn1**t$  in the figure) shows a strong correlation peak at the center where the target is located and a minor peak where the circular object is located. From the plots in Figure 7.13, as the input SNR decreases, the background noise in the correlation pattern increases along with the power of the false target (circular object). The peak can still be recognized in the plot up to  $tmgn8**t$ ; i.e.,  $SNR_i = -6.2$  dB. Scenes with lower  $SNR_i$  are nothing but noise and the correlator fails to detect the target.

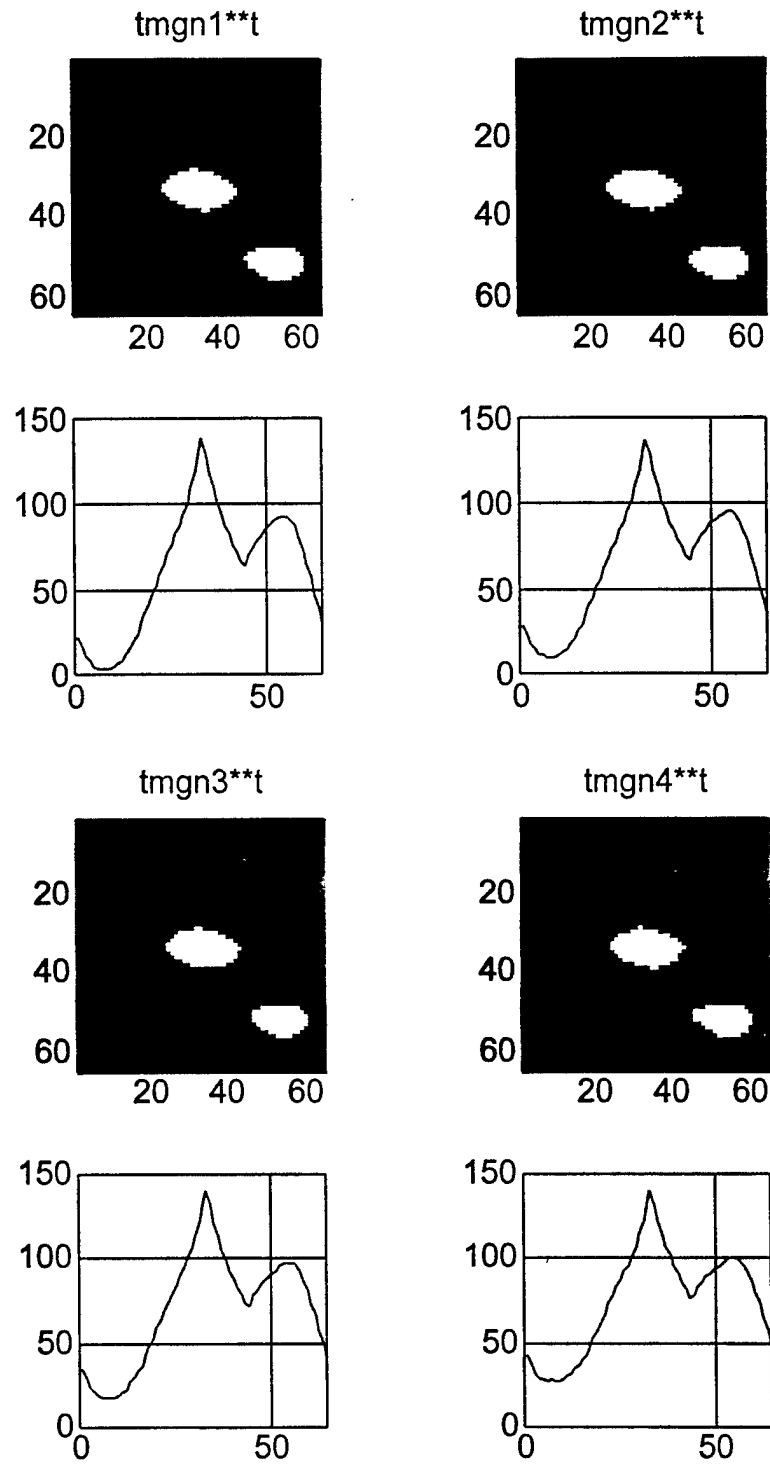


FIGURE 7.13. CORRELATION PATTERN OF NOISY INPUTS WITH TARGET

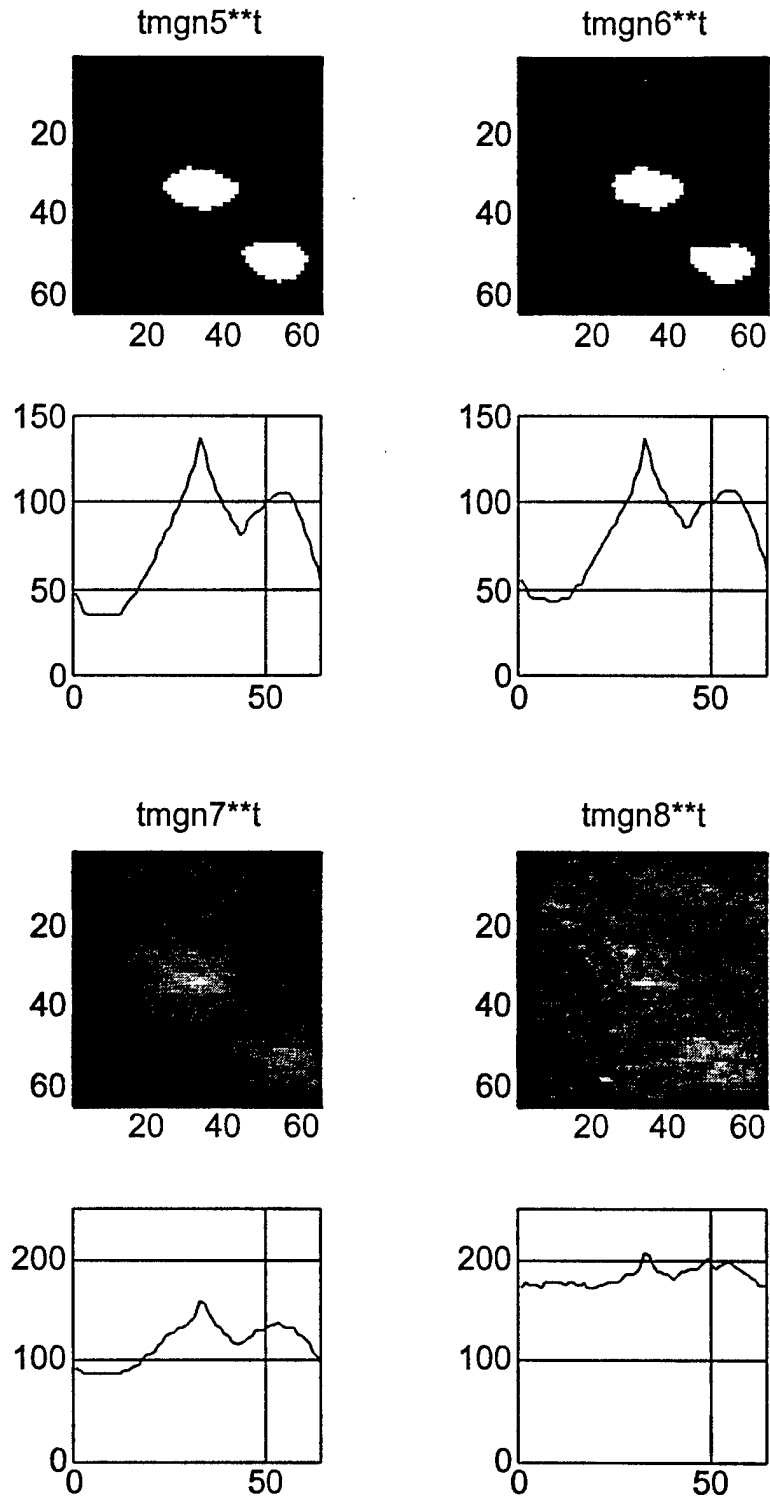


FIGURE 7.13. CORRELATION PATTERN OF NOISY INPUTS WITH TARGET (CONTINUED)

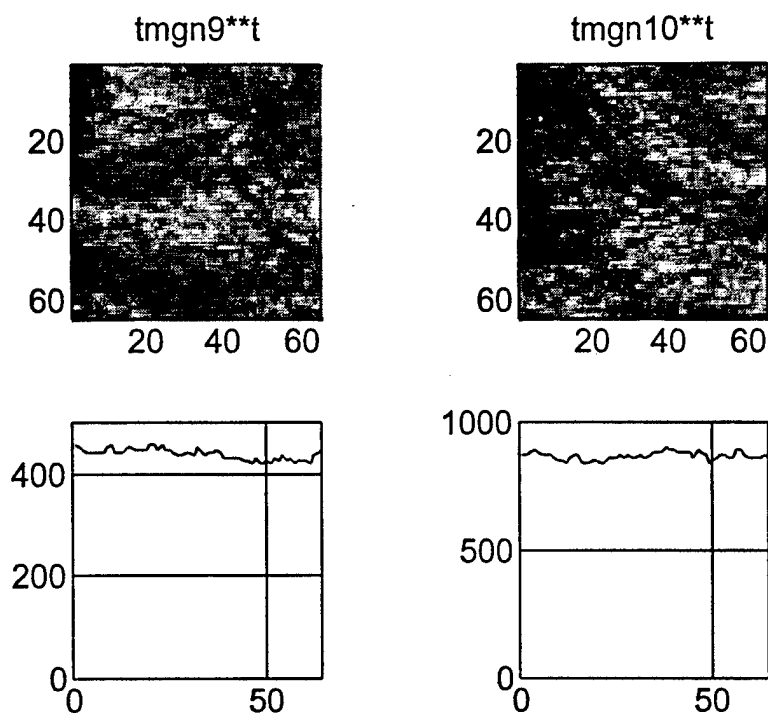
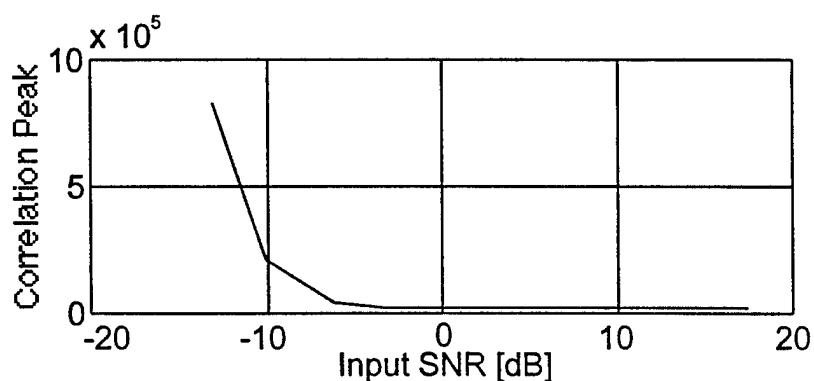
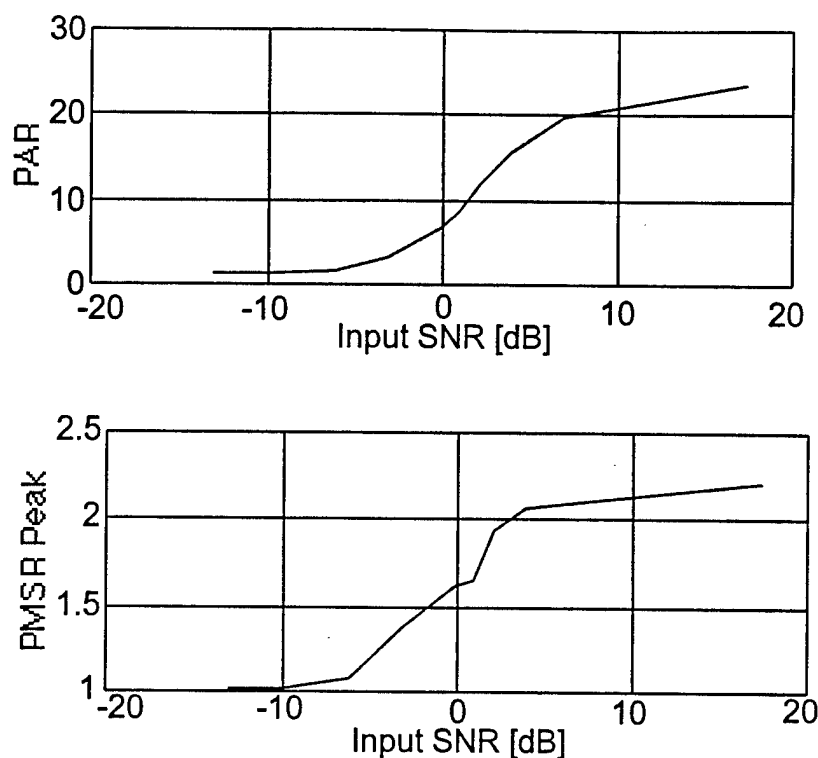


FIGURE 7.13. CORRELATION PATTERN OF NOISY INPUTS WITH TARGET (CONTINUED)

Correlator performance parameters are shown in Figure 7.14. The correlation peak is higher for low SNRs because of the increase in the input scene energy contributed by the high noise level. The PAR increases as the  $\text{SNR}_i$  increases; i.e., the correlation peak gets sharper by the increase of the  $\text{SNR}_i$ . The PMSR, also increases with increasing  $\text{SNR}_i$ . This increase lowers the probability of false alarm.

FIGURE 7.14. PERFORMANCE PARAMETERS AS A FUNCTION OF  $\text{SNR}_i$

FIGURE 7.14. PERFORMANCE PARAMETERS AS A FUNCTION OF  $\text{SNR}_i$  (CONTINUED)

The next set of experiments uses the correlator with a BPOF. Correlation patterns are shown in Figure 7.15 in the same format as that in Figure 7.13. The correlation peaks are much sharper than those for the matched filter results. The sidelobe peak is also much smaller for this case. The matched filter showed slightly better detection for higher noise levels, as in the case for *tmgn8*, otherwise the performance of the BPOF system is far better. The performance parameters are plotted in Figure 7.16. The correlation peak, as before, is larger for low  $\text{SNR}_i$ . The PAR increases rapidly with the increase of the  $\text{SNR}_i$ . It is almost an order of magnitude larger than the PAR results for the matched filter case. The PMSR shows similar results as the PAR. Both of these measures confirm the evidence shown in Figure 7.15 of the sharper correlation peak.

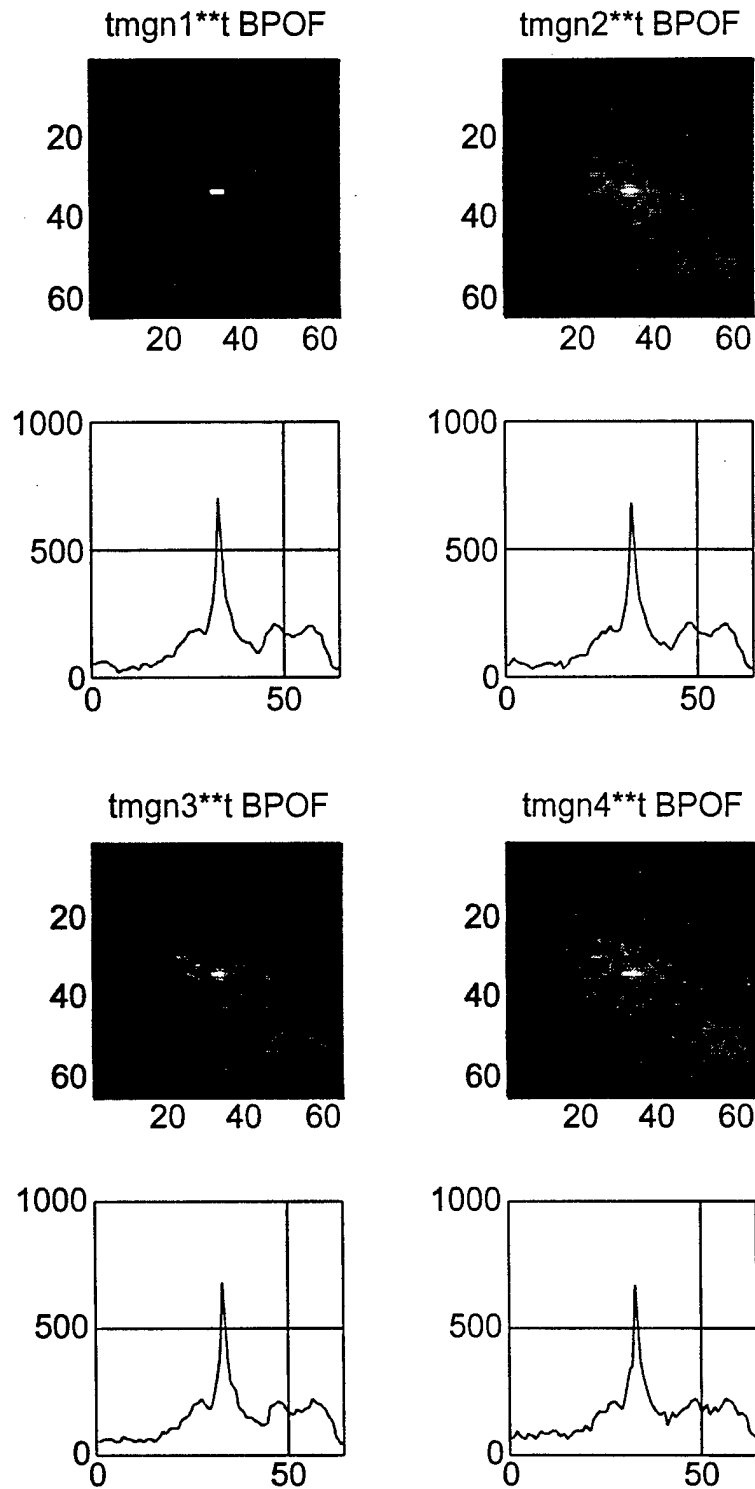


FIGURE 7.15. CORRELATION PATTERNS FOR NOISY INPUT SCENE USING A BPOF



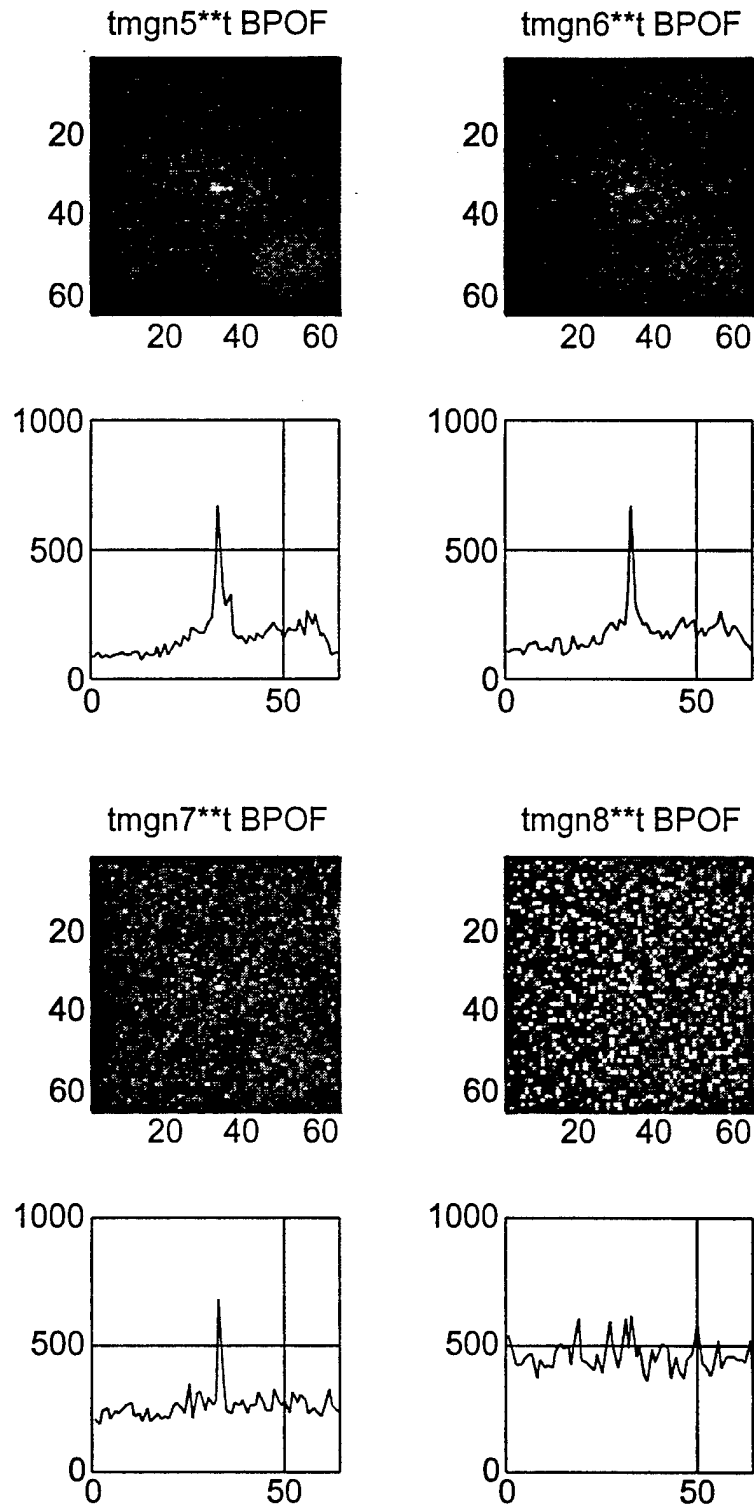


FIGURE 7.15. CORRELATION PATTERNS FOR NOISY INPUT SCENE USING A BPOF (CONTINUED)

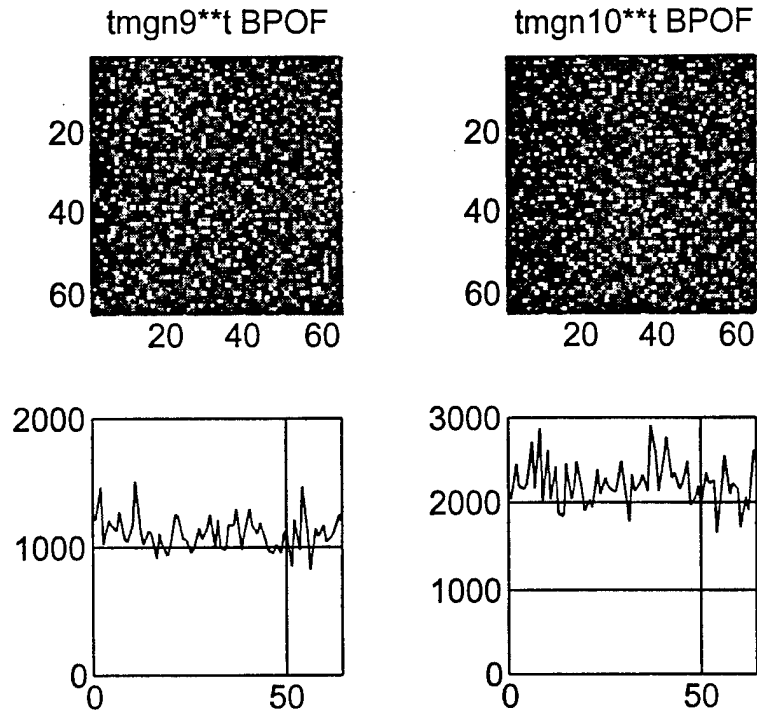


FIGURE 7.15. CORRELATION PATTERNS FOR NOISY INPUT SCENE USING A BPOF (CONTINUED)

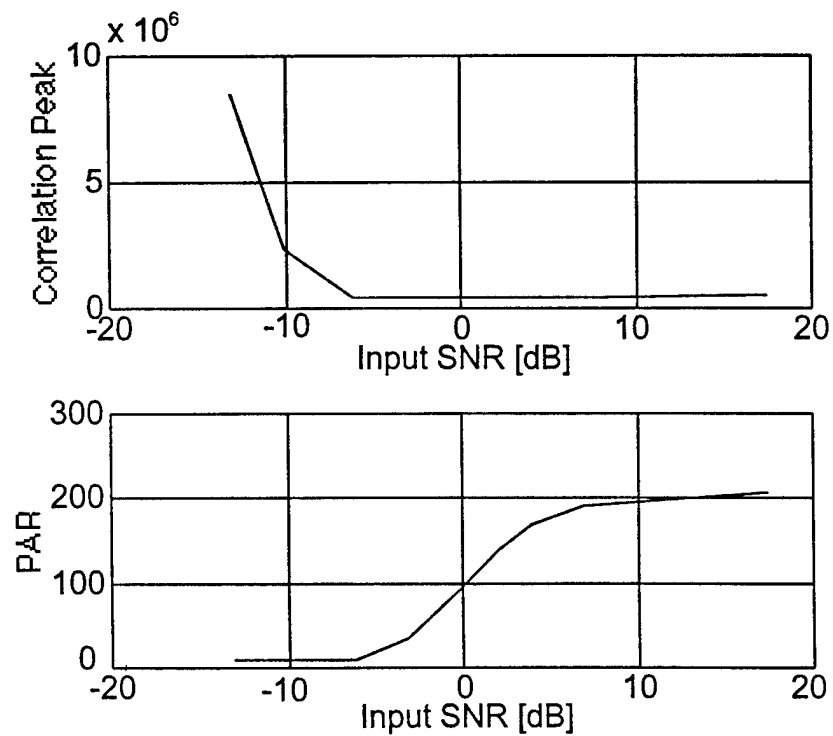


FIGURE 7.16. PERFORMANCE PARAMETERS FOR NOISY INPUT AND BPOF

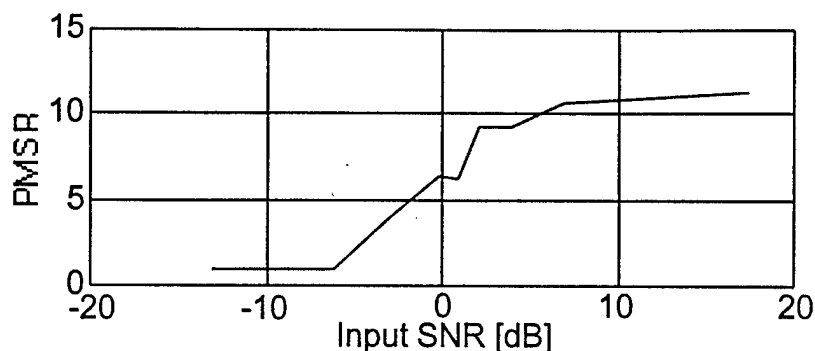


FIGURE 7.16. PERFORMANCE PARAMETERS FOR NOISY INPUT AND BPOF (CONTINUED)

7.4.1.4 Quantization of Noise Corrupted Input. In the previous section, the input is assumed to be represented optically in a continuous fashion. As mentioned before, this is not realistic because of the limitations of the SLMs available. In this section, the affect of the binarization of the input image on the correlator performance is studied.

In Figure 7.17, the binarized version of noise corrupted input images is given for the range of SNR used in the previous section. When the SNR<sub>i</sub> is less than zero, it becomes difficult if not impossible to visually detect the target.

In Figure 7.18, the correlation patterns are given both as intensity distribution and plots of the maximum value along each column in the pattern. The background noise bias is high even for large SNRs. This makes the capability of detecting the correlation peak and thresholding difficult. This is reflected in the plots for the PAR and PMSR given in Figure 7.19.

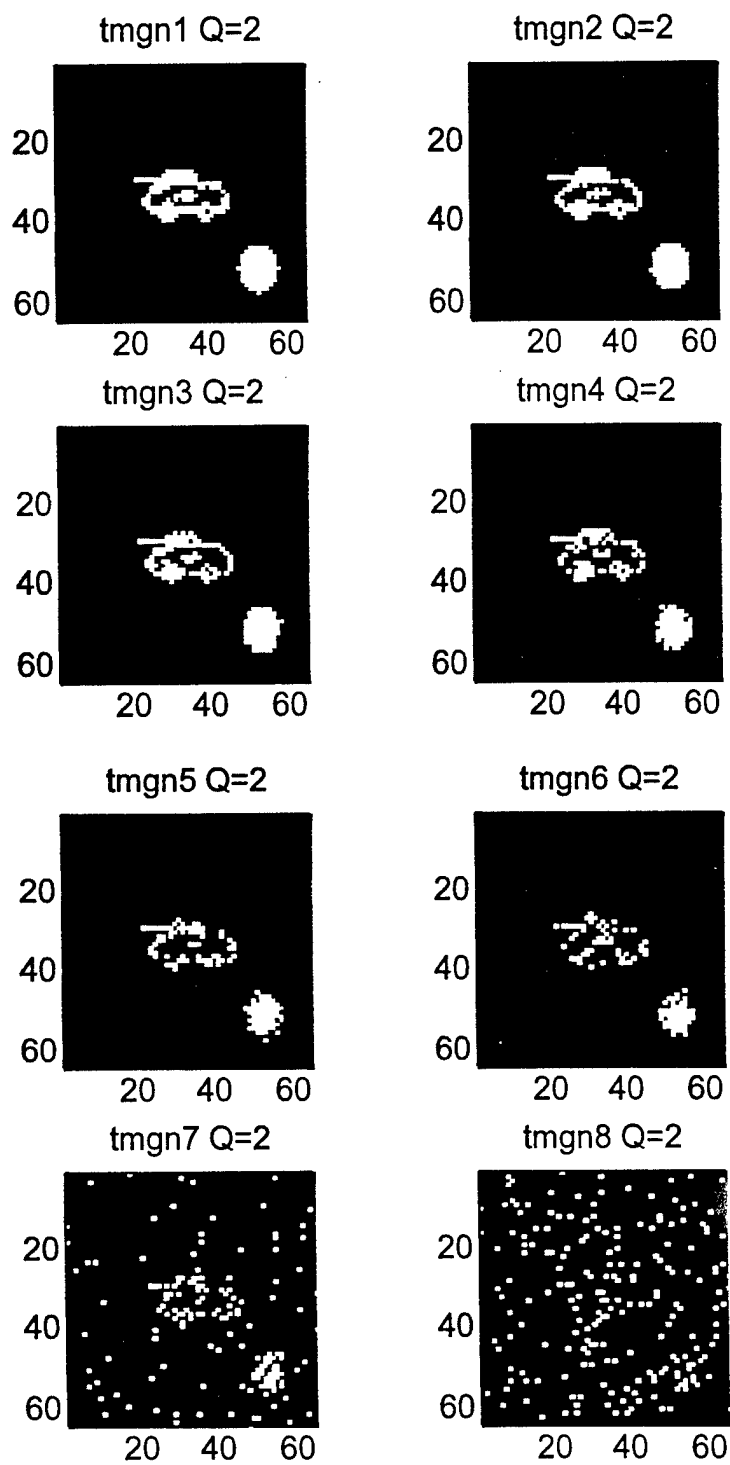


FIGURE 7.17. BINARIZED NOISY INPUT SCENE

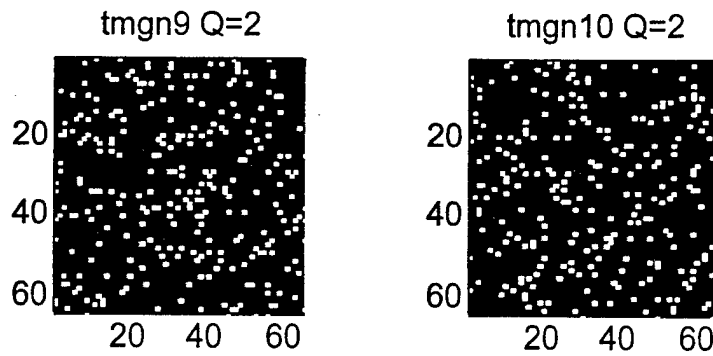


FIGURE 7.17. BINARIZED NOISY INPUT SCENE (CONTINUED)

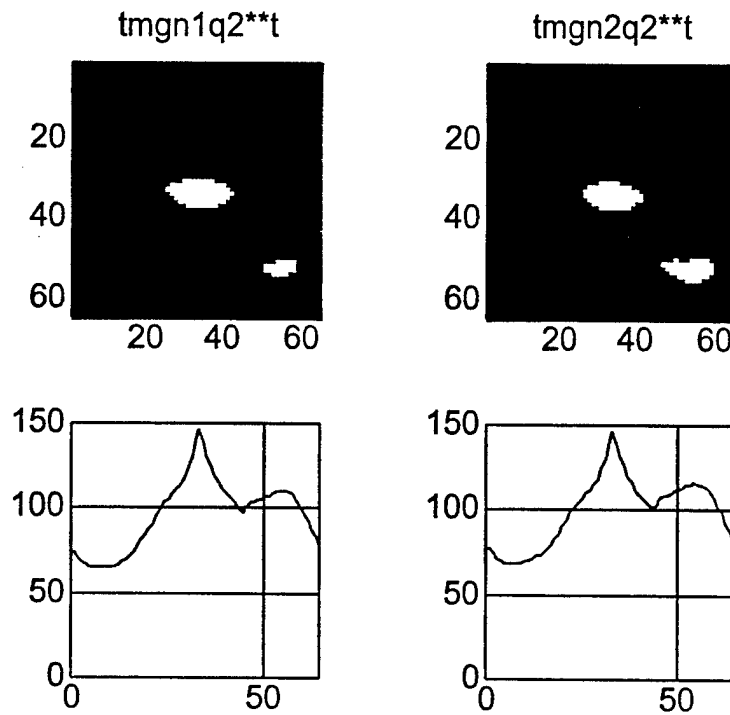


FIGURE 7.18. CORRELATION PATTERNS FOR BINARIZED NOISY INPUT SCENE USING A CMF

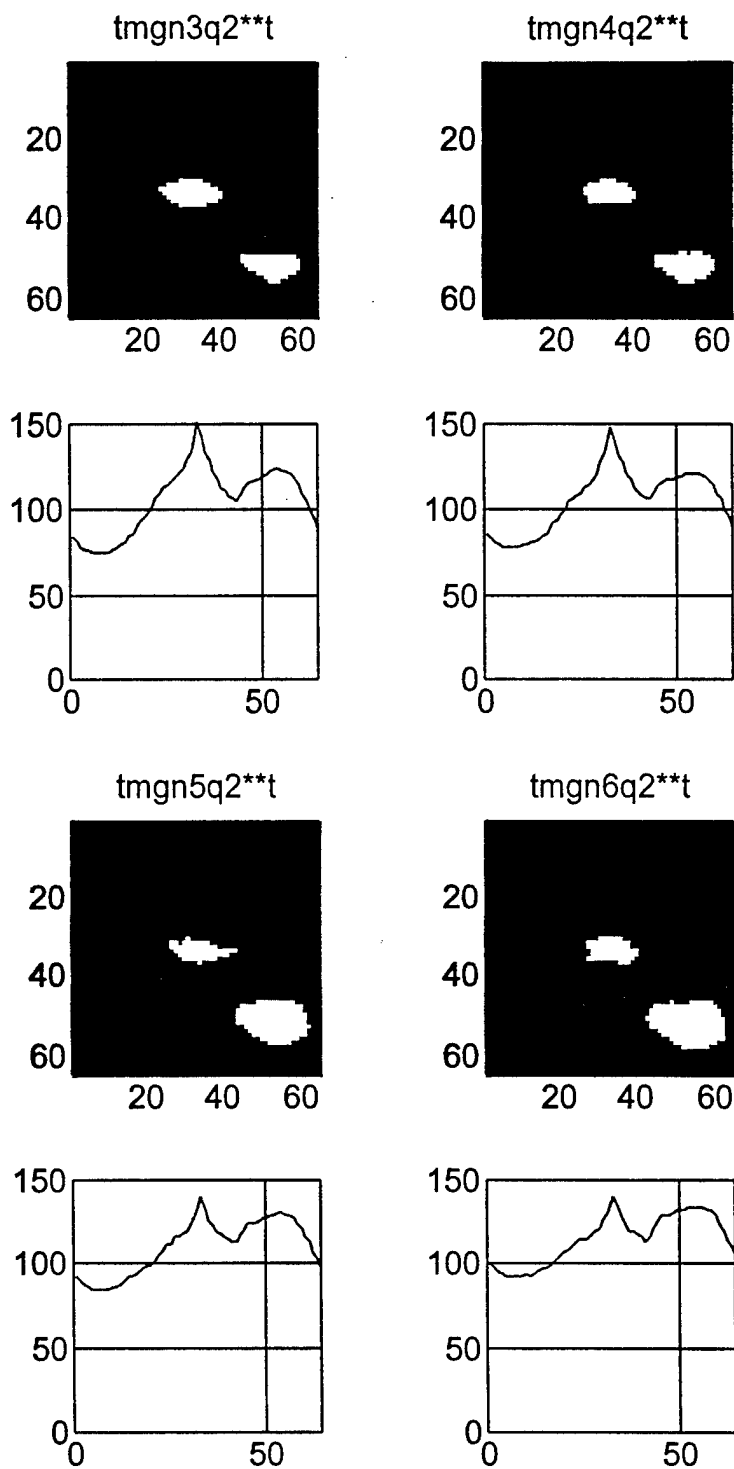


FIGURE 7.18. CORRELATION PATTERNS FOR BINARIZED NOISY INPUT SCENE USING A CMF (CONTINUED)

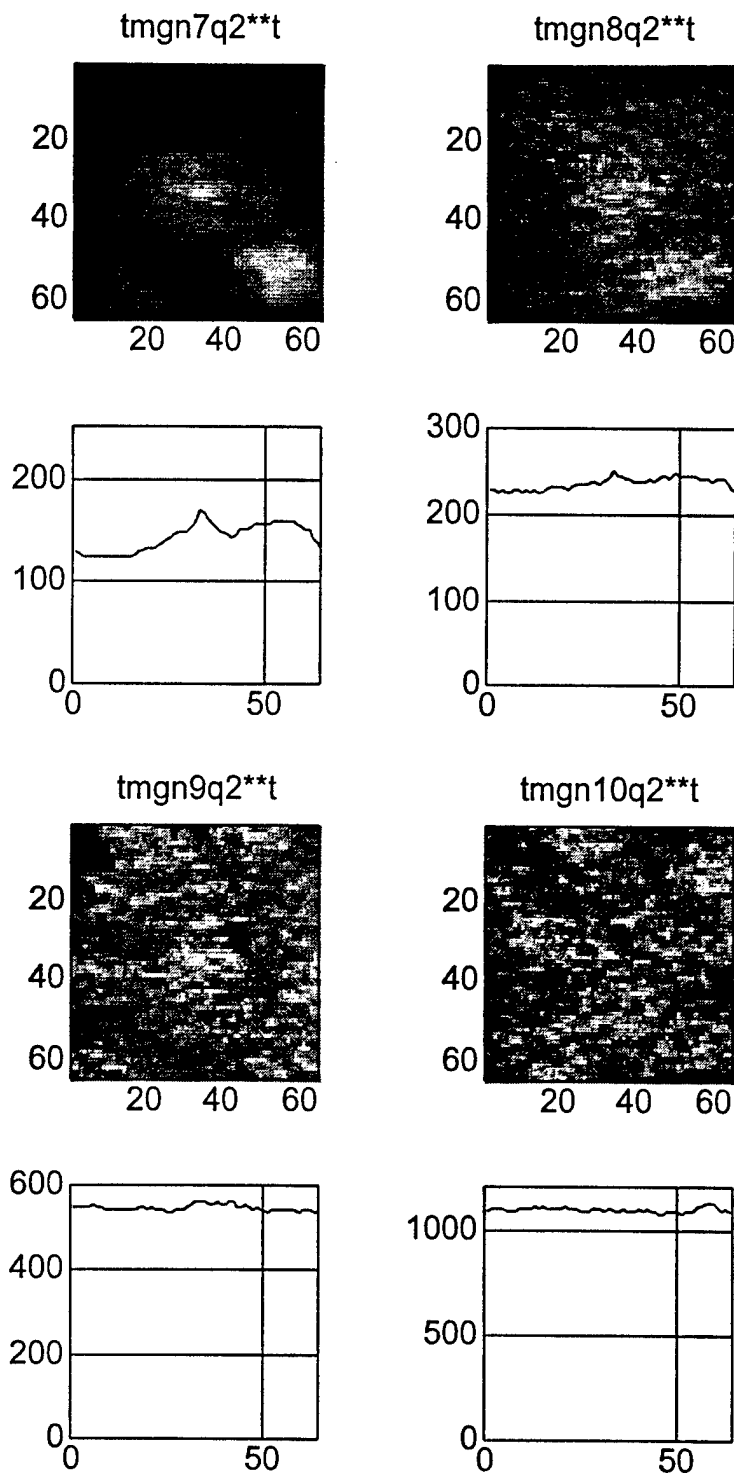


FIGURE 7.18. CORRELATION PATTERNS FOR BINARIZED NOISY INPUT SCENE USING A CMF (CONTINUED)

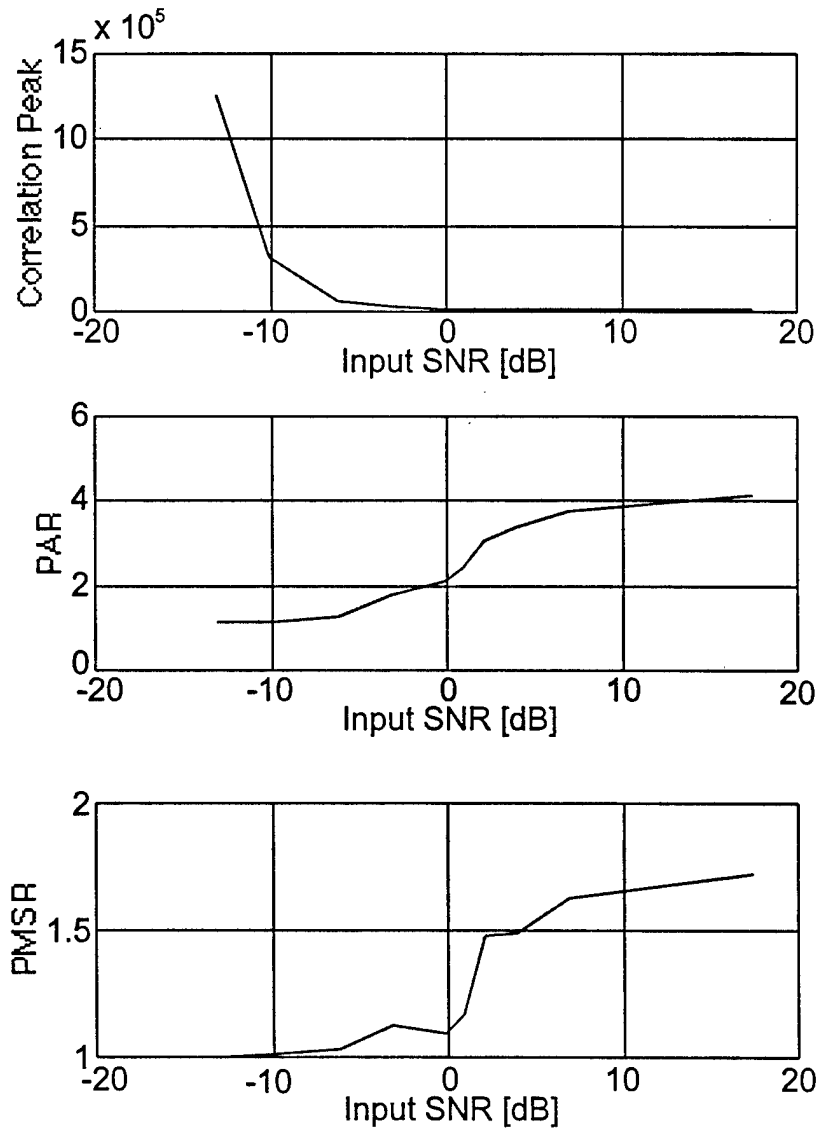


FIGURE 7.19. PERFORMANCE PARAMETERS FOR  
BINARIZED NOISY INPUT AND CMF



#### 7.4.2 Experimentally Collected Target Data

This section studies the correlator performance for detecting a target in images experimentally collected. In these scenes, the target is present in different environments and backgrounds. The target's statistics are given in Appendix B. The targets have a somewhat spherical shape and are darker than the background. Both large and small targets might appear in a scene. In the same image, there is the possibility of the existence of more than one target and also partial targets. For this test, six images are considered and are labeled as: b1, b7, d1, d2, w1, and w2. The images are shown in Figure 7.20. The images are all in 128x128 pixel format with 256 gray levels. In Figure 7.21 each of the images is shown along with a plot of a line scan along one or more targets. As an example, image b1 is shown along with a plot of the intensity along line 95 and is labeled as b1(95), similar scans are done for the other images.

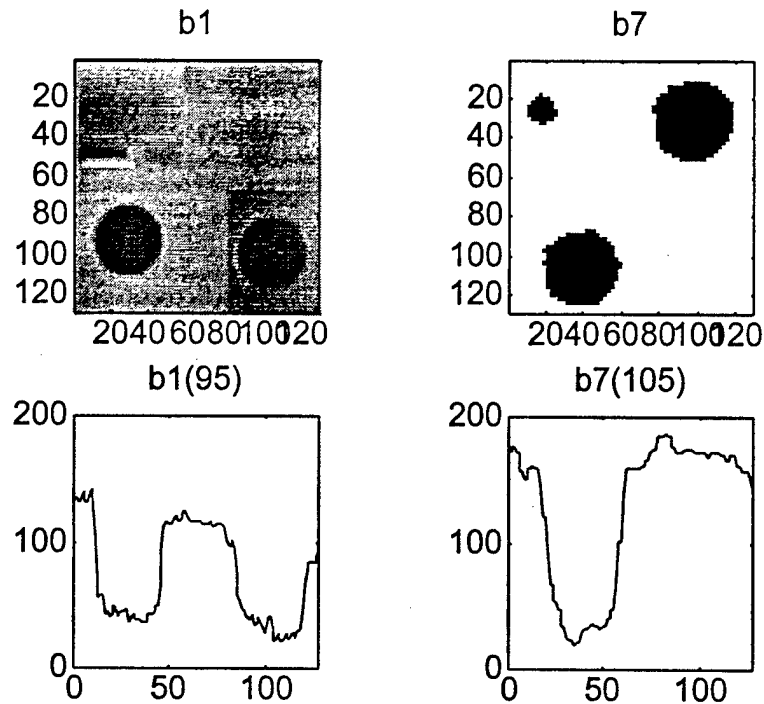


FIGURE 7.20. EXPERIMENTALLY COLLECTED IMAGES

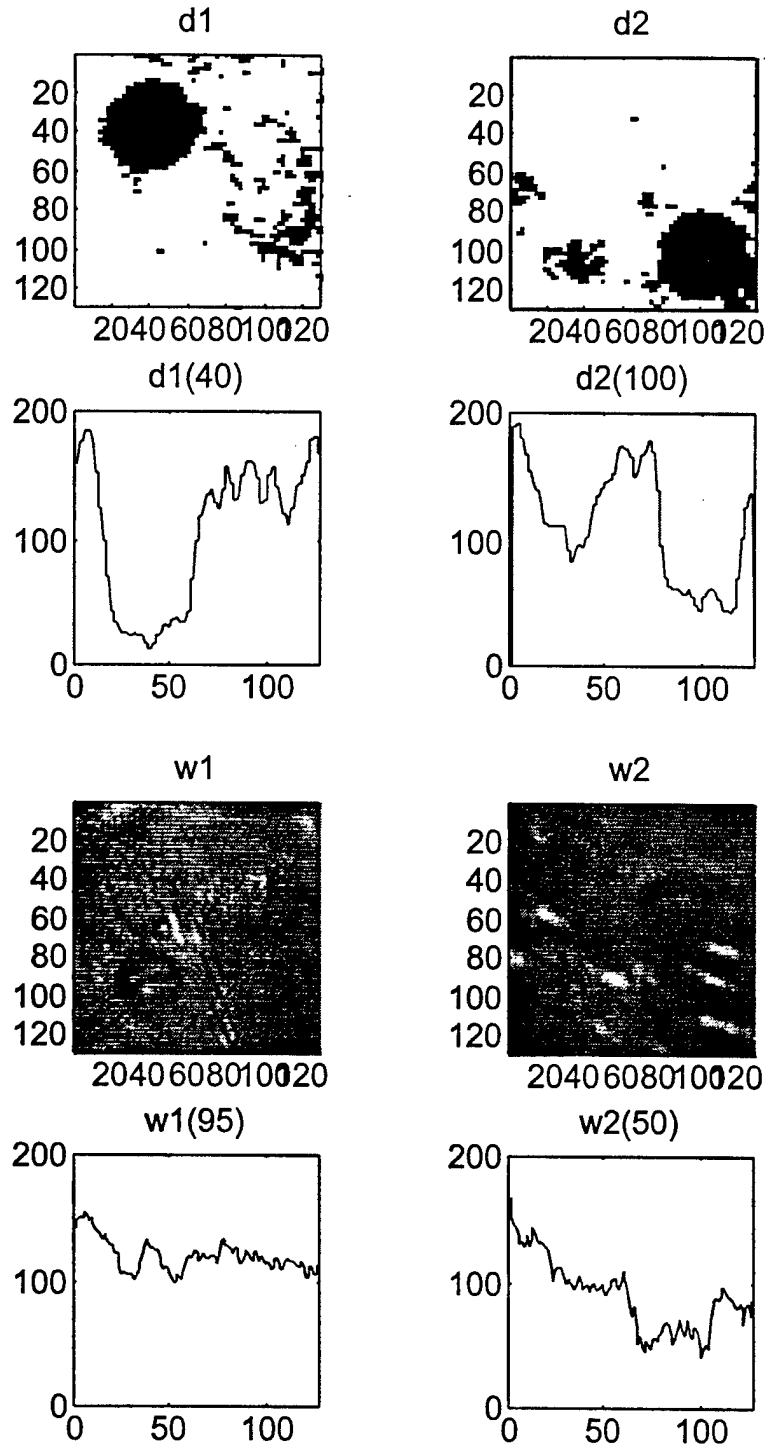


FIGURE 7.20 EXPERIMENTALLY COLLECTED IMAGES (CONTINUED)

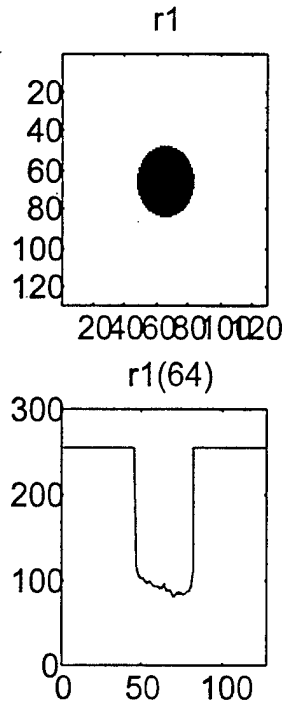


FIGURE 7.21. REFERENCE TARGET IMAGE

**7.4.2.1 Continuous Input Image.** A matched filter was computed for the reference target image and used in the computer simulation to detect the targets shown in Figure 7.20. The autocorrelation of the target is given in Figure 7.22 and it shows a sharp correlation peak. The intensity pattern of the cross correlations between the six input images and the target is given in Figure 7.23. Each cross-correlation intensity pattern is accompanied by a plot of the maximum value along each column of the pattern. In the image b1, there are two targets that are clear, while there is one faded target in the upper left corner. The correlation pattern of b1\*\*t has two strong correlation peaks, which are evident in the plots, and a weak peak appears in the upper left corner, which might be difficult to see in the printout because of the printer limitations. Scene b7 has two standard targets and a smaller target in the upper left corner. The correlation pattern for b7 shows the three correlation peaks, with the peak indicating the smaller target having less energy. Scenes d1, d2, and w2 each has only one target and the corresponding correlation pattern has one peak at the proper locations of the targets. Scene w1 has a full target and a partial target. The correlation pattern has two peaks at the proper locations of the targets.

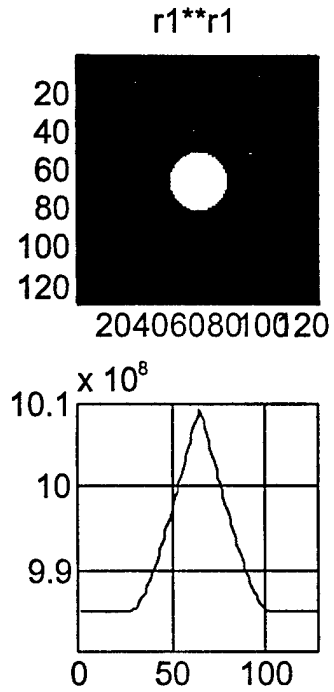


FIGURE 7.22. AUTOCORRELATION PATTERN OF TARGET

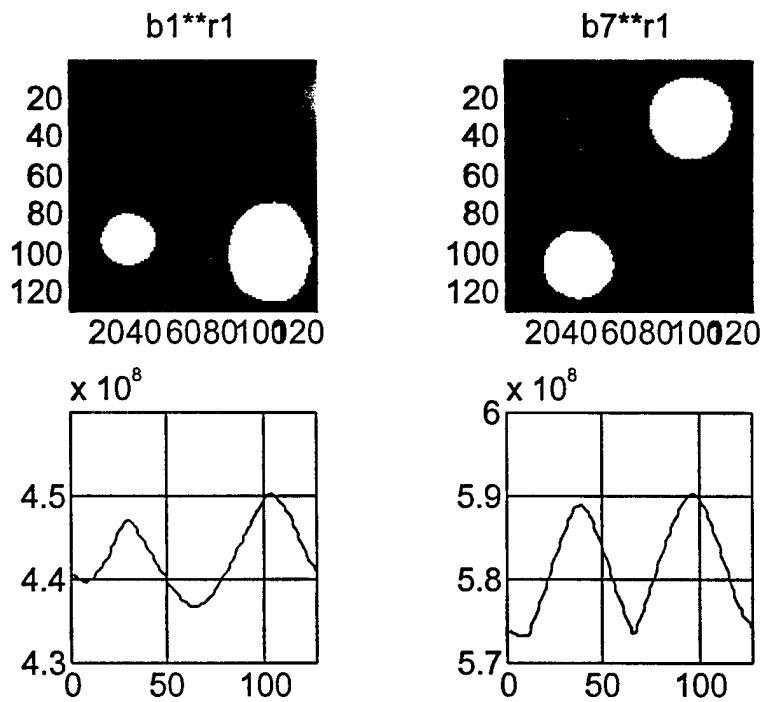


FIGURE 7.23. CROSS-CORRELATION OF INPUT SCENES WITH TARGET

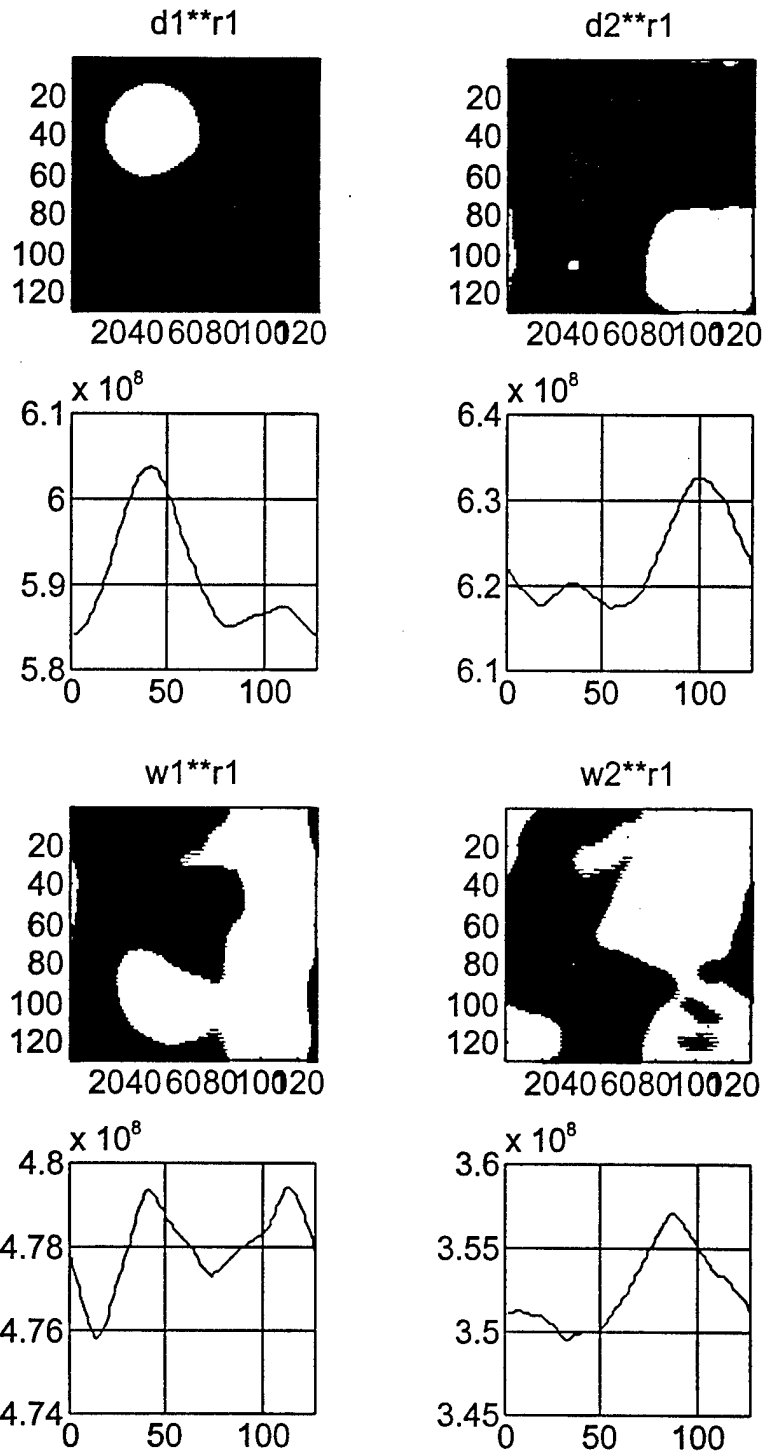


FIGURE 7.23. CROSS-CORRELATION OF INPUT SCENES WITH TARGET (CONTINUED)

The correlator performance measures were computed and tabulated in Table 7.3. The values for PAR and PMSR are not high because of high background noise. These values can be improved by postprocessing techniques.

TABLE 7.3. CORRELATION PERFORMANCE FOR MATCHED FILTER

Parameter	l**r1	b1**r1	b7**r1	d1**r1	d2**r1	w1**r1	w2**r1
Peak x1.0e+06	1.0191	0.2028	0.3485	0.3645	0.4003	0.2298	0.1275
PAR	1.0469	1.0567	1.0604	1.0652	1.0523	1.0099	1.0430
PMSR	1.0095	1.0046	1.0047	1.0036	1.0028	1.0001	1.0033

Next a POF of the target was used. The correlation results of such are shown in Figures 7.24 and 7.25. The autocorrelation peak is strong as expected and is much sharper than for the CMF. The cross-correlation patterns of the six scenes with the target are shown in Figure 7.25. The targets in b1, b2, and d1 are detected by the system, as indicated by the strong correlation peaks, except for the faded target in b1. The system failed to detect the target in d2, w1, and w2 scenes.

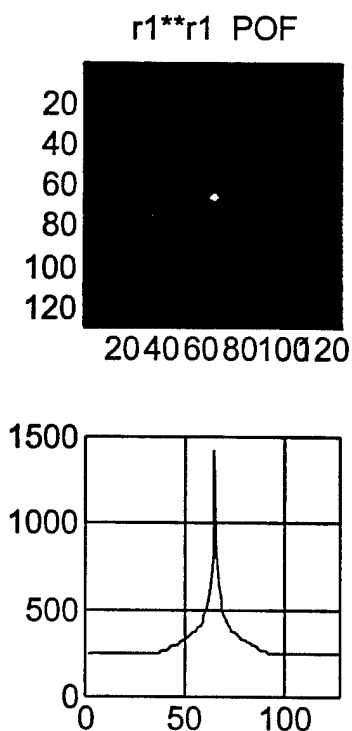


FIGURE 7.24. AUTOCORRELATION OF TARGET USING POF

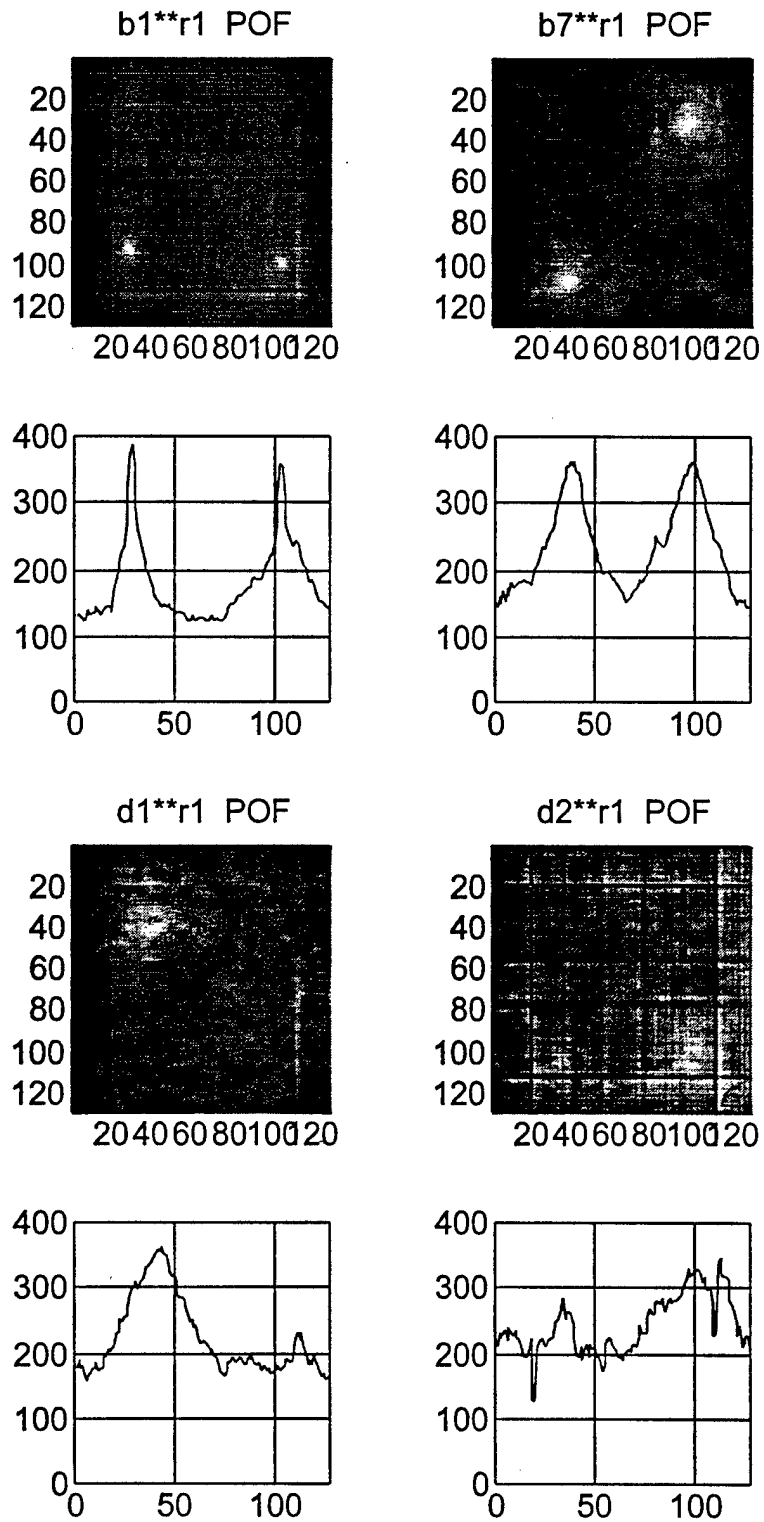


FIGURE 7.25. CROSS-CORRELATION INTENSITY PATTERNS FOR INPUT SCENES WITH TARGET

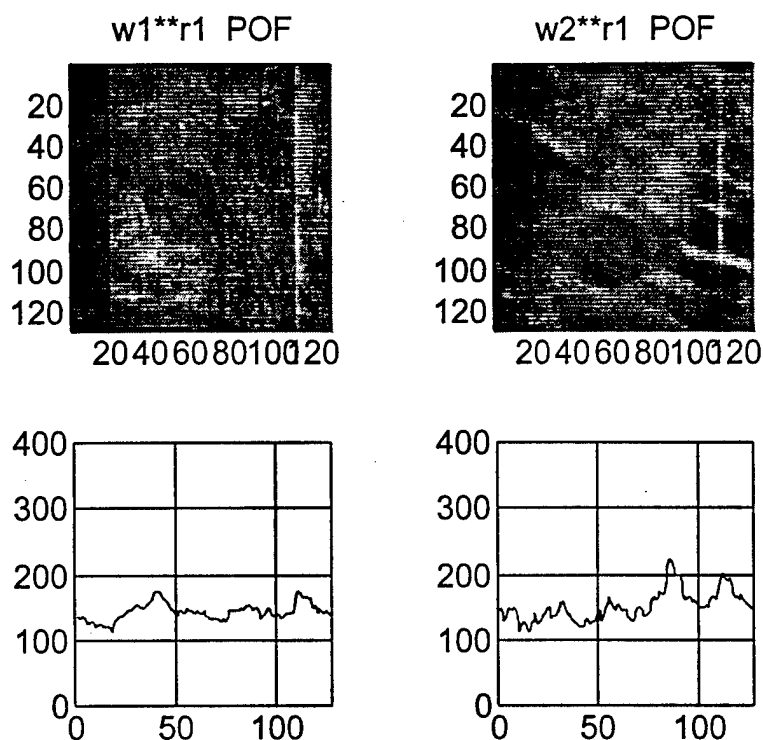


FIGURE 7.25. CROSS-CORRELATION INTENSITY PATTERNS  
FOR INPUT SCENES WITH TARGET (CONTINUED)

The correlator performance measures were computed and tabulated in Table 7.4. The values for PAR and PMSR are not high because of the high background noise. These numbers can be improved by postprocessing techniques. The results for the PAR are much higher here than in the CMF case as given in Table 7.3. This indicated that the correlation peaks are sharper in the POF case.

TABLE 7.4. CORRELATION PERFORMANCE FOR POF

Parameter	r1**r1	b1**r1	b7**r1	d1**r1	d2**r1	w1**r1	w2**r1
Peak x1.0e+06	2.0275	0.1492	0.1325	0.1323	0.1187	0.0306	0.0498
PAR	32.9070	11.5391	5.9203	5.7708	4.5651	2.1495	5.8794
PMSR	0.4250	1.1729	1.0056	1.1524	1.0663	1.0260	1.2366

A BPOF of the target was used. The results of these correlations are shown in Figures 7.26 and 7.27. The autocorrelation peak is strong as expected and is much sharper than for the CMF case. The cross-correlation patterns of the six scenes with the target are shown in Figure 7.27. The targets in b1, b2, and d1 are detected by the system, as indicated by the strong correlation peaks except for the faded target in b1. The system failed to detect the target in d2, w1, and w2 scenes. These results are almost identical to the POF.



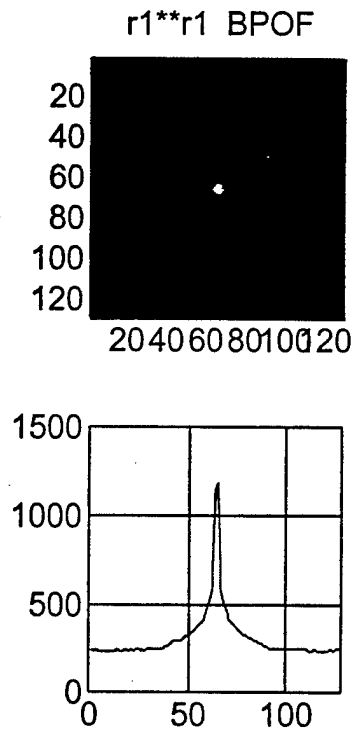


FIGURE 7.26. AUTOCORRELATION PATTERN OF TARGET USING BPOF

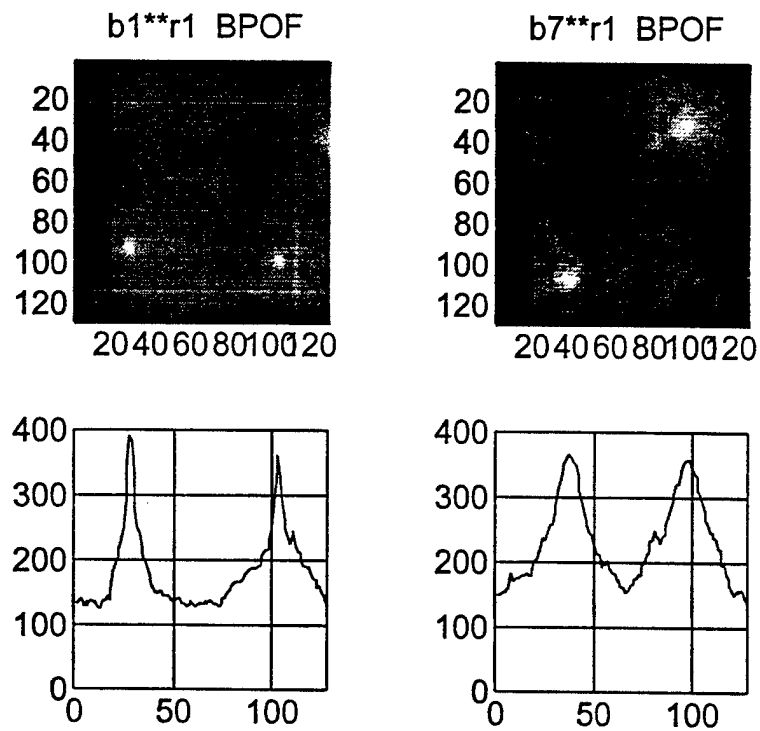


FIGURE 7.27. CROSS-CORRELATION INTENSITY PATTERNS FOR INPUT SCENES USING BPOF

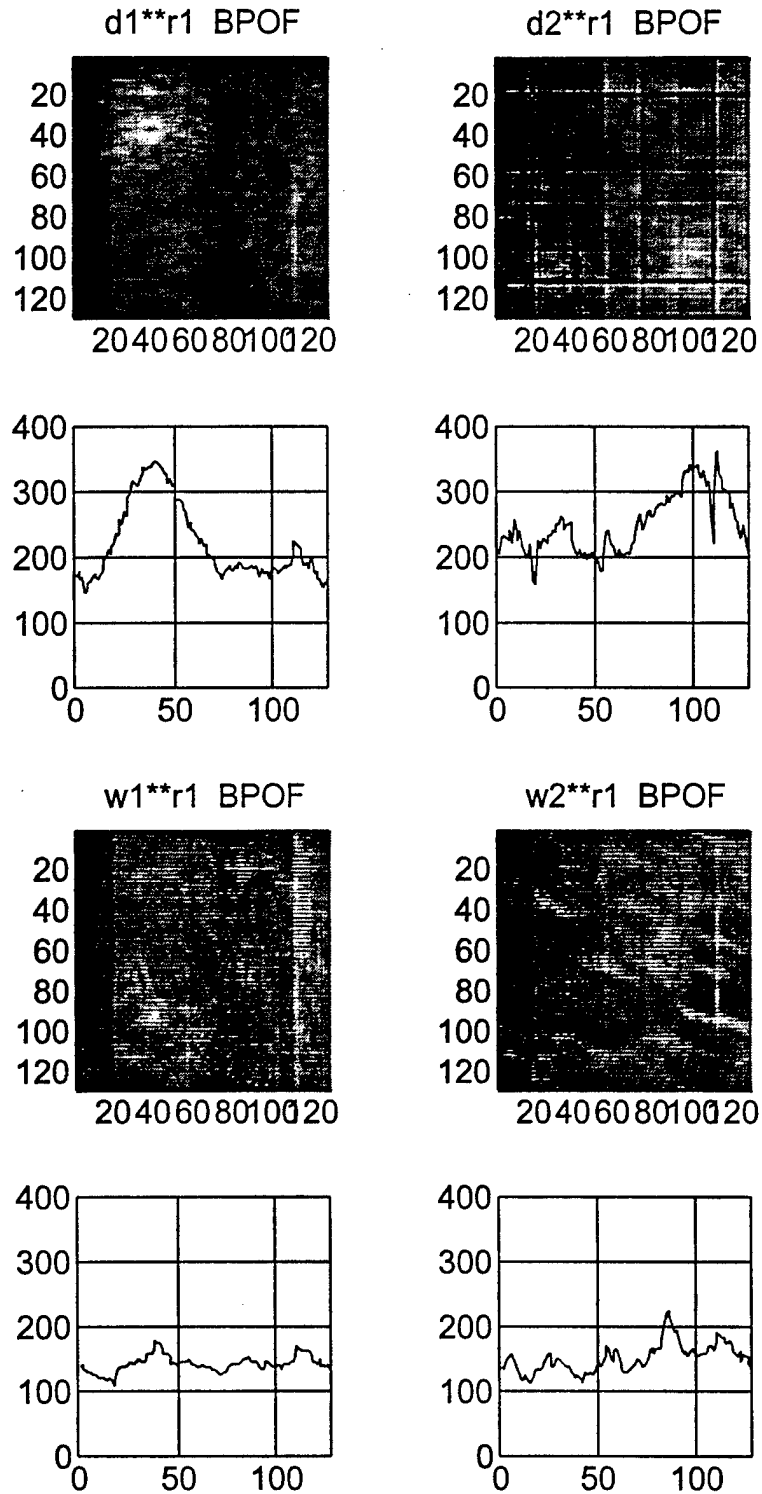


FIGURE 7.27. CROSS-CORRELATION INTENSITY PATTERNS FOR INPUT SCENES USING BPOF (CONTINUED)

The correlator performance measures were computed and tabulated in Table 7.5. The values for PAR and PMSR are similar to those for the POF case. The results for the PAR are much larger here than in the CMF case as given in Table 7.3.

TABLE 7.5. CORRELATION PERFORMANCE FOR BPOF

Parameter	r1**r1	b1**r1	b7**r1	d1**r1	d2**r1	w1**r1	w2**r1
Peak x1.0e+06	1.4064	0.1545	0.1337	0.1192	0.1303	0.0324	0.0502
PAR	22.8254	11.9470	5.9731	5.1997	5.0103	2.2753	5.9281
PMSR	6.7169	1.1767	1.0311	1.0011	1.1107	1.0991	1.3544

**7.4.2.2 Quantization of the Input Image.** This section considers quantization effect on the correlator performance for detecting targets among the experimentally collected data images. First, the set of six images were binarized and correlated with a complex matched filter and a binary POF. Second, the two images b1 and w2 were quantized with  $Q=2, 4, 8, 16$ , and 32 levels and correlated with a CMF and then with a BPOF.

The binarized set of images are shown in Figure 7.28. Binarization of the images enhanced greatly b1 and b2 and somewhat d1 and d2, but w1 and w2 were degraded. The intensity patterns of the cross correlation between the six input images and the target is given in Figure 7.29. Each cross-correlation intensity pattern is accompanied by a plot of its maximum value along each column. These plots are placed below the corresponding correlation intensity pattern. The correlation pattern of b1\*\*t has two strong correlation peaks corresponding to the two targets present in the image. These intensity patterns have a high contrast ratio. Image b1, as discussed in the previous section, has a weak target in the upper left corner. This weak target has been removed from the image in the binarization process. Scene b7 has two targets and a smaller scale target in the upper left corner. The correlation pattern for b7 shows the three correlation peaks with the lower magnitude peak indicating the smaller scale target. Scenes d1 and d2 each has one target, and the corresponding correlation pattern each has one strong peak at the proper location of the target, and a few false peaks. The correlation patterns for w1 and w2 are completely obscured with no correlation peaks. This is due to loss of target information during the binarization process. The binarization of the image was able to enhance the performance of the correlator for the cases where the targets are clearly distinguished from the background. In the presence of strong clutter, the binarization caused the target information to be lost.

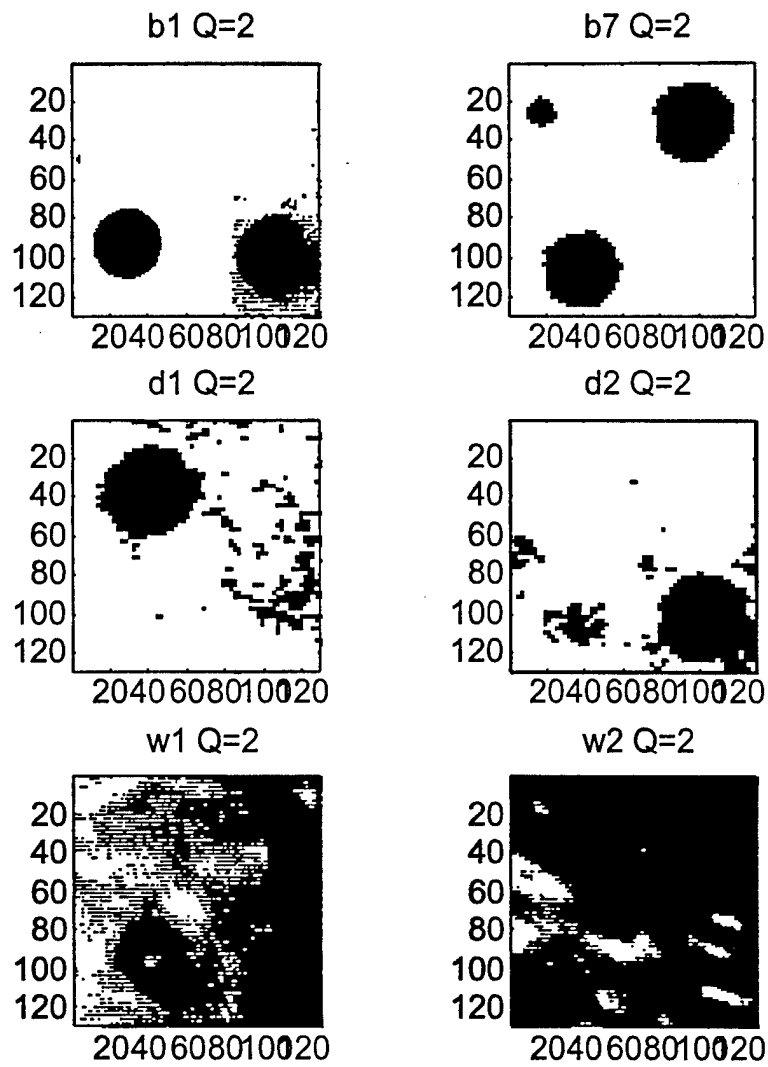


FIGURE 7.28. BINARIZED INPUT IMAGES

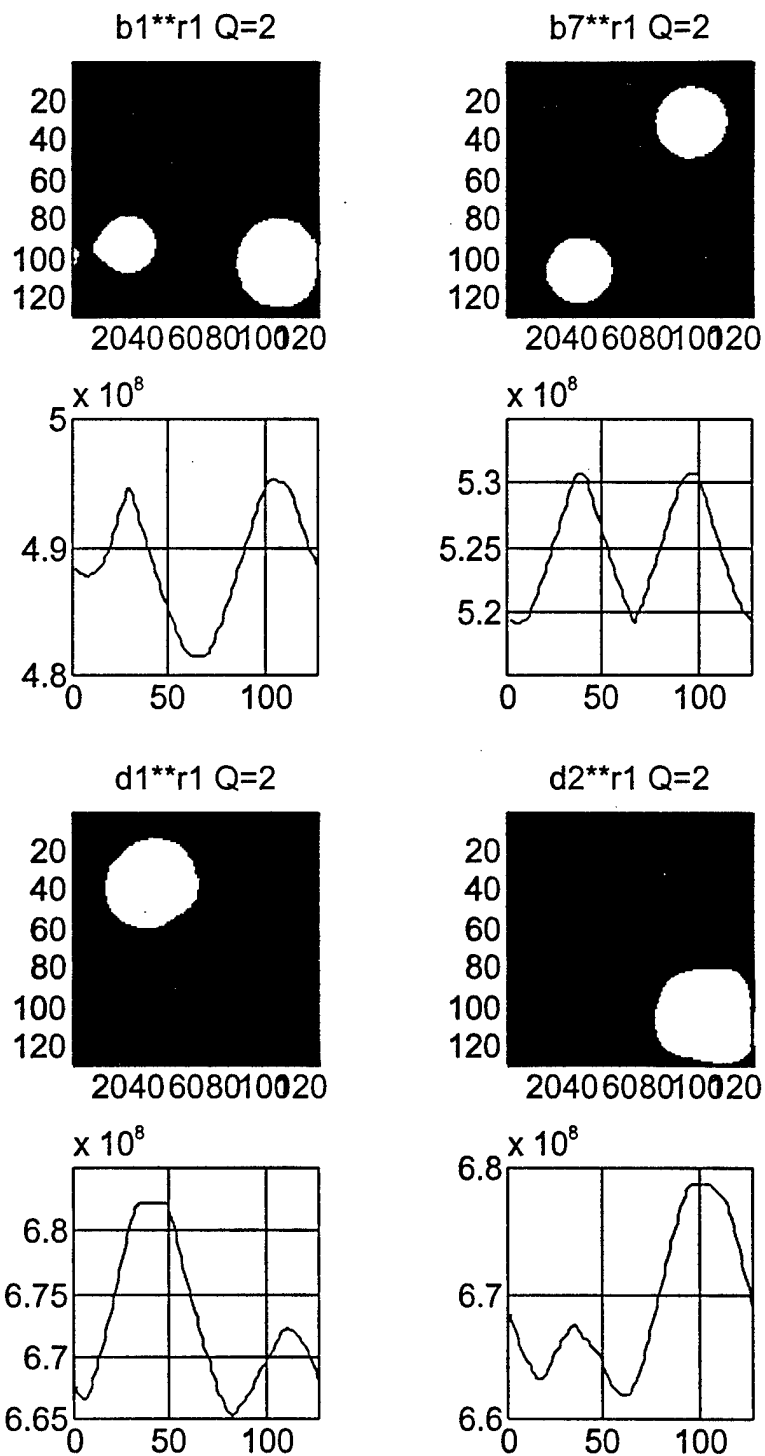


FIGURE 7.29. CROSS-CORRELATION OF BINARIZED INPUT SCENES WITH TARGET

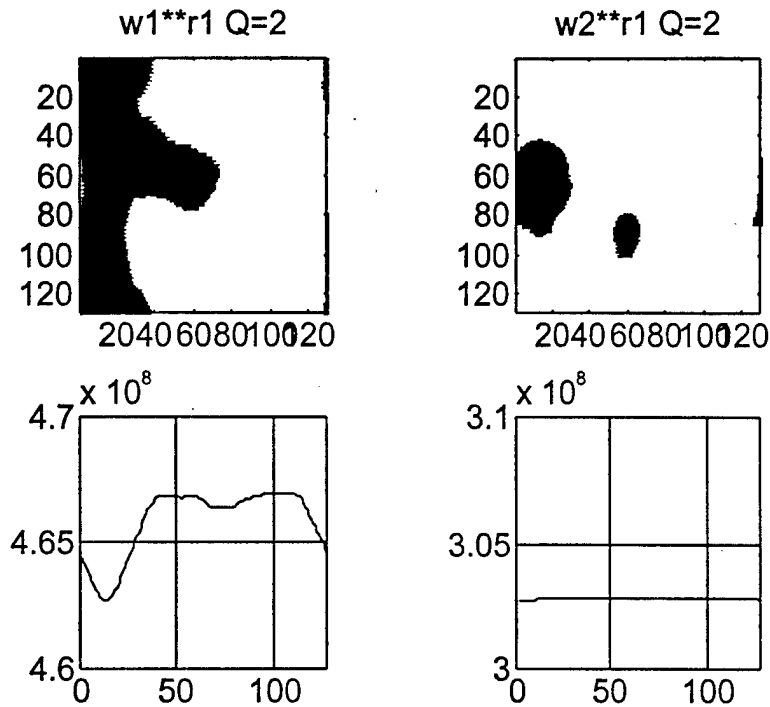


FIGURE 7.29. CROSS-CORRELATION OF BINARIZED  
INPUT SCENES WITH TARGET (CONTINUED)

A BPOF of the target was used with binary input images. The cross-correlation patterns of the six scenes with the target are shown in Figure 7.30. The targets in b1 and b2 are detected by the system and are indicated by the strong correlation peaks except for the faded target in b1. Cross correlations for d1 and d2 indicate weak correlation peaks at the target positions. The system failed to detect the target in scenes w1 and w2.

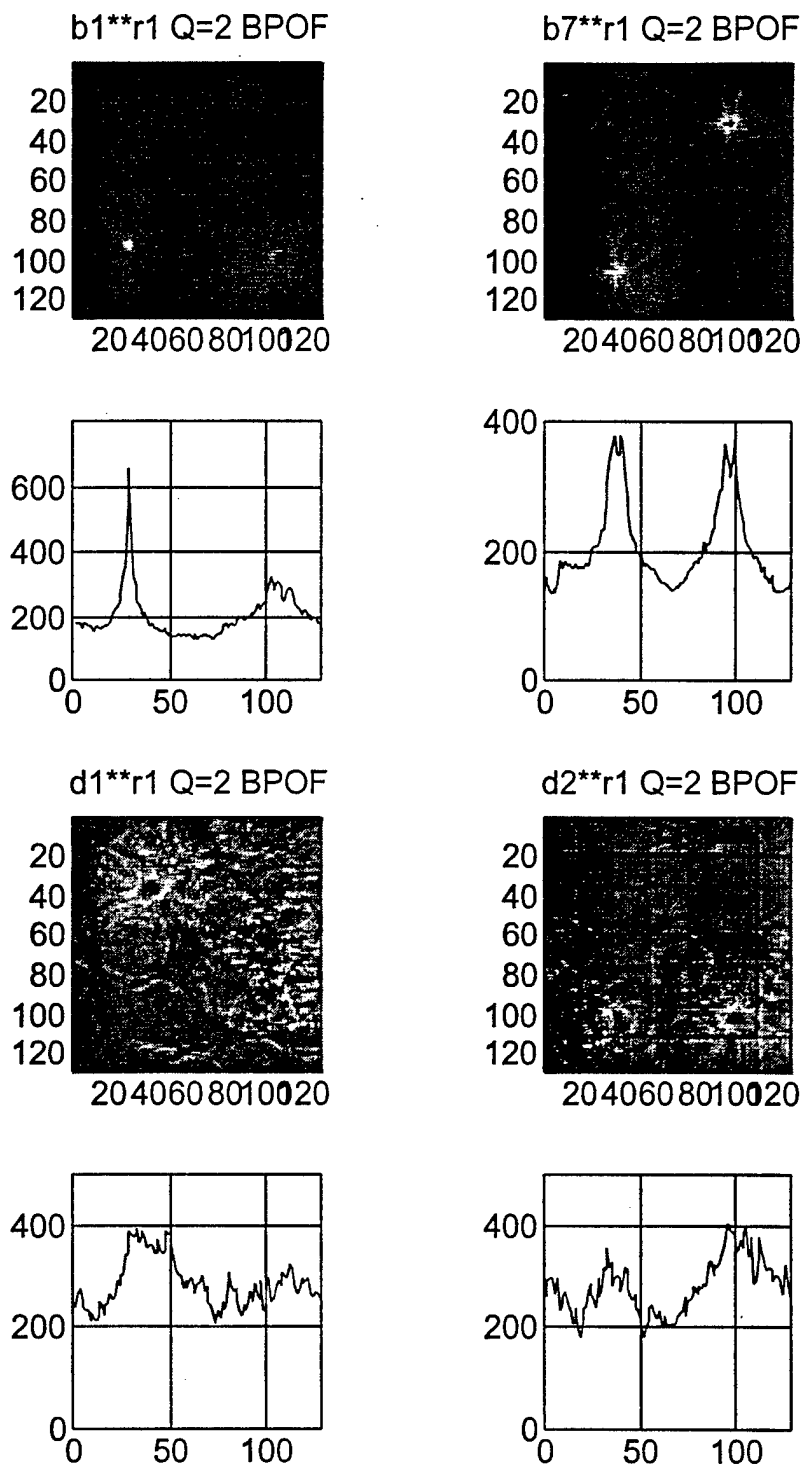


FIGURE 7.30. CROSS-CORRELATION OF BINARIZED  
INPUT SCENES WITH TARGET USING BPOF

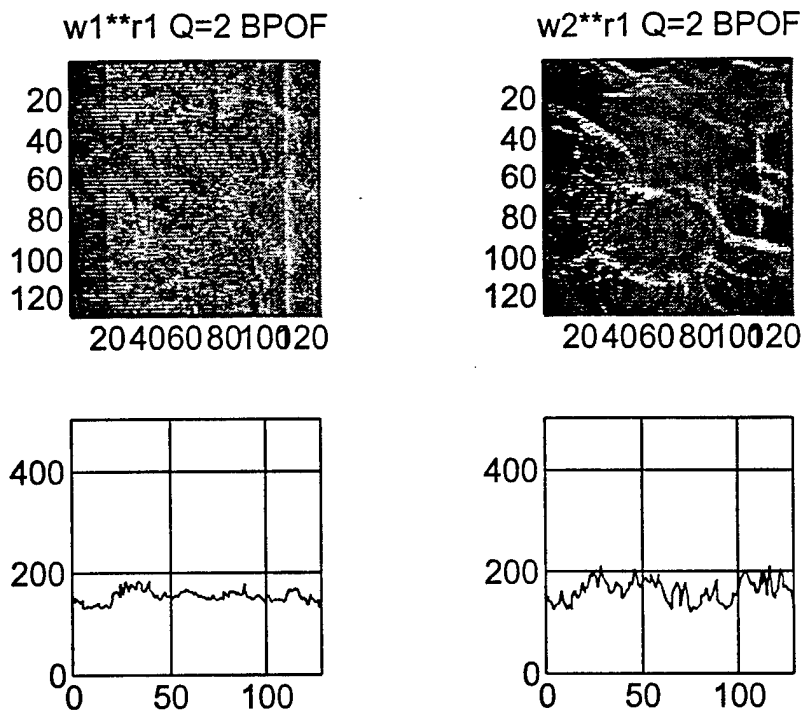


FIGURE 7.30. CROSS-CORRELATION OF BINARIZED INPUT SCENES WITH TARGET USING BPOF (CONTINUED)

The correlator performance measures were computed and tabulated in Table 7.6. The results for the PAR and PMSR are slightly smaller than in the continuous case as given in Table 7.5.

TABLE 7.6. CORRELATION PERFORMANCE FOR BINARY INPUT AND BPOF

Parameter	Input Image					
	b1	b7	d1	d2	w1	w2
Peak x1.0e+05	4.2808	1.4465	1.5303	1.6368	0.3473	0.4517
PAR	27.3123	8.1478	5.0998	5.4955	2.5176	6.6007
PMSR	4.0330	1.0057	1.0073	1.0365	1.0059	1.0179

Next the case for quantizing b1 and w1 scenes with  $Q=2, 4, 8, 16$ , and  $32$  is considered. These quantized and continuous images are given in Figures 7.31 and 7.32.



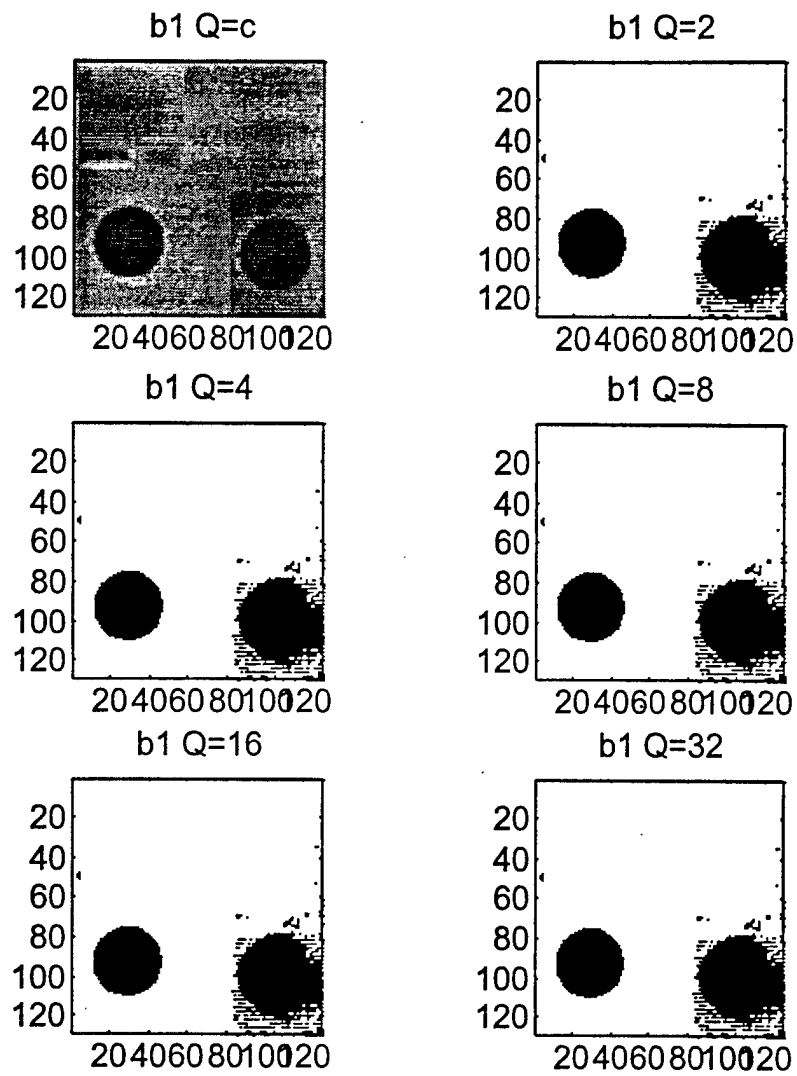
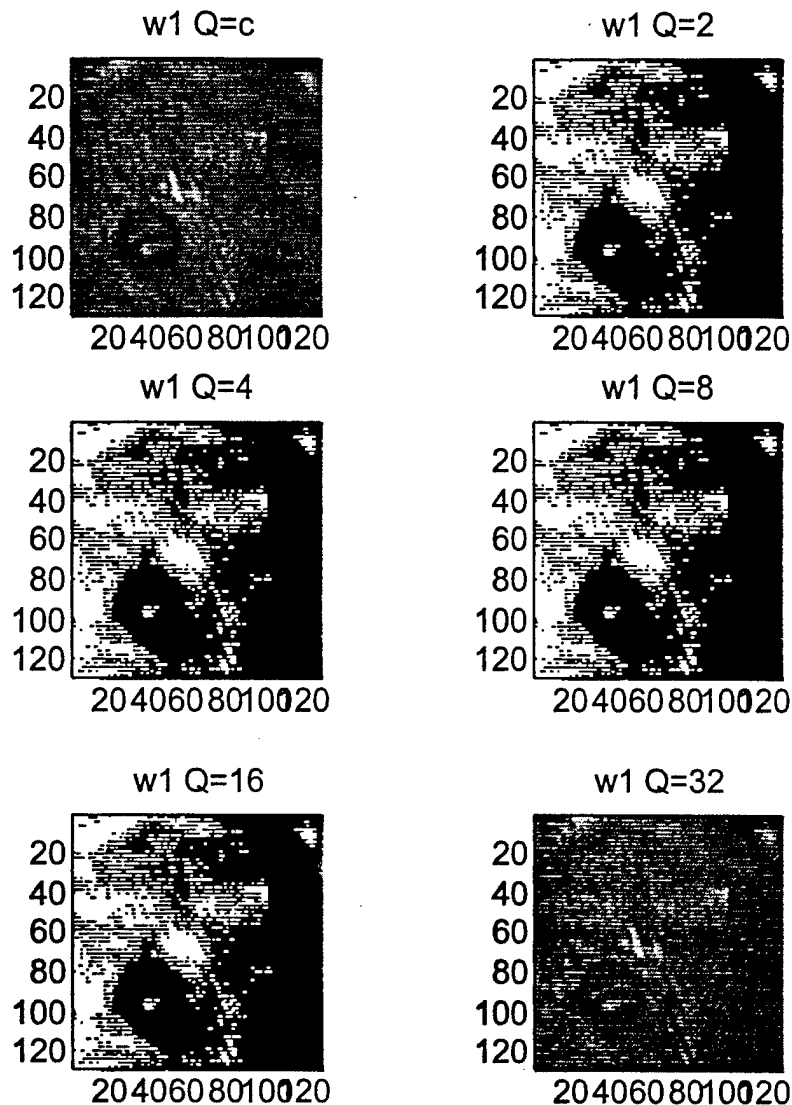
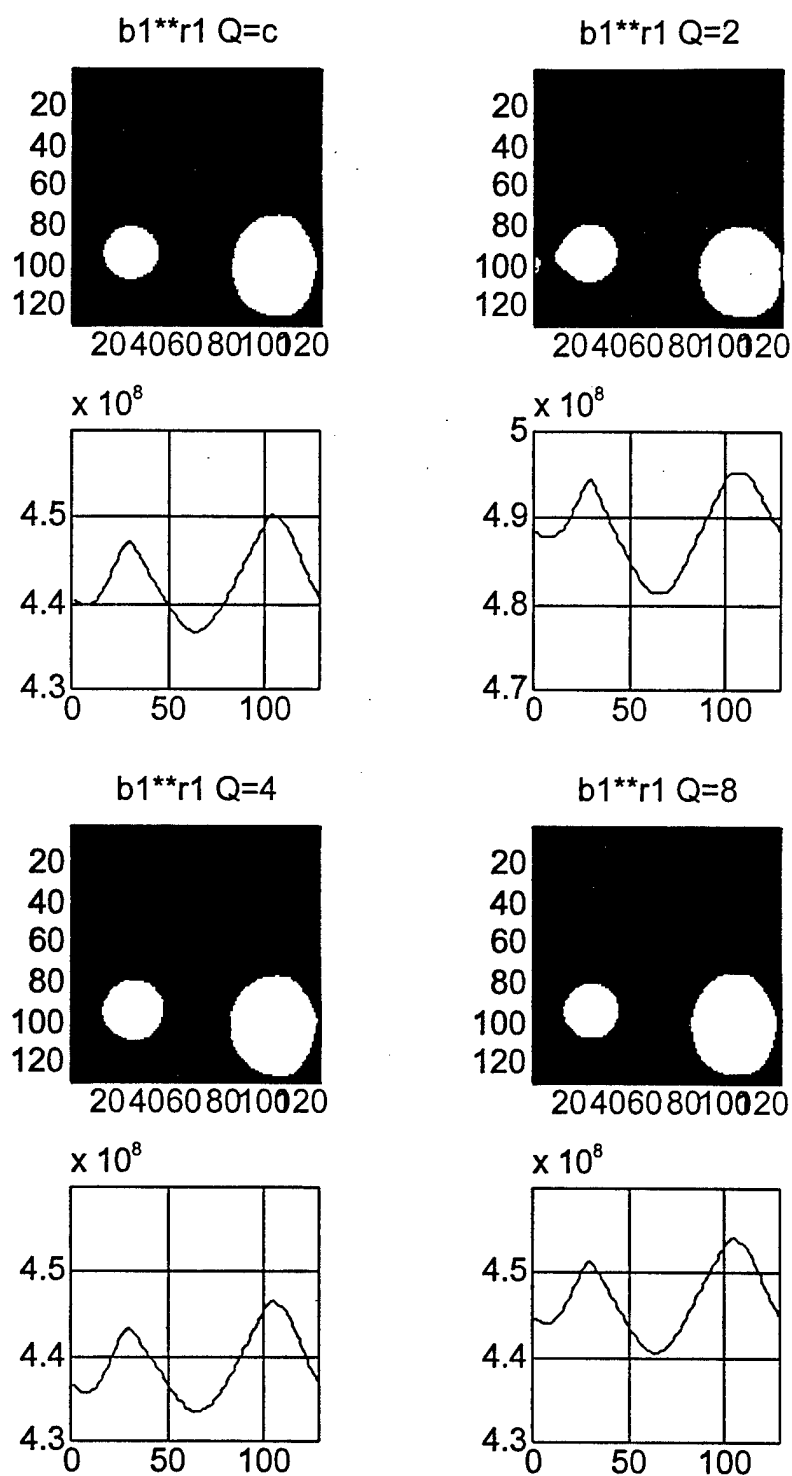


FIGURE 7.31. QUANTIZED INPUT SCENE b1 WITH Q=16 AND 32

FIGURE 7.32. QUANTIZED INPUT SCENE  $w1$  WITH  $Q=c, 2, 4, 8, 16,$  AND  $32$ 

The intensity pattern of the cross correlation between the two quantized input images and the target is given in Figures 7.33 and 7.34 for scene  $b1$  and  $w1$ , respectively. Each cross-correlation intensity pattern is accompanied by a plot of the maximum value along each column of the pattern. These plots are placed below the corresponding correlation intensity patterns. The correlation pattern of  $b1^{**}t$  has two strong correlation peaks corresponding to the two targets present in the image. These intensity patterns have a high contrast ratio. The weak target in  $b1$  has been removed from the image for  $Q=2$  and it starts to show up for  $Q=4$  and higher. So for the targets in this image to be detected, at least four gray levels are needed. Scene  $w1$  has two targets--a full and a partial one. For  $Q=2$ , the cross-correlation pattern failed to detect any of the targets in the scene. For gray levels  $Q=4$  and higher, the two peaks started to appear. In the case when  $Q=8$ , the pattern was similar to a higher quantization level.

FIGURE 7.33. CROSS-CORRELATION INTENSITY PATTERN FOR QUANTIZED  $b_1$  USING CMF

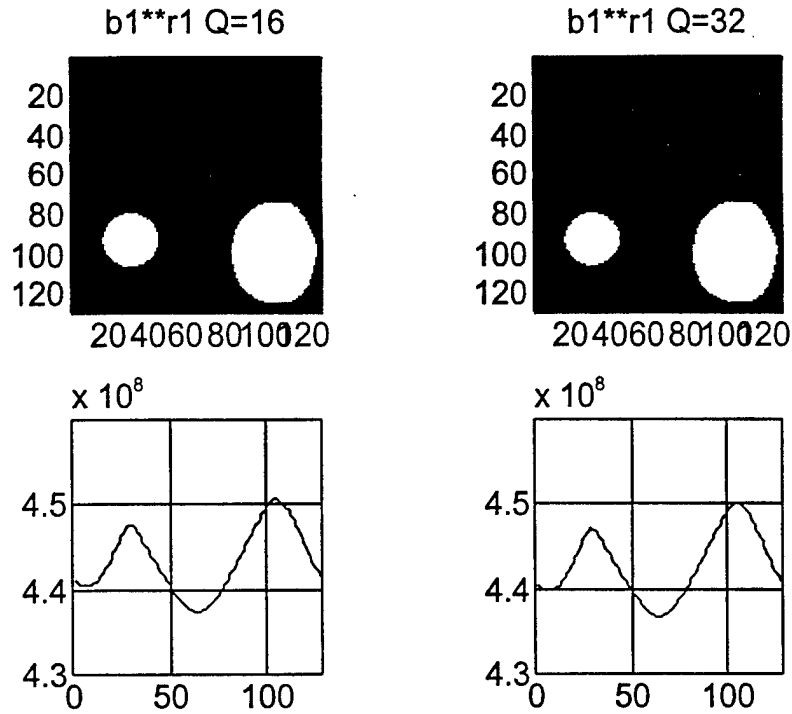


FIGURE 7.33. CROSS-CORRELATION INTENSITY PATTERN FOR QUANTIZED  $b_1$  USING CMF (CONTINUED)

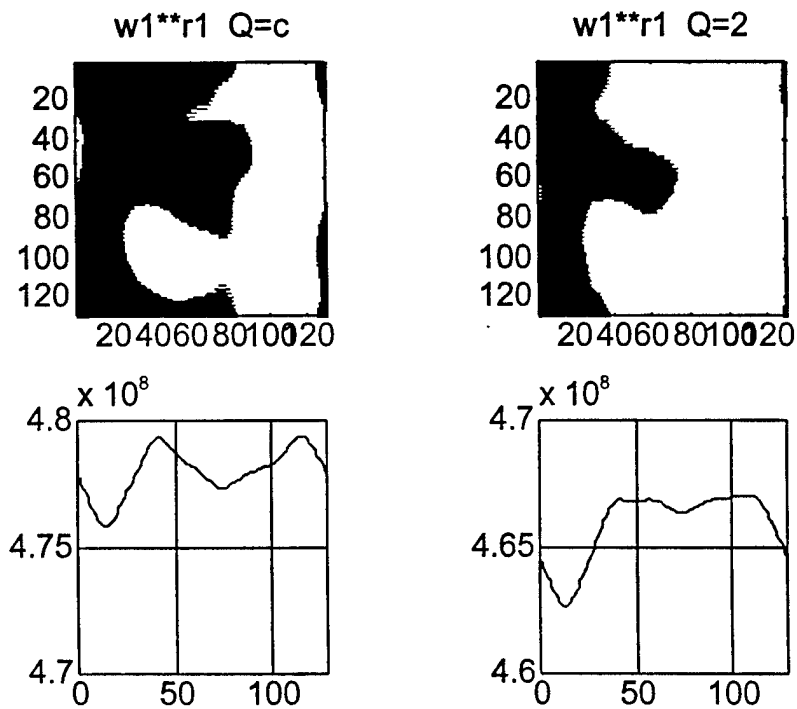


FIGURE 7.34. CROSS-CORRELATION INTENSITY PATTERN FOR QUANTIZED  $w_1$  USING CMF

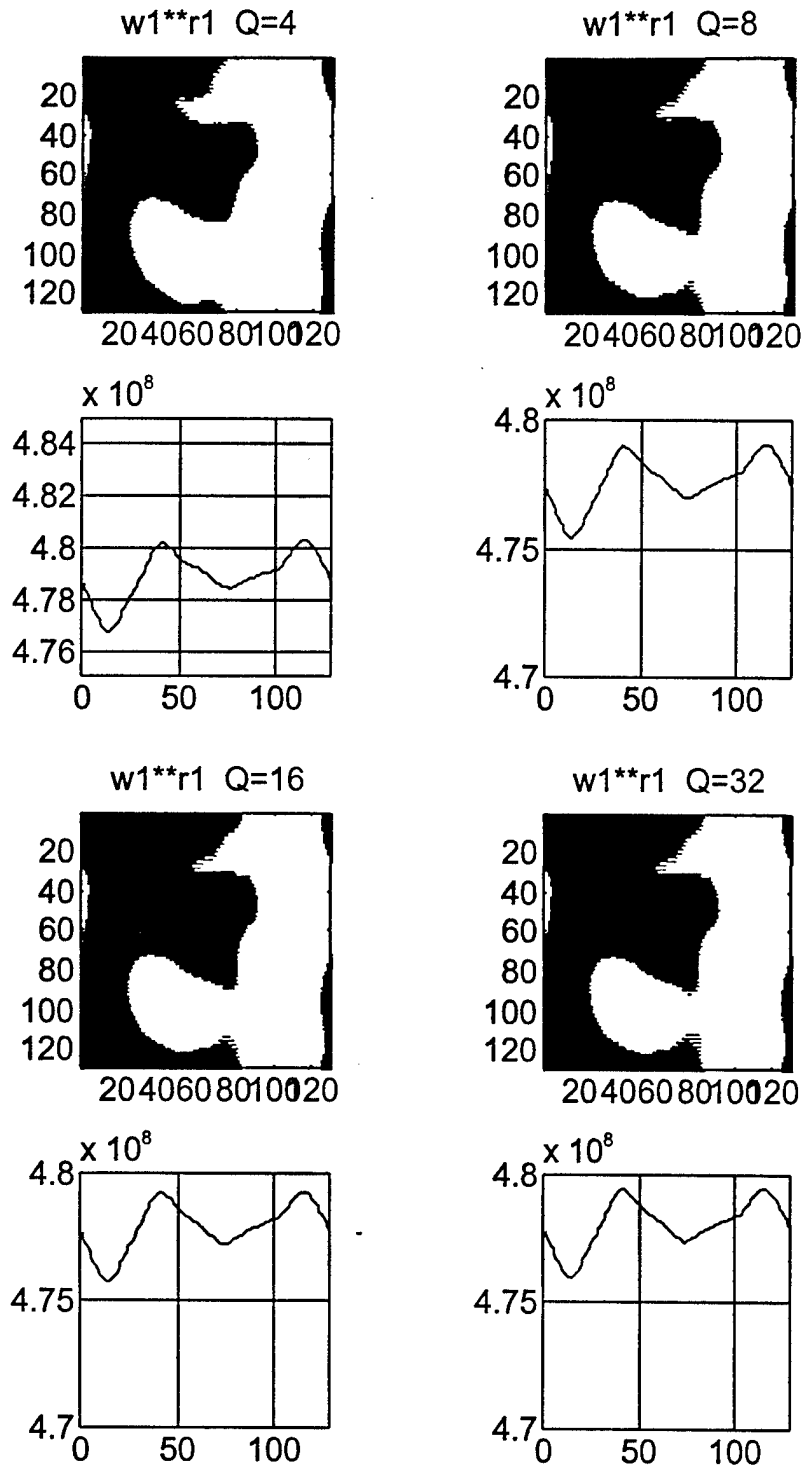


FIGURE 7.34. CROSS-CORRELATION INTENSITY PATTERN FOR QUANTIZED  $w_1$  USING CMF (CONTINUED)

The correlation performance measures for b1 quantized are given in Table 7.7 and for w1 quantized in Table 7.8. The values for PAR and PMSR increase with quantization levels. The increase reaching a maximum when Q=8.

TABLE 7.7. CORRELATION PERFORMANCE FOR QUANTIZED b1 SCENE

	Quantization Level					
Parameter	Q=c	Q=2	Q=4	Q=8	Q=16	Q=32
Peak x1.0e+07	2.0275	2.4523	1.9944	2.0642	2.0322	2.0271
PAR	1.0567	1.0492	1.0570	1.0557	1.0564	1.0566
PMSR	1.0046	1.0016	1.0038	1.0044	1.0046	1.0047

TABLE 7.8. CORRELATION PERFORMANCE FOR QUANTIZED w1 SCENE

	Quantization Level					
Parameter	Q=c	Q=2	Q=4	Q=8	Q=16	Q=32
Peak x1.0e+07	2.2983	2.1810	2.3072	2.2952	2.2973	2.2991
PAR	1.0099	1.0087	1.0098	1.0101	1.0099	1.0099
PMSR	1.0001	1.0000	1.0001	1.0002	1.0001	1.0001

## 8.0 IMAGES WITH LIMITED PIXEL RESOLUTION

The amount of information contained in an image is characterized by its pixel resolution. If the same image is given in a 32x32 and 128x128 formats, the later will contain more detailed information than the former. A reduction in the pixel resolution results in a loss of information. This information can be essential in identifying and recognizing a target. In pattern recognition, images with targets of limited pixel resolution are expected to be more difficult to detect. This section provides information on the affect of limited pixel resolution on target detection. The simulation study will be done using experimentally collected images. These are real images of targets of interest.

### 8.1 LIMITED PIXEL RESOLUTION SIMULATION

The limited resolution effect is studied by reducing the pixel count of the images. This limited resolution can be the result of either small targets or reduced optical resolution. In this section, simulations are performed by taking the 128x128 images and reducing them to 64x64, 32x32, and 16x16 images. This reduction in resolution will result in making the target contain a smaller number of pixels. The number of target (circular shaped mine) pixels for these images are given in Table 8.1.

TABLE 8.1. REDUCED RESOLUTION PIXEL COUNT

Image Size (pixels)	Target Size (pixels)
128x128	1020
64x64	255
32x32	65
16x16	17

The images are shown in Figures 8.1 to 8.6. Each image is shown in the size formats given in Table 8.1. The targets in these images lose their circular shape as the resolution decreases and become less recognizable, especially some of the faded ones. The targets in images beach1 and beach7 are preserved at all size formats. In image dune2, target 1 disappeared completely in the 16x16 image. In image water1, the half target, target 2, started to fade away in the 32x32 image format. Thus, reduction in pixel resolution can cause some of the target to be lost from the image, which make it undetectable.

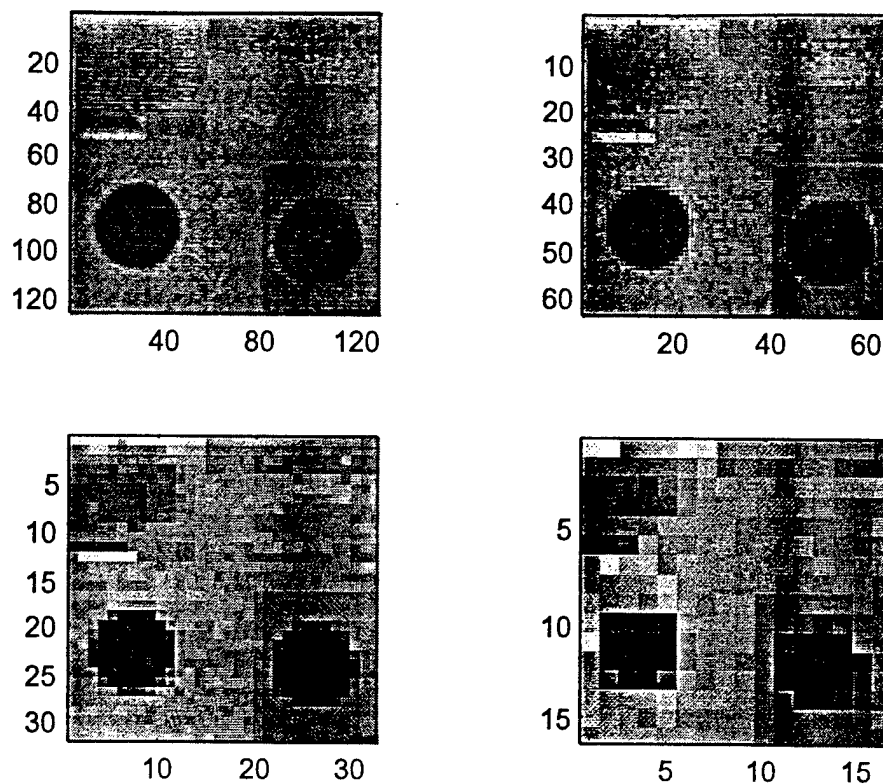


FIGURE 8.1. IMAGE BEACH1

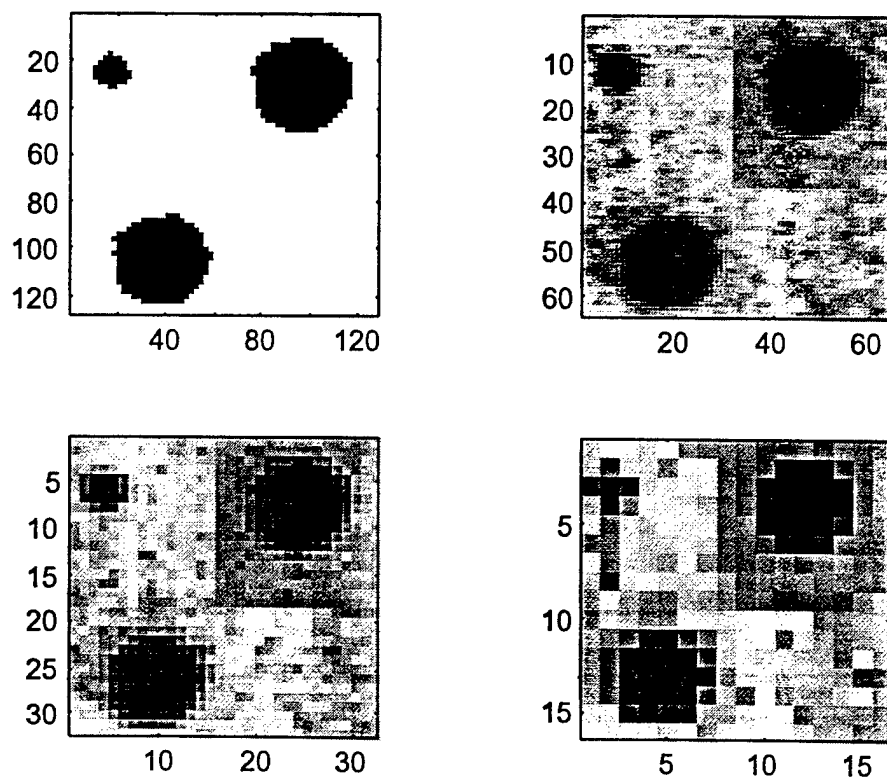


FIGURE 8.2. IMAGE BEACH7



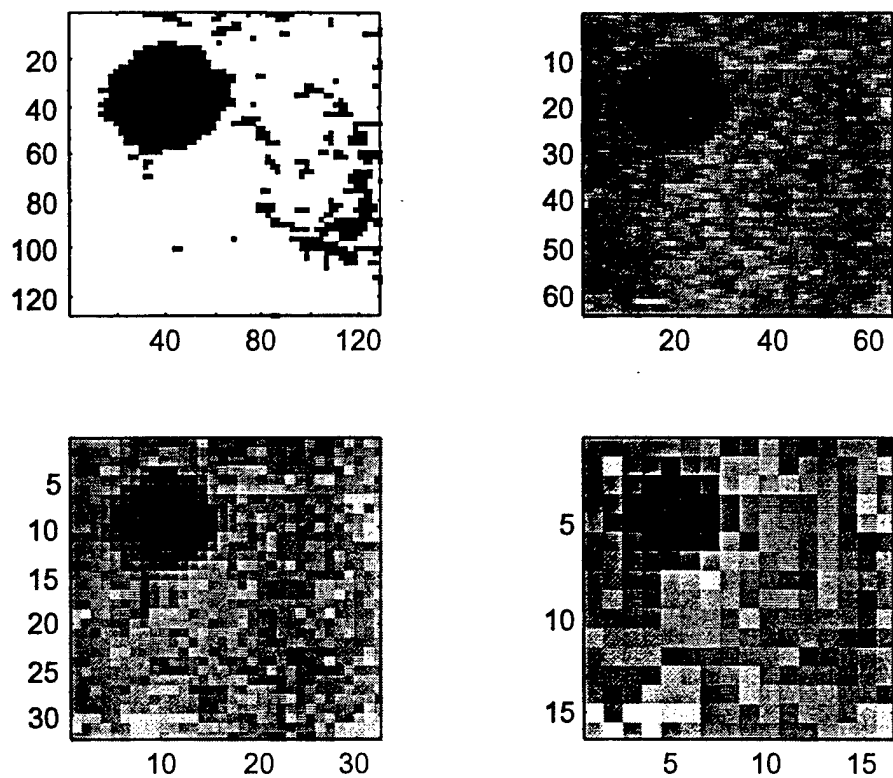


FIGURE 8.3. IMAGE DUNE1

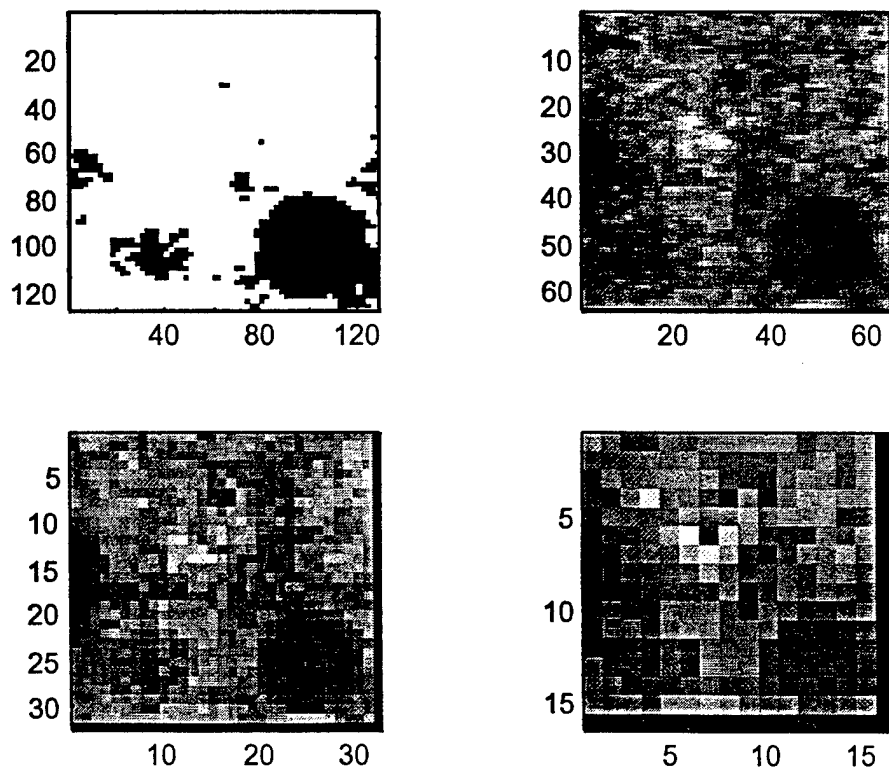


FIGURE 8.4. IMAGE DUNE2

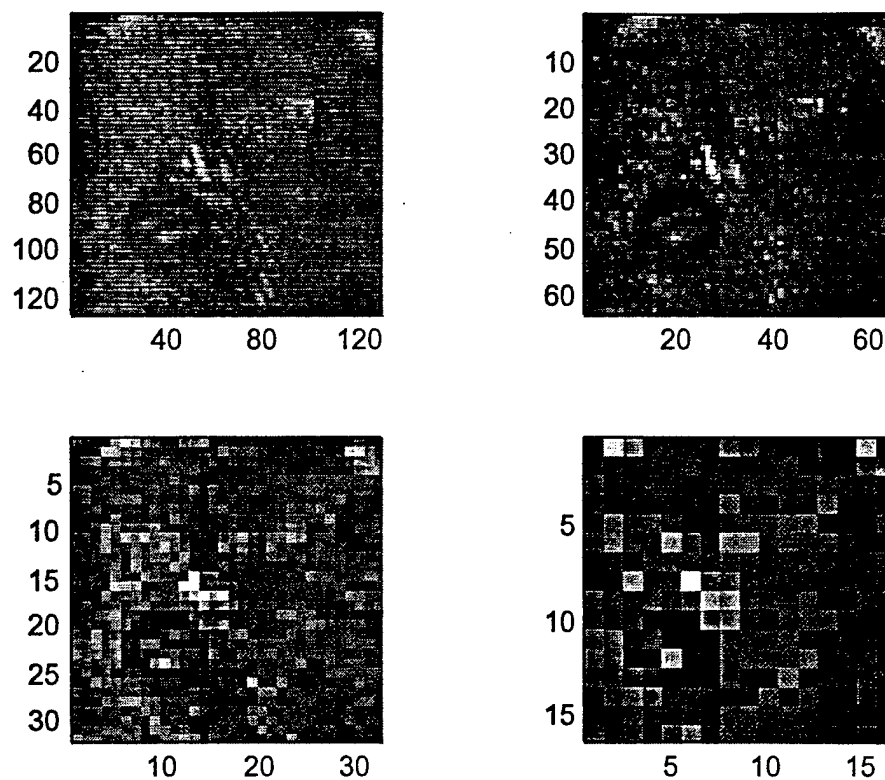


FIGURE 8.5. IMAGE WATER1

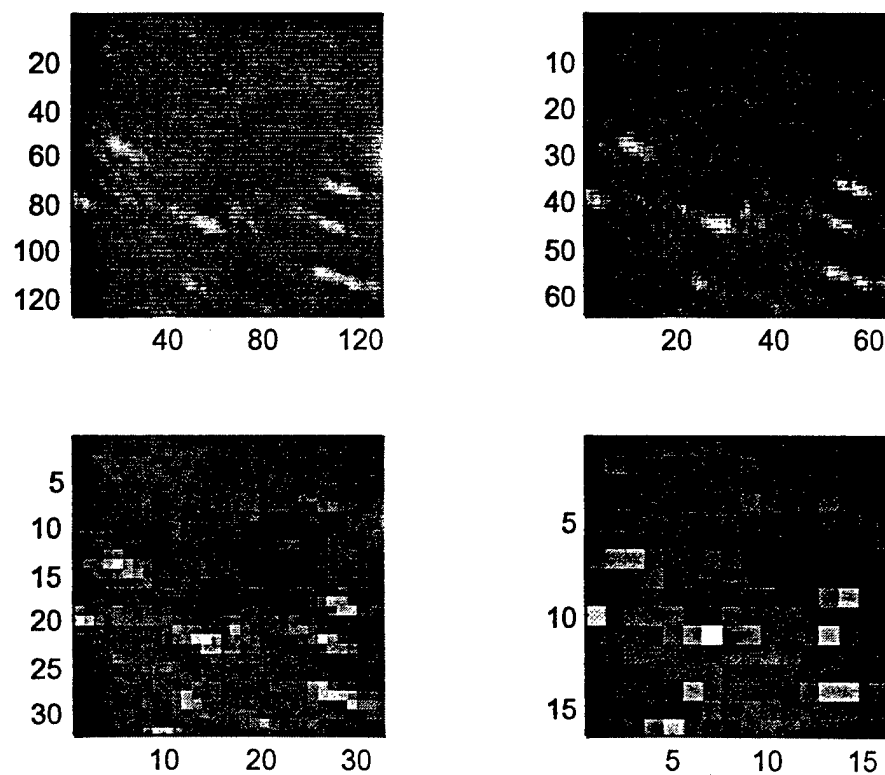


FIGURE 8.6. IMAGE WATER2

## 8.2 LIMITED PIXEL RESOLUTION AND CORRELATOR

The affect of the pixel resolution on the optical correlator performance is studied using the generated images with reduced resolution. Each of the images was used as the input to an optical correlator system and a filter of the same resolution was generated for the target for detection purposes. In each case, the correlation between the input and the target was computed. The different correlator performance metrics were determined for each of the targets in the images. The results of these calculations are given in Table 8.2.

TABLE 8.2. REDUCED RESOLUTION PERFORMANCE RESULTS

Resolution/ Image	beach1 (2)			beach1 (3)		
	PEAK	PAR	PMSR	PEAK	PAR	PMSR
128	11.8859		1.7320	17.8446	8.7366	2.6003
64	14.7924		1.9324	22.8387	8.2715	2.9836
32	8.4351		1.2048	22.7662	8.1196	3.2518
16	7.3194		1.0000	19.2162	8.4653	2.6254
Resolution/ Image	beach7 (2)			beach7 (3)		
	PEAK	PAR	PMSR	PEAK	PAR	PMSR
128	26.5385	8.4806	3.6722	30.2238	9.6583	4.1821
64	28.2965	8.4570	3.9104	32.2557	9.6403	4.4576
32	28.7276	8.3414	4.2349	32.7576	9.5112	4.8288
16	27.5312	7.1630	3.0179	32.8739	9.0903	3.6035
Resolution/ Image	dune1 (1)			dune2 (2)		
	PEAK	PAR	PMSR	PEAK	PAR	PMSR
128	41.7058	9.1804	3.0676	38.0706	5.9580	2.2844
64	44.3031	9.1894	3.0112	40.5828	5.9785	2.0713
32	44.9580	9.1617	3.6525	41.1607	5.1492	1.9477
16	47.6370	8.7462	3.3955	46.7985	4.1200	4.7334
Resolution/ Image	water1 (1)			water2 (2)		
	PEAK	PAR	PMSR	PEAK	PAR	PMSR
128	1.2225	3.5604	1.3543	13.2441	3.6734	1.6299
64	1.4037	4.5036	1.9504	11.5585	3.5627	1.6660
32	1.2941	4.4959	1.7348	11.1232	3.4612	1.6299
16	0.9952	3.8712	1.3761	11.4197	3.1260	1.6054

The relation between the correlator performance metrics (PAR and PMSR) and the pixel resolution of the input images for some of the targets in Table 8.2 are plotted in Figures 8.7 and 8.8.

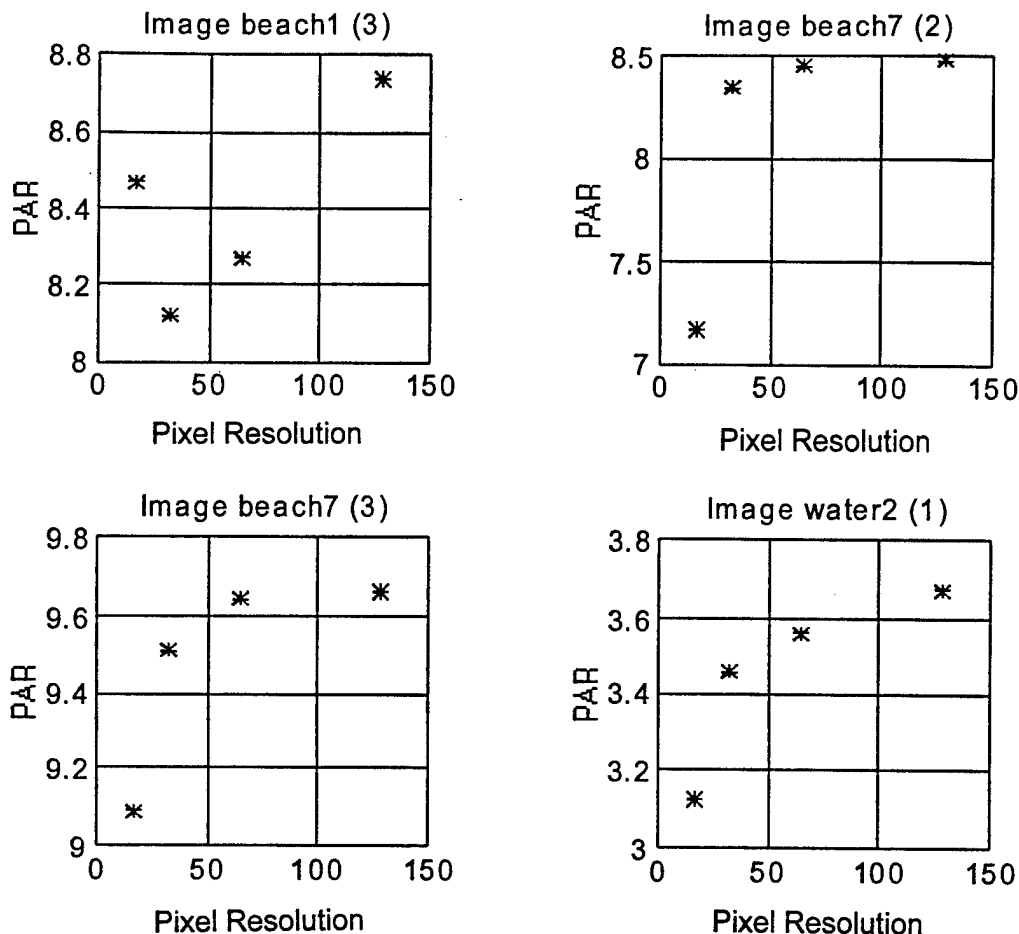


FIGURE 8.7. PERFORMANCE MEASURE PAR  
AS A FUNCTION OF IMAGE PIXEL RESOLUTION

The PAR value increases as the pixel resolution of the image increases as shown in Figure 8.1. This relationship is not linear but has similar characteristics for the different targets used. The increase in the PAR with an increase in the resolution might not be true for all targets as can be seen from the data in Table 8.2. Targets with smaller contrast signal-to-noise ratio (CSNR) values tend not to follow this general characteristic. This can be understood because such targets have statistics closer to the background and thus are more difficult to detect. The variations in the PAR values are between 5 and 18 percent. This change is not large and will not affect the detection process significantly.

The PMSR values, as shown in Figure 8.8, do not have a particular trend as the pixel resolution of the images increase. The overall change in the PMSR can be as large as 50 percent in some cases.

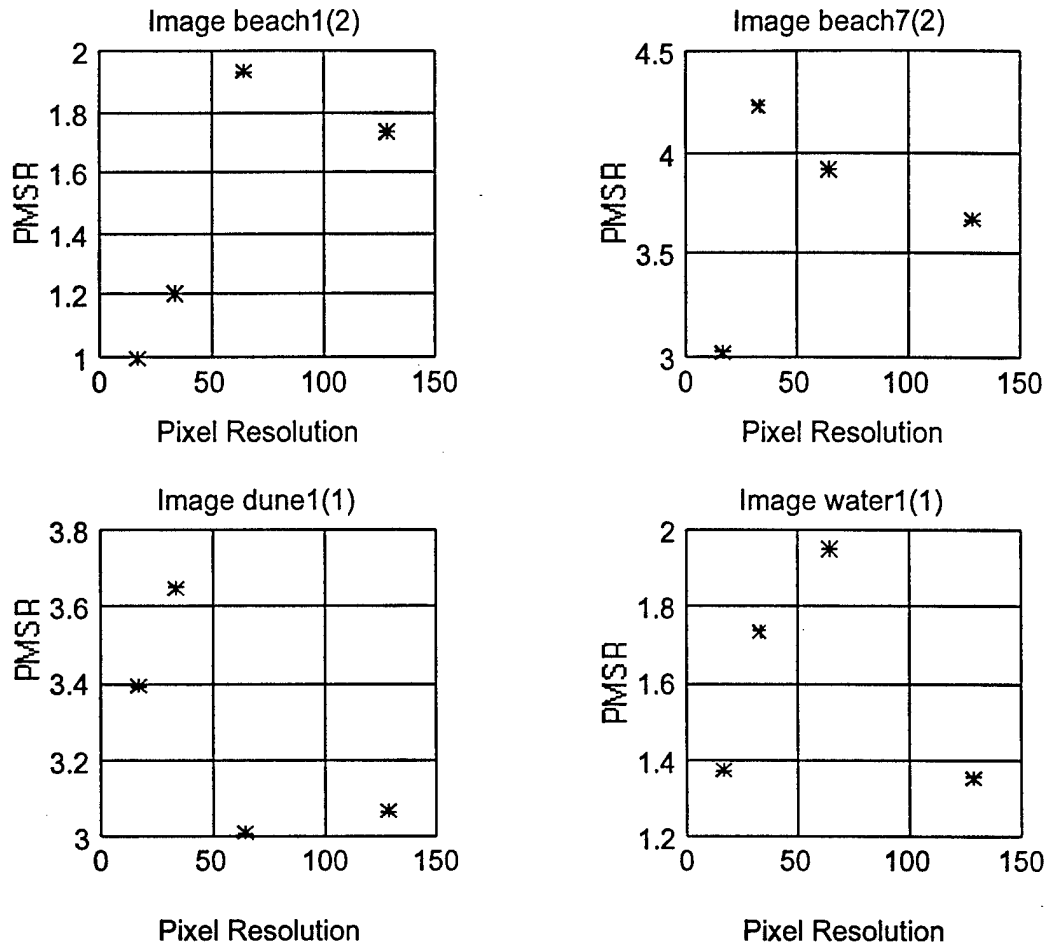


FIGURE 8.8. PERFORMANCE MEASURE PMSR AS A  
FUNCTION OF IMAGE PIXEL RESOLUTION

In summary, limited pixel resolution has some affect on the performance metrics of the correlator. The PAR variations are less than 20 percent. This change will not affect the detectability of the target if PAR was the metric used. Reducing the resolution caused a minor loss in detectability, especially for targets with large CSNR values. This is an important result in the sense that the resolution of the images can be reduced to a smaller format without suffering a significant reduction in the detectability of the targets. This is not the case when CSNR is small. A smaller image format can drastically reduce the computing time of the detection process. For example, a reduction of the resolution from 128x128 to 32x32 reduces the computing time to 1/16 of the original time. This improves the overall throughput of the system.

## 9.0 THRESHOLDING

Thresholding is an essential element in the final stage of the detection process in the optical correlator system. This is performed on the data collected by the photodetector array at the output correlation plane. Thresholding criteria determines if the peak in the correlation plane indicates the presence of a target in the image. This criteria must be based on the selected performance metric; correlation peak, PAR, and/or the PMSR.

To determine which of these metrics is to be used as a thresholding parameter, a study was conducted to characterize the minelike targets in the images according to the difficulty of their detection.

### 9.1 MINELIKE TARGET CHARACTERIZATION

The images have a general characteristic of a noisy background. The intensity distribution of the noisy background as well as the intensity distributions of the targets tends to follow, in the images considered, Gaussian statistics. The statistics, mean and variance of the intensity, of both the target and the background determines the difficulty of the detection. A number of parameters can be used to quantify the difficulty of detection of the targets. In this study, the parameters will be limited to the following:

1. The contrast ratio (CR), which is given by

$$CR = \frac{(\text{Background mean} - \text{Target mean})}{(\text{Background mean} + \text{Target mean})} \quad (9.1)$$

2. The target-to-background ratio (TBR)

$$TBR = \frac{\text{Target mean}}{\text{Background mean}} \quad (9.2)$$

3. CSNR

$$CSNR = \frac{(\text{Background mean} - \text{Target mean})}{\sqrt{\text{Background Variance} + \text{Target Variance}}} \quad (9.3)$$

The first two of these parameters does not take into account the variations of the background and the target intensities. Images with the same background and target means but different variances have different levels of detectability. This makes the third parameter, CSNR, the more robust and general of the three. A CSNR of zero indicates the impossibility of detection, while a CSNR of infinity indicates the easiest level of detection. So the larger the parameter CSNR, the easier the detection of the target.

This report is limited to the characterization of the targets according to the CSNR parameter. The six images and the targets existing in them are defined in Appendix B, along with their statistics.

The results of the simulation computation of the optical correlator metrics in terms of the CSNR of the targets is given in Table 9.1. Targets with no entries for the performance metrics were not detected with the optical correlator. The experiments were conducted using three different spatial filter formats.

The data for the target beach1 is not available because it was not detected. The parameter PAR\_B is a special case of the PAR. It is defined as the peak-to-the-mean of the intensity of the correlation plane after blocking an area of 41x41 pixels (which is slightly larger than the target size) around the correlation peak. Some of the data in Table 9.1 is presented in a graphical format in Figures 9.1 to 9.3.

The curves in Figures 9.1 to 9.3 show the relationship between the performance metrics and the CSNR. In general, all the metrics increase with the increase of the CSNR of the targets. This in particular is evident for the curves in Figure 9.1, where the CMF was used in the correlator system. The BPOF based correlator system illustrates the worst relationship. For the matched filter case, the relationship is linear between the correlation peak, the PAR, and the PAR\_B metrics. For the POF and the BPOF cases, the relationship is not linear but has the same trend.

TABLE 9.1. CORRELATOR PERFORMANCE RESULTS\*

IMAGE	CSNR	CMF			
		PEAK	PAR	PAR_B	PMSR
beach1 (1)	0.1693				
beach1 (2)	2.9079	11.8859	5.8193	15.9438	1.7320
beach1 (3)	4.0987	17.8446	8.7366	23.9368	2.6003
beach7 (2)	6.1736	26.5385	8.4806	48.0475	3.6722
beach7 (3)	6.9342	30.2238	9.6583	54.7198	4.1821
dune1 (1)	4.4073	41.7058	9.1804	22.6053	3.0676
dune2 (2)	3.4258	38.0706	5.9580	12.1300	2.2844
water1 (1)	1.0935	1.2225	3.5604	6.4109	1.3543
water2 (1)	1.5080	13.2441	3.6734	4.8366	1.6299

IMAGE	CSNR	POF			
		PEAK	PAR	PAR_B	PMSR
beach1 (1)	0.1693				
beach1 (2)	2.9079	1.4897e5	11.5853	18.6388	4.4992
beach1 (3)	4.0987	1.27e5	9.8762	15.8892	3.8355
beach7 (2)	6.1736	9.0136e4	10.9117	27.3717	4.2014
beach7 (3)	6.9342	8.9533e4	10.8382	27.1886	4.1733
dune1 (1)	4.4073	1.0747e5	7.8099	11.1585	1.9203
dune2 (2)	3.4258	0.9112e5	3.5047	5.9696	1.1256
water1 (1)	1.0935	9.6506e3	5.0407	7.7421	1.4524
water2 (1)	1.5080	4.9784e4	5.8809	8.9201	1.5518

IMAGE	CSNR	BPOF			
		PEAK	PAR	PAR_B	PMSR
beach1 (1)	0.1693				
beach1 (2)	2.9079	1.5419e5	12.0039	19.3429	4.7476
beach1 (3)	4.0987	1.3101e5	10.1995	16.4352	4.0339
beach7 (2)	6.1736	9.008e4	11.2687	28.7109	3.8783
beach7 (3)	6.9342	8.6776e4	10.8554	27.6578	3.7360
dune1 (1)	4.4073	9.2155e4	7.3559	10.6256	1.5759
dune2 (2)	3.4258	1.3024e5	5.0118	7.8222	1.9062
water1 (1)	1.0935	1.1184e5	5.2553	7.1518	1.2848
water2 (1)	1.5080	5.0167e5	5.9340	7.2808	1.3545

\* The number between the brackets is the target number in that particular image.



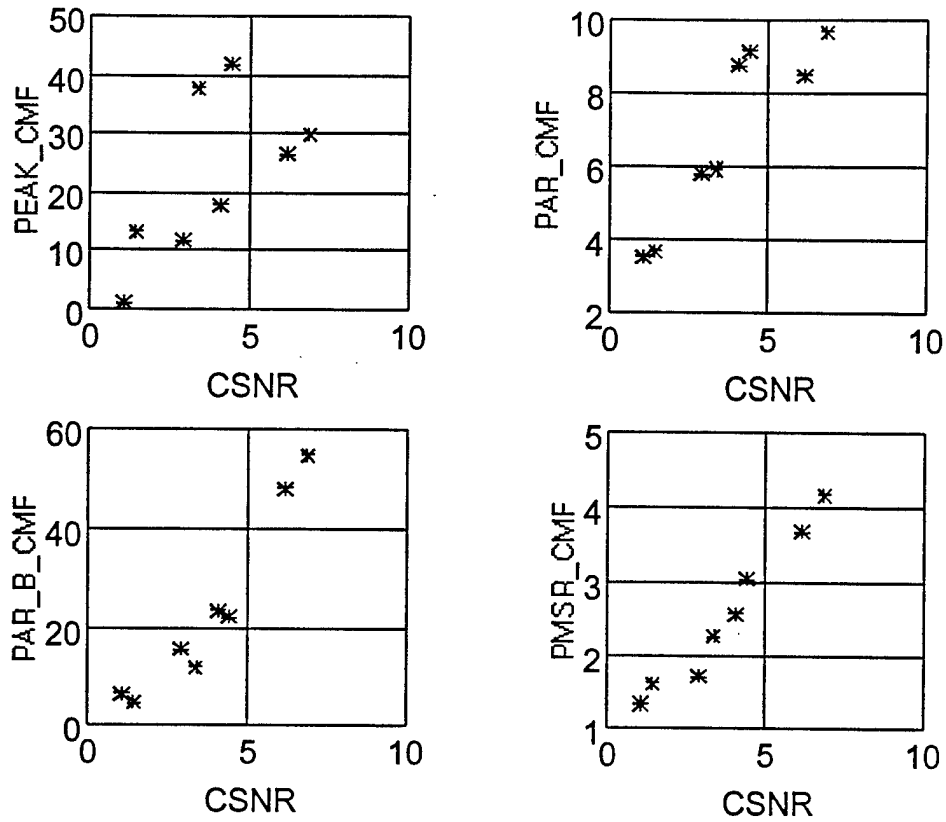


FIGURE 9.1. PERFORMANCE PARAMETERS AS A FUNCTION OF CSNR FOR CMF CASE

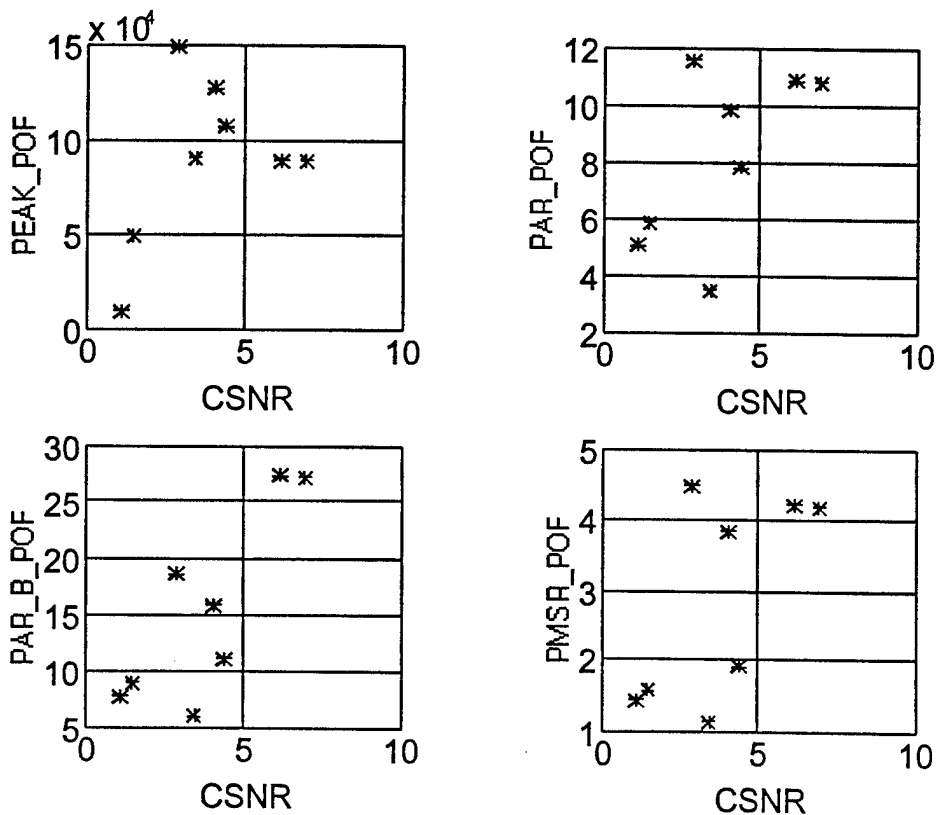


FIGURE 9.2. PERFORMANCE PARAMETERS AS A FUNCTION OF CSNR FOR POF CASE

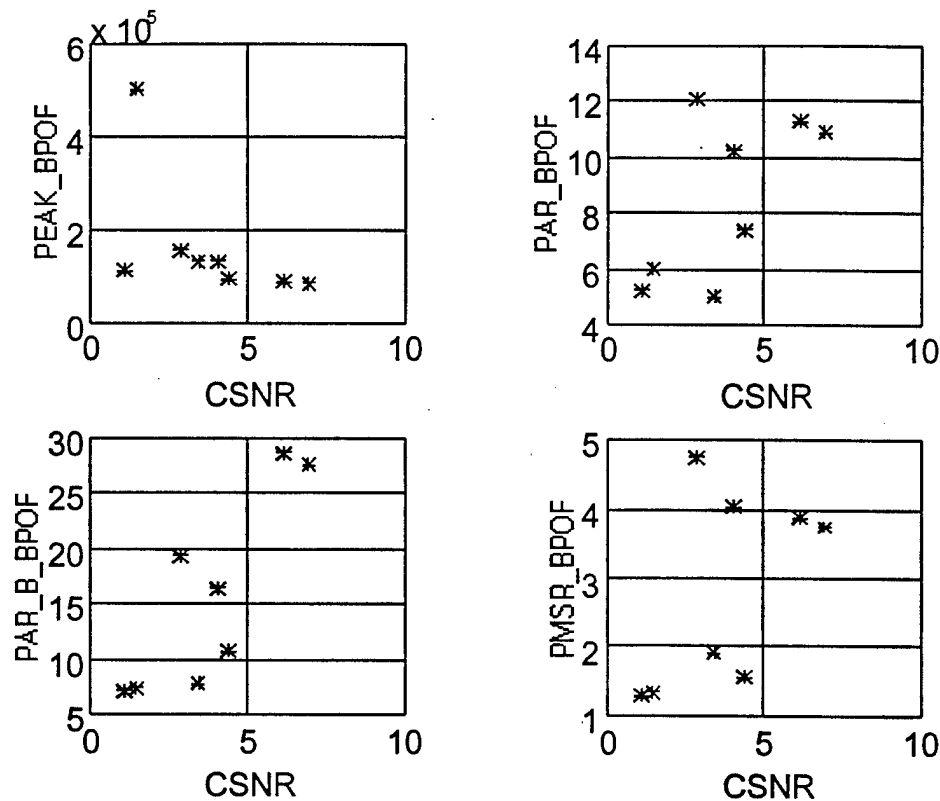


FIGURE 9.3. PERFORMANCE PARAMETERS AS A FUNCTION OF CSNR FOR BPOF CASE

## 9.2 THRESHOLDING PARAMETER

A threshold parameter is chosen to ensure a high target detectability rate with low false alarms. Among the metrics considered, both PAR and PAR\_B gave the best performance as illustrated in Figures 9.1 to 9.3. However, PAR is the more suitable metric for the threshold parameter. Using these images, the PAR value for non-targets was less than unity for the CMF case. Therefore, setting the threshold value for PAR at three will be sufficient for detecting most targets and rejecting most non-targets. Choosing PAR closer to unity will pick up some of the faded targets but also some of the false correlation peaks. Results in this section are shown using both thresholds,  $PAR_{th} = 3$  and 5. These results are shown in Figures 9.4 to 9.7. For each of these figures, the correlation was computed and the correlation peaks were identified that satisfy the thresholding requirement. The peaks that satisfy these conditions are located in the image by superimposing a cross-hair at the position of the detected target over the input image.

In the CMF case, Figure 9.4, the targets were all detected except for the faded target in beach1. Some of the target's edges were detected and labeled as separate targets. The reason for this is that the correlation target by itself forms a cone with a base width about twice the size of the target. All of it could have been blocked when the peak was located instead of blocking only

a square of 41x41 pixels. If that were done, the edges would not be detected but adjacent targets might be missed.

In the POF case, Figure 9.5, and the BPOF case, Figure 9.6, all the targets were detected but so were a number of false targets (water1 and water2). Also the edges in a number of targets were detected as in the CMF case. Detecting false targets could have been avoided if, for example, the threshold value was raised for the PAR to five.

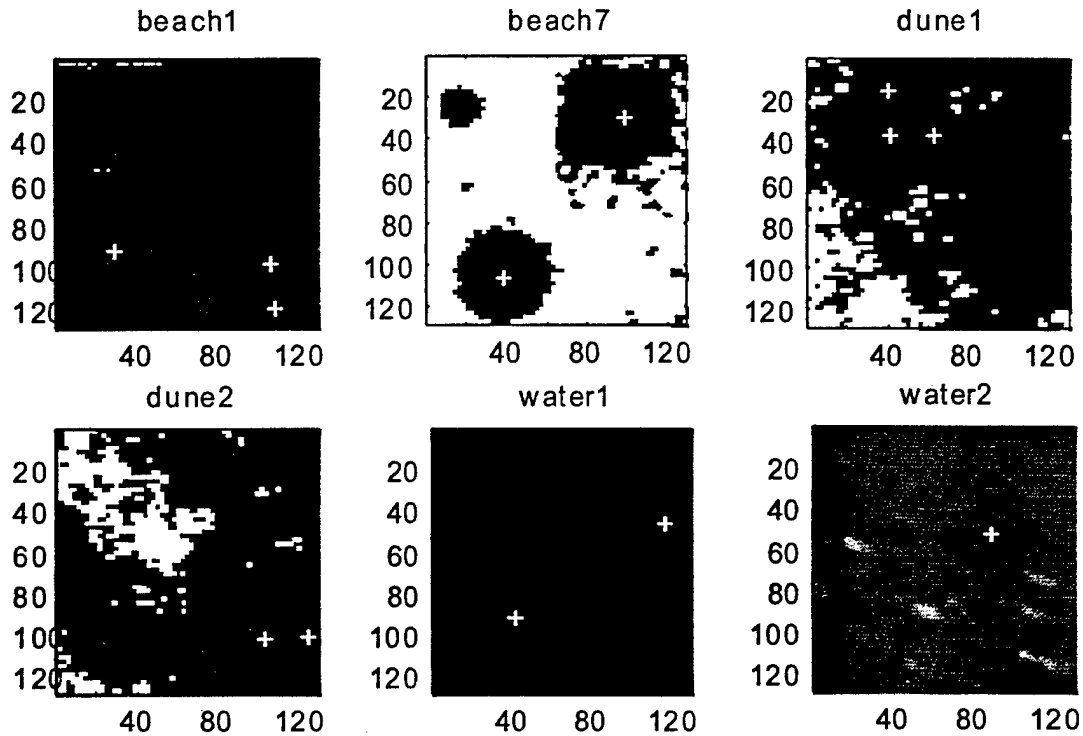


FIGURE 9.4. IMAGES AND TARGET LOCATION AS DETECTED BY CORRELATOR  
(SPATIAL FILTER USED IS CMF AND  $PAR_{th} = 3$ )

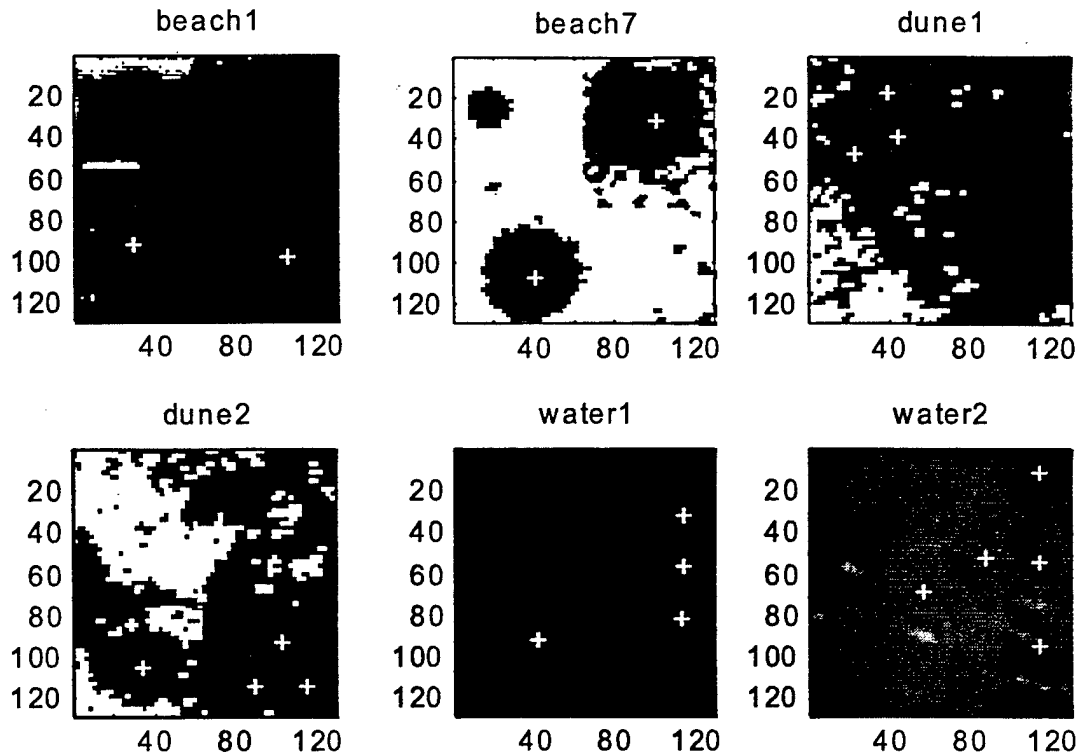


FIGURE 9.5. IMAGES AND TARGET LOCATION AS DETECTED BY CORRELATOR  
(SPATIAL FILTER USED IS POF AND  $PAR_{th}=3$ )

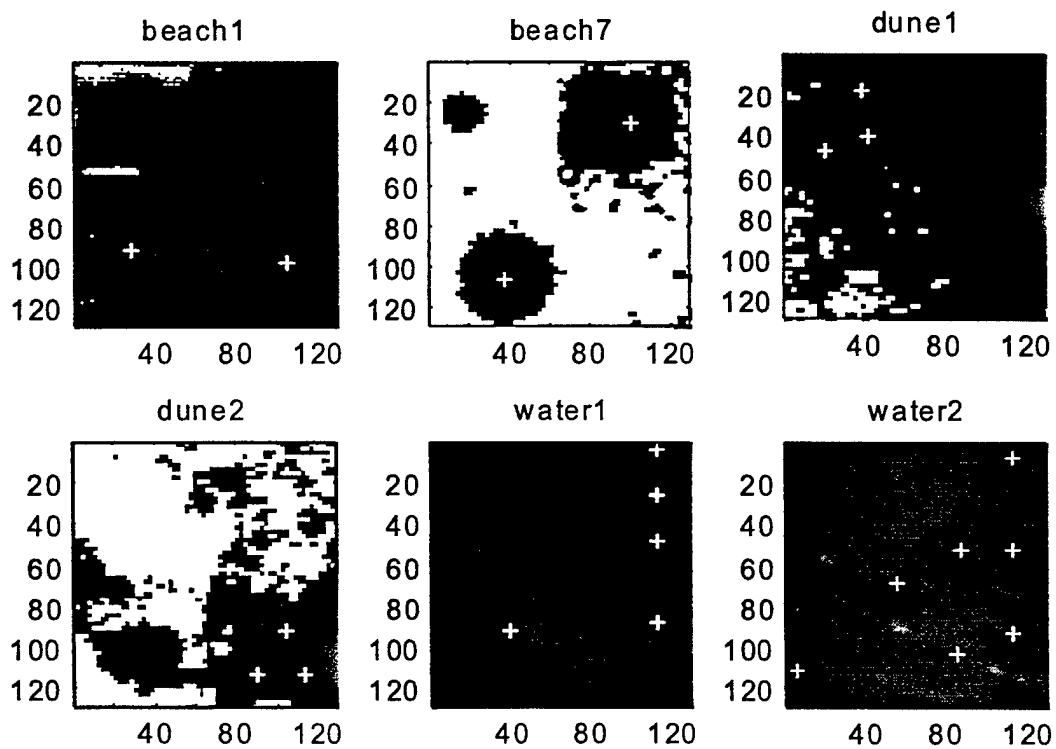


FIGURE 9.6. IMAGES AND TARGET LOCATION AS DETECTED BY CORRELATOR  
(SPATIAL FILTER USED IS BPOF AND  $PAR_{th}=3$ )

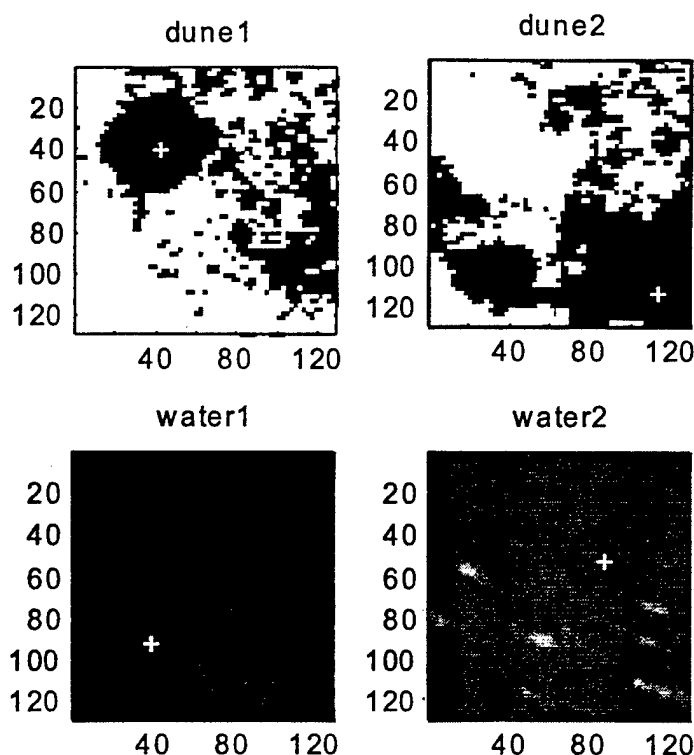


FIGURE 9.7. IMAGES AND TARGET LOCATION AS DETECTED BY CORRELATOR  
(SPATIAL FILTER USED IS BPOF AND  $PAR_{th}=5$ )

Increasing the threshold value to  $PAR=5$  is shown to eliminate the detection of the false targets, Figure 9.7. The increase of  $PAR$  to five caused the loss of one of the targets in image *water1*.

In summary, these results show that thresholding is an essential step in the detection procedure. Choosing the proper metric and its thresholding value can determine the performance of the pattern recognition system. It was shown through the investigation of the real images that the metric  $PAR$  is the proper metric to be used as the thresholding parameter for determining and detecting the targets in minefield images. The value for the threshold is shown to depend on the type of filter used in the system. But all filter formats demonstrated excellent detection and low false detection rates.

The thresholding parameter value can be chosen after calibrating the system with a set of typical images. Lowering the threshold will increase the sensitivity of the system, which increases the false detection rate; while increasing it will lower the false alarm rate. The optimum threshold value then depends on the situation and strategic needs for using the system. Setting the threshold at the proper level is important for obtaining a constant false alarm rate. In some applications, the threshold can be uniform over the output field; while for other applications, it can be varied to compensate for variations in background illumination or other uncontrollable factors.

## 10.0 SUMMARY AND CONCLUSIONS

Optical correlators are the core of many optical image processing systems. Pattern recognition systems, morphological image processors, and neural networks are a few of the examples that use optical correlators. This study has presented a fundamental analysis, simulation, and evaluation of optical correlators in their use for minelike target detection.

A theoretical foundation based on diffraction theory for optical correlators was presented. This background is instrumental in understanding the operation, characteristics, and limitations of correlator systems. Optical and optoelectronic components of the correlator systems along with their characteristics have also been presented. The affect of discretization in spatial light modulators and detector arrays on the performance of the overall system were analyzed. Power budget and speed analysis of the system were discussed and formulas governing them were derived.

Modeling of the correlator using linear system theory were presented within the framework of Fourier optics. Deviations from Fourier optics in some practical systems can be studied using the Fresnel diffraction theory presented in this report. A computer model for the correlator was developed allowing the user to control and specify the different parameters of the system.

Numerical experiments for testing different aspects of the correlator were carried out using a number of images both computer generated and experimentally collected. In-plane translation affects on the correlation peak were studied. It was shown that a translation of a few pixels (three or four) can cause the correlation peak to drop to half of its original value. This emphasizes the importance of alignment in a correlator system.

Two aspects of the implementation of the system, quantization and noise, were extensively studied. The affect of quantization of the input image and the filter on the overall performance of the correlator was considered. This was done using different spatial filter formats: CMF, POF, and BPOF. For each of these experiments performance metrics (correlation peak, PAR, and PMSR) were computed to evaluate the system. Quantization with few gray levels, two to four levels, degrades the performance of the correlator severely, especially when the signal is buried in background noise (low CSNR). Gray levels of eight or higher showed good performance. The results regarding the quantization effects were quite the same for all the images considered. It was shown that at least eight gray levels are needed for good performance of the correlator system to detect the targets considered. Effects of noise in the input image were also investigated. The optical correlator was shown to be capable of detecting targets in experimentally collected data even for low SNRs, about -2 dB. Best results in the presence of

noise were achieved using the CMF. Correlator systems using POF and BPOF failed to detect some of the faint targets in the image.

Limited pixel resolution of the images has some affect on the performance metrics of the correlator. The PAR variations are less than 20 percent for the minelike targets considered. This change will not affect the detectability of the target if PAR was the metric used. Reducing the resolution caused only a minor loss in detectability, especially for targets with large CSNR values. This is an important result in the sense that resolution of the images can be reduced to a smaller format without suffering a significant reduction in the detectability of the targets. This is not the case when CSNR is small. A smaller image format can drastically reduce the computing time of the detection process. For example, a reduction of the resolution from 128x128 to 32x32 reduces the computing time to 1/16 of the original time. This improves the overall throughput of the system.

Thresholding is an essential step in the detection process. Choosing the proper metric and its thresholding value can determine the performance of the system. It was shown in the investigation of the images that the metric PAR is the best metric for detecting minelike targets. The value for the threshold is shown to depend on the type of filter used. But all filter formats demonstrated excellent detection and low false alarm rates.

The thresholding parameter value can be chosen after calibrating the system with a set of typical images. Lowering the threshold will increase the sensitivity of the system, which increases the false detection rate; while increasing it will lower the false alarm rate. The optimum threshold value then depends on the situation and strategic needs for using the system. Setting the threshold at the proper level is important for obtaining a constant false alarm rate. In some applications, the threshold can be uniform over the output field; while for other applications it can be varied to compensate for variations in background illumination or other uncontrollable factors.

In summary, optical correlators show great capabilities in detecting minelike targets. Good performance was demonstrated even for targets with low CSNR values ( $< 1.0$ ). The parallelism and speed of these systems, as high as three orders of magnitude relative to digital implementations, make them prime candidates for preliminary screening of images for minelike targets and should be investigated further.

## 11.0 REFERENCES

1. Suganda, Jutamulia, ed., *Optical Correlators*, SPIE Milestone Series, Vol. MS76, 1993.
2. Abushagur, Mustafa A.G. and Caulfield, H. John, *Fourier Optics*, SPIE Milestone Series, Vol. MS105, 1995.
3. James, M., *Pattern Recognition*, BSP Professional Books, Oxford, 1987.
4. Vasilenko, G.I. and Tisbu'kin, L.M., *Image Recognition by Holography*, Consultants Bureau, 1989.
5. Collings, Neil, *Optical Pattern Recognition Using Holographic Techniques*, Addison-Wesley, 1988.
6. VanderLugt, A.B., "Signal Detection by Complex Spatial Filtering," *IEEE Trans. Inf. Th.* 10, pp. 139-145, 1964.
7. Goodman, J.W., *Introduction to Fourier Optics*, McGraw-Hill, 1967.
8. Weaver, C.S. and Goodman, J.W., "A Technique for Optically Convolver Two Functions," *Appl. Opt.* 5, pp. 1248-49, 1966.
9. VanderLugt, A.B., "The Effects of Small Displacements of Spatial Filters," *Appl. Opt.* 6, pp. 1221-25, 1967.
10. Guenther, B.D., et. al, "Coherent Optical Processing: Another Approach," *IEEE J. Qu. Elect.* 15, pp. 1348-62, 1979.
11. Casasent, D.P. and Psaltis, D., "Position, Rotation, and Scale Invariant Optical Correlators," *Appl. Opt.* 15, pp. 1795-99, 1976.
12. Hsu, Y. and Arsenault, H.H., "Optical Pattern Recognition Using Circular Harmonic Expansion," *Appl. Opt.* 21, pp. 4016-19, 1982.
13. Schils, G.F. and Sweeney, D.W., "Rotationally Invariant Correlation Filtering," *J. Opt. Soc. Am. A* 2, pp. 1411-18, 1985.



## REFERENCES (Continued)

14. Jensen, A.S.; Lindvold, L.; and Ramussen, E., "Transformation of Image Positions, Rotations, and Sizes into Shift Parameters," *Appl. Opt.* 26, pp. 1775-81, 1987.
15. Mersereau, K. and Morris, G.M., "Scale, Rotation, and Shift Invariant Image Recognition," *Appl. Opt.* 25, pp. 2338-42, 1987.
16. Rosen, J. and Sharmir, J., "Scale Invariant Pattern Recognition with Logarithmic Radial Harmonic Filters," *Appl. Opt.* 28, pp. 240-44, 1989.
17. Rau, J.E., "Detection of Differences in Real Distribution," *J. Opt. Soc. Am.* 56, pp. 1830-39, 1966.
18. Yu, F.T.S. and Lu, X.J., "A Realtime Programmable Joint Transform Correlator," *Opt. Commun.* 52, pp. 1248-49, 1984.
19. Johnson, F.T.J.; Barnes, T.H.; Eiju, T.; Haskell, T.G.; and Matsuda, K., "Analysis of a Joint Transform Correlator Using a Phase-Only Spatial Light Modulator," *Opt. Eng.* 30, pp. 1947-57, 1991.
20. Javidi, B. and Horner, J.L., "Single SLM Joint Transform Correlator," *Appl. Opt.* 28, pp. 1027-32, 1989.
21. VanderLugt, Anthony, *Optical Signal Processing*, John Wiley & Sons, NY, 1992.
22. Vijaya Kumar, B.V.K. and Casasent, D., "Binarization Effects in a Correlator with Noisy Input Data" *Appl. Opt.* 20, pp. 1433-37, 1981.
23. Shanmugam, K.S., *Digital and Analog Communication System*, John Wiley & Sons, NY, 1979.
24. Vijaya Kumar, B.V.K. and Hassebrook, L., "Performance Measures for Correlation Filters," *Appl. Opt.* 29, pp. 2997-3006, 1990.
25. Inbar, H.; Konforti, N.; Marom, E., "Modified Joint Transform Correlator Binarized by Error-Diffusion. I. Spatially Constant Noise-Dependent Range Limit," *Appl. Opt.* 33, pp. 4434-4443, 1994.

**APPENDIX A**  
**SYSTEM COMPONENTS AND PARAMETERS**

## A.1 SYSTEM COMPONENTS

A typical 4f in-line correlator system is assembled using a set of optical and optoelectronic components, which are partially listed. A dedicated computer system is usually used to control the flow of data and also used as the interface between the user and the system.

1. Light Source
2. Lens (Spatial Filter)
3. Spatial Light Modulator (SLM) (Input and Filter)
4. Fourier Transform Lens
5. Fourier Transform Lens
6. Output Detector Array
7. Mirrors
8. Beam Splitters
9. Polarizers

## A.2. COMPONENT PARAMETERS

The following is a detailed list of the components parameters and characteristics need to be considered in the design of a correlator system.

### LIGHT SOURCE

- a. Power Emitted
- b. Beam Profile
- c. Wavelength
- d. Spectral Width
- e. Coherence Length
- f. Source Size (Emitting Surface) for LD
- g. Rise Time

## LENS (SPATIAL FILTER)

- a. Focal Lengths
- b. Aperture Size
- c. Surface Curvatures
- d. Surface Tolerance
- e. Glass Type
- f. Index of Refraction at Operating Wavelength
- g. Pinhole Size

## SLM (INPUT AND FILTER)

- a. SLM Type
- b. Transmissivity or Reflectivity
- c. Physical Size
- d. Resolution in Pixels
- e. Pixel Size
- f. Pixel Spacing
- g. Fill Factor
- h. Surface Flatness
- i. Addressing Speed
- j. Gray Levels

## FOURIER TRANSFORM LENS

- a. Focal Length
- b. Aperture Size
- c. Surface Curvatures
- d. Tolerance
- e. Glass Type
- f. Index of Refraction at Operating Wavelength

## OUTPUT DETECTOR ARRAY

- a. Detector Type
- b. Reflectivity
- c. Physical Size
- d. Array Size
- e. Active Area Size
- f. Detector Spacing
- g. Fill Factor
- h. Responsivity
- i. Reading Speed
- j. Dynamic Range (Bit Resolution)

## MIRRORS

- a. Size
- b. Reflectance
- c. Surface Flatness

## BEAM SPLITTERS

- a. Size
- b. Splitting Ratio
- c. Polarization Effect and Ratio
- d. Surface Flatness

## POLARIZERS

- a. Extinction Ratio
- b. Reflectance
- c. Absorption Factor
- d. Surface Flatness

**APPENDIX B**  
**MINELIKE TARGETS DATA**

The experimentally collected minelike target images used in this study are given in this appendix. Each of the targets in an image is identified along with its statistics. The background mean and standard deviation is computed using the National Institute of Health (NIH) image (public domain) processing software provided by the NIH, and given in Tables B.1 to B.4. Also the mean and standard deviation (std) of the region close to the target is computed and labeled as IB. The targets are shown in Figures B.1 to B.3 and are identified by a circle drawn around them and a number to identify each.

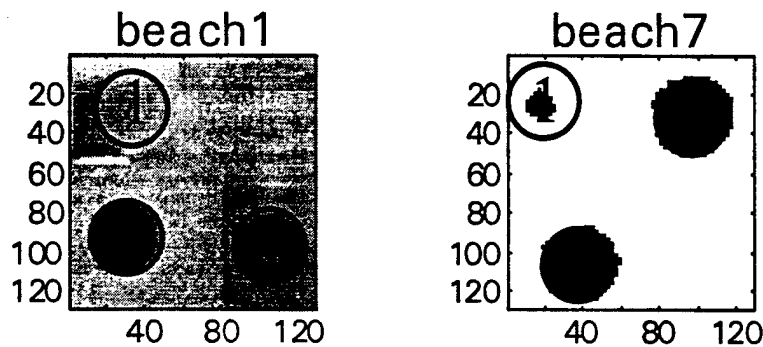


FIGURE B.1 BEACH 1 AND BEACH 7 IMAGES

TABLE B.1. BEACH 1 TARGET AND BACKGROUND STATISTICS

Parameter	Background	beach1		
		(1)	(2)	(3)
mean	119.65	116.62	51.97	32.38
std.	14.9	9.92	17.88	15.21
minimum	69	92.8	20.86	0.72
maximum	176.25	148.19	122.29	87.04
IB mean		130.58	132	91.39
IB std.		15.38	9.02	7.67

TABLE B.2. BEACH 7 TARGET AND BACKGROUND STATISTICS

Parameter	Background	beach7		
		(1)	(2)	(3)
mean	164.46	148.1	43.44	34.94
std.	12.75	35.35	14.89	13.65
minimum	115.24	59.95	20.09	11
maximum	188	185.2	90.06	94.95
IB mean		172.3	149.97	127.52
IB std		7.3	18.76	21.28

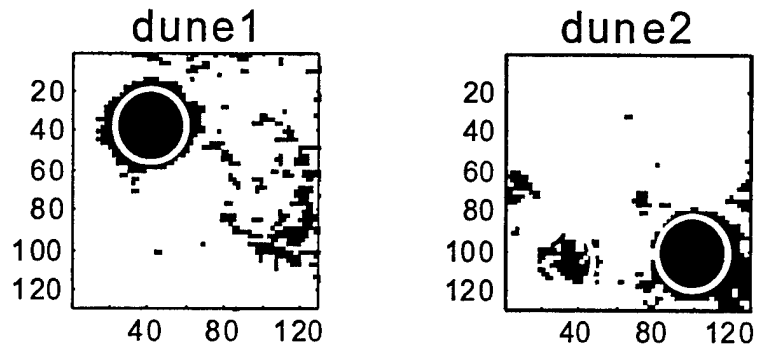


FIGURE B.2. DUNE 1 AND DUNE 2 IMAGES

TABLE B.3. DUNE 1 AND DUNE 2 IMAGES

Parameter	Background for dune1	dune1 (1)	Background for dune2	dune2 (1)	dune2 (2)
mean	154.77	26.63	168.84	132.32	53.24
std.	27.01	10.76	32.39	23.86	9.8
minimum	15	1	1	84	28
maximum	254	70	254	213	83
IB mean		117.58		174.86	124.87
IB std		41.79		19.26	28.21



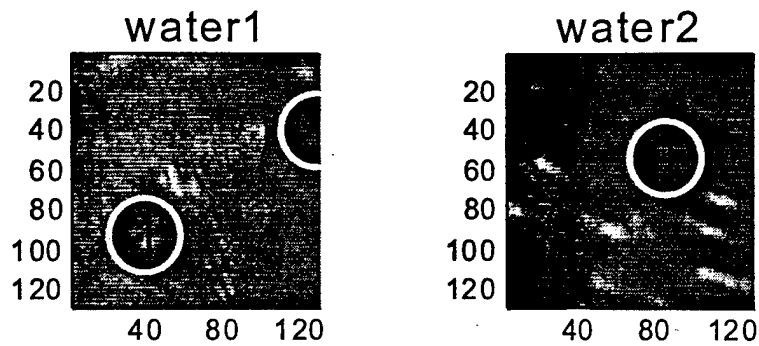


FIGURE B.3. WATER1 AND WATER2 IMAGES

TABLE B.4. WATER1 AND WATER2 IMAGES

Parameter	Background for water1	water1 (1)	water1 (2)	Background for water2	water2 (1)
mean	120.52	104.71		90.87	40.48
std.	10.96	943		28.31	17.75
minimum	86.83	83.96		22	1
maximum	171	133.95		254	102
IB mean		124.62			72.95
IB std		10.74			26.68

The performance parameters defined in Section 8.0 for these targets are given in Table B.5.

TABLE B.5. CORRELATOR PERFORMANCE RESULTS

TARGET	CSNR*	TBR**	CR***	IB CSNR	IB TBR	IB CR
beach1 (1)	0.1693	1.026	0.0128	0.7628	1.1197	0.0565
beach1 (2)	2.9079	2.3023	0.3944	3.9962	2.5399	0.4350
beach1 (3)	4.0987	3.6952	0.574	3.4642	2.8224	0.4768
beach7 (2)	6.1736	3.7859	0.5821	4.4478	3.4523	0.5508
beach7 (3)	6.9342	4.7069	0.6495	3.6619	3.6497	0.5699
dune1 (1)	4.4073	5.8119	0.7064	2.1076	4.4153	0.6307
dune1 (2)	0.9123	1.276	.1213	1.3944	1.3215	0.1385
dune2 (2)	3.4258	3.1713	0.5205	2.3986	2.3454	0.4022
water1 (1)	1.0935	1.1510	.0702	1.3930	1.1901	0.0868
water2 (2)	1.5080	2.2448	0.3836	1.0133	1.8021	0.2863

\*CNR=Contrast Signal-to-Noise Ratio

\*\*TBR=Target-to-Background Ratio

\*\*\*CR=Contrast Ratio

**APPENDIX C**  
**COMPUTER MODEL FOR OPTICAL CORRELATOR**

A computer model was developed and demonstrated for an optical correlator. This model is based on the theory developed in Section 3.0. It is built based on a MATLAB® platform. The model has a graphical user interface (GUI) that provides a friendly operation environment. The general attributes of the model are

- User friendly
- Allows the user to select the parameters of the correlator system through simple buttons
- Optical components, such as lenses and spatial light modulators, can be specified
- Spatial filters to be used in the system
- Quantization levels for input, filter or both can be chosen
- Thresholding parameter PAR can be specified
- Input image, filter, correlation, and target locations can be displayed graphically

### OPERATION PROCEDURE

Using the optical correlator computer model is facilitated through MATLAB. The procedure for a typical session is as follows:

1. Run MATLAB.
2. In the MATLAB Command window load the input image (e.g., a file named: `input_image`), and load the target (e.g., a file named `target`). This is done through the following command in MATLAB.

*{>>load input\_image;load target;}*

Statements between {} and in italics are MATLAB commands.

3. Rename the input image and target as `fname` and `fltr`, respectively.

```
{>>fname=input_image;fltr=target;}
```

4. Run optical correlator model through the following command.

```
{>>optical_correlator}
```

5. At this point MATLAB will run the optical correlator model and a graphics window will appear. This window is shown in Figure C.1.
6. Clicking on the input and target button displays the input and target images.
7. Clicking on the filter button will allow the user to choose one of three spatial filter formats: CMF, POF, or BPOF. Click on one of these choices.
8. Clicking on the correlation button allows three output format: image, plot, or both. Clicking on one of these choices will display the correlator output in the chosen format.
9. Clicking on the threshold button allows the user to display an input image with a cross-hair on each target detected in the input. After pressing on this button, the user needs to click on the command window and type the value for the PAR threshold followed by a carriage return.
10. Clicking on the graphical windows shows two images; the top is an image of the correlation output and the bottom is the input image with a cross-hair placed on each target detected (as in Section 9.0 figures).
11. To test another input, repeat the steps starting at step 2.

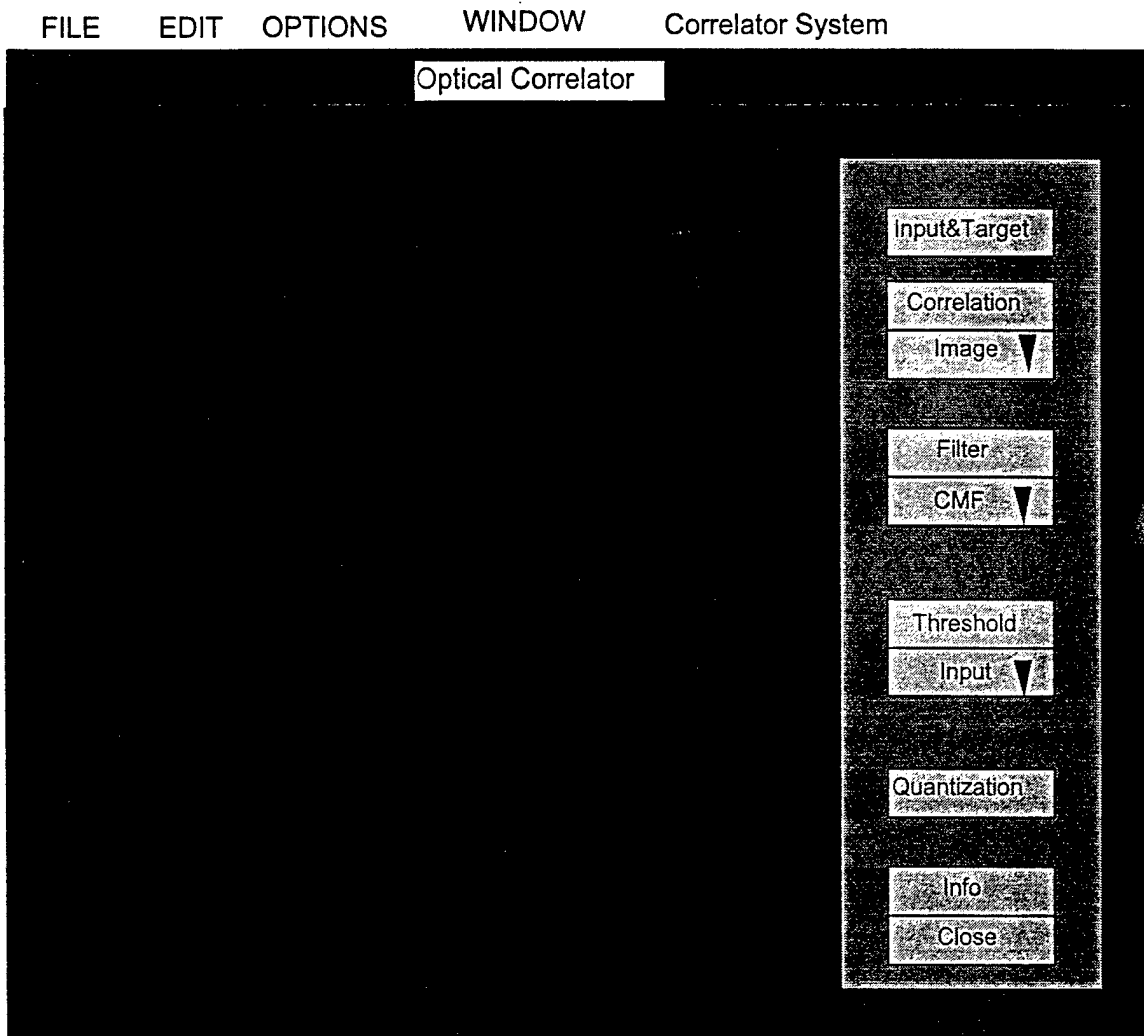


FIGURE C.1. MATLAB COMMAND WINDOW AND FUNCTIONS

**DISTRIBUTION**

	COPIES		COPIES
<b>DOD ACTIVITIES (CONUS)</b>		ATTN M ABUSHAGUR	1
ATTN CODE 321 (W CHING)	1	DEPT OF ELEC COMPUTER ENGR	
CHIEF OF NAVAL RESEARCH		UNIV OF ALABAMA HUNTSVILLE	
BALLSTON TOWER		HUNTSVILLE AL 25899	
800 N QUINCY ST			
ARLINGTON VA 22217-5660		<b>INTERNAL</b>	
ATTN AWT (D VAUGHN)	1	CODE E29L (TECHNICAL LIBRARY)	4
COMMANDING GENERAL		CODE 110A (HENDERSON)	5
MARCORSYSCOM		CODE 0532 (MSC)	5
QUANTICO VA 22134-5080			
ATTN PMO 210	1		
PMO 407	1		
PROGRAM EXECUTIVE OFFICER			
MINE WARFARE			
2531 JEFFERSON DAVIS HWY			
ARLINGTON VA 22242-5167			
ATTN LIBRARY	1		
NAVAL RESEARCH LABORATORY			
4555 OVERLOOK DR SW			
WASHINGTON DC 20375-5320			
DEFENSE TECHNICAL INFORMATION CENTER			
8725 JOHN J KINGMAN RD			
SUITE 0944			
FT BELVOIR VA 22060-6218	2		
<b>NON-DOD ACTIVITIES (CONUS)</b>			
THE CNA CORPORATION			
PO BOX 16268			
ALEXANDRIA VA 22302-0268	1		
ATTN GIFT AND EXCHANGE DIV	4		
LIBRARY OF CONGRESS			
WASHINGTON DC 20540			